Heliyon 10 (2024) e24348

Contents lists available at ScienceDirect

Heliyon

journal homepage: www.cell.com/heliyon

Review article

Advances in amelioration of plasma electrolytic oxidation coatings on biodegradable magnesium and alloys

Biying Shi [a,1], Yu Ru Li [a,1], Jiaqi Xu [a,1], Jiawei Zou [a], Zili Zhou [a], Qi Jia [b], Heng Bo Jiang [a,*], Kai Liu [a,**]

[a] *The CONVERSATIONALIST Club & Department of Stomatological Technology, School of Stomatology, Shandong First Medical University, Jinan 250117, Shandong, China*

[b] *Department and Research Institute of Dental Biomaterials and Bioengineering, Yonsei University College of Dentistry, Seoul 03722, Republic of Korea*

ARTICLE INFO

Keywords:
Mg alloys
Plasma electrolytic oxidation
Biodegradability
Corrosion resistance
Biocompatibility

ABSTRACT

Magnesium and its alloys are considered excellent materials for biodegradable implants because of their good biocompatibility and biodegradability as well as their mechanical properties. However, the rapid degradation rate severely limits their clinical applications. Plasma electrolytic oxidation (PEO), also known as micro-arc oxidation (MAO), is an effective surface modification technique. However, there are many pores and cracks on the coating surface under conventional PEO process. The corrosive products tend to penetrate deeply into the substrate, reducing its corrosion resistance and the biocompatibility, which makes PEO-coated Mg difficult to meet the long-term needs of *in vivo* implants. Hence, it is necessary to modify the PEO coating. This review discusses the formation mechanism and the influential parameters of PEO coatings on Mg. This is followed by a review of the latest research of the pretreatment and typical amelioration of PEO coating on biodegradable Mg alloys in the past 5 years, including calcium phosphate (Ca–P) coating, layered double hydroxide (LDH)-PEO coating, ZrO_2 incorporated-PEO coating, antibacterial ingredients-PEO coating, drug-PEO coating, polymer-PEO composite coating, Plasma electrolytic fluorination (PEF) coating and self-healing coating. Meanwhile, the improvements of morphology, corrosion resistance, wear resistance, biocompatibility, antibacterial abilities, and drug loading abilities and the preparation methods of the modified PEO coatings are deeply discussed as well. Finally, the challenges and prospects of PEO coatings are discussed in detail for the purpose of promoting the clinical application of biodegradable Mg alloys.

1. Introduction

Currently, the incidence of fractures is mounting dramatically worldwide, with approximately 455 million fractures reported worldwide in 2019 [1]. In the United States alone, over 3.1 million orthopedic procedures are performed each year [2]. Researchers predict that, by 2050, the quantity of fracture events in China is going to reach 5.99 million per year at an estimated cost of $25.43

* Corresponding author.
** Corresponding author.
E-mail addresses: hengbojiang@foxmail.com (H.B. Jiang), liukaifancy@163.com (K. Liu).
[1] These authors contributed equally to this work.

https://doi.org/10.1016/j.heliyon.2024.e24348
Received 3 August 2023; Received in revised form 4 December 2023; Accepted 8 January 2024
Available online 11 January 2024

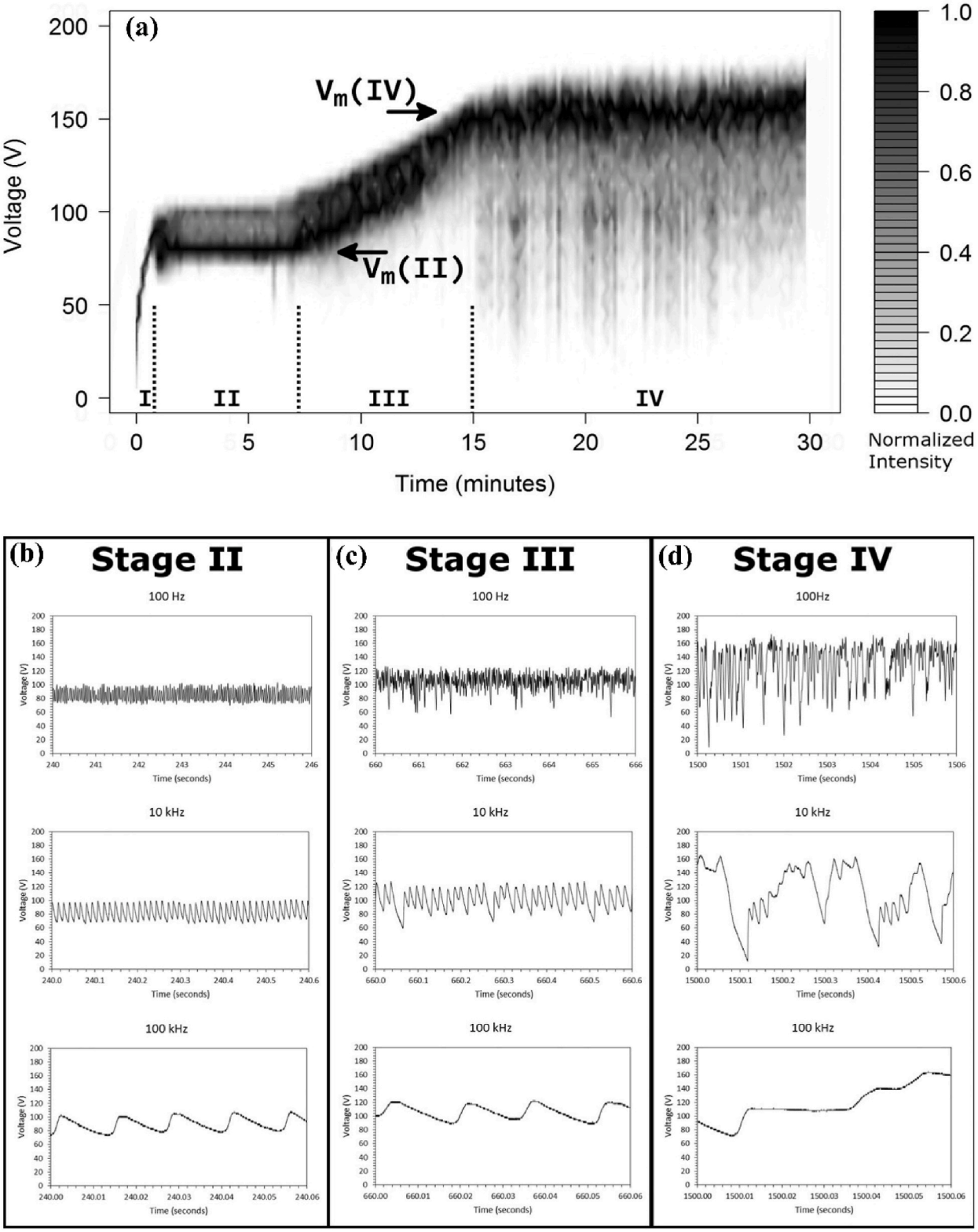

Fig. 1. (a) Normalized time-dependent histogram of voltage. Voltage transients measured at different sampling rates during (b) stage II, (c) stage III, and (d) stage IV [50].

billion [3]. However, non-biodegradable traditional metallic materials, such as titanium, are often used in bone repair surgery, which require second surgeries to remove, adding extra pain and financial burden to patients. Hence, there is a growing demand for biodegradable implants in surgical procedures. In contrast, Mg alloys have low density (1.35–1.85 g/cm^3), elastic modulus comparable to bone, high specific strength, biodegradability and good biocompatibility, which not only ensures that the implant can effectively reduce the stress shielding but also increases the bone mass to a certain extent. Besides, the degradation products are mainly Mg^{2+}, which is biocompatible, i.e., exerting an irritating effect on the growth of certain cells and new tissues [4], especially for mesenchymal

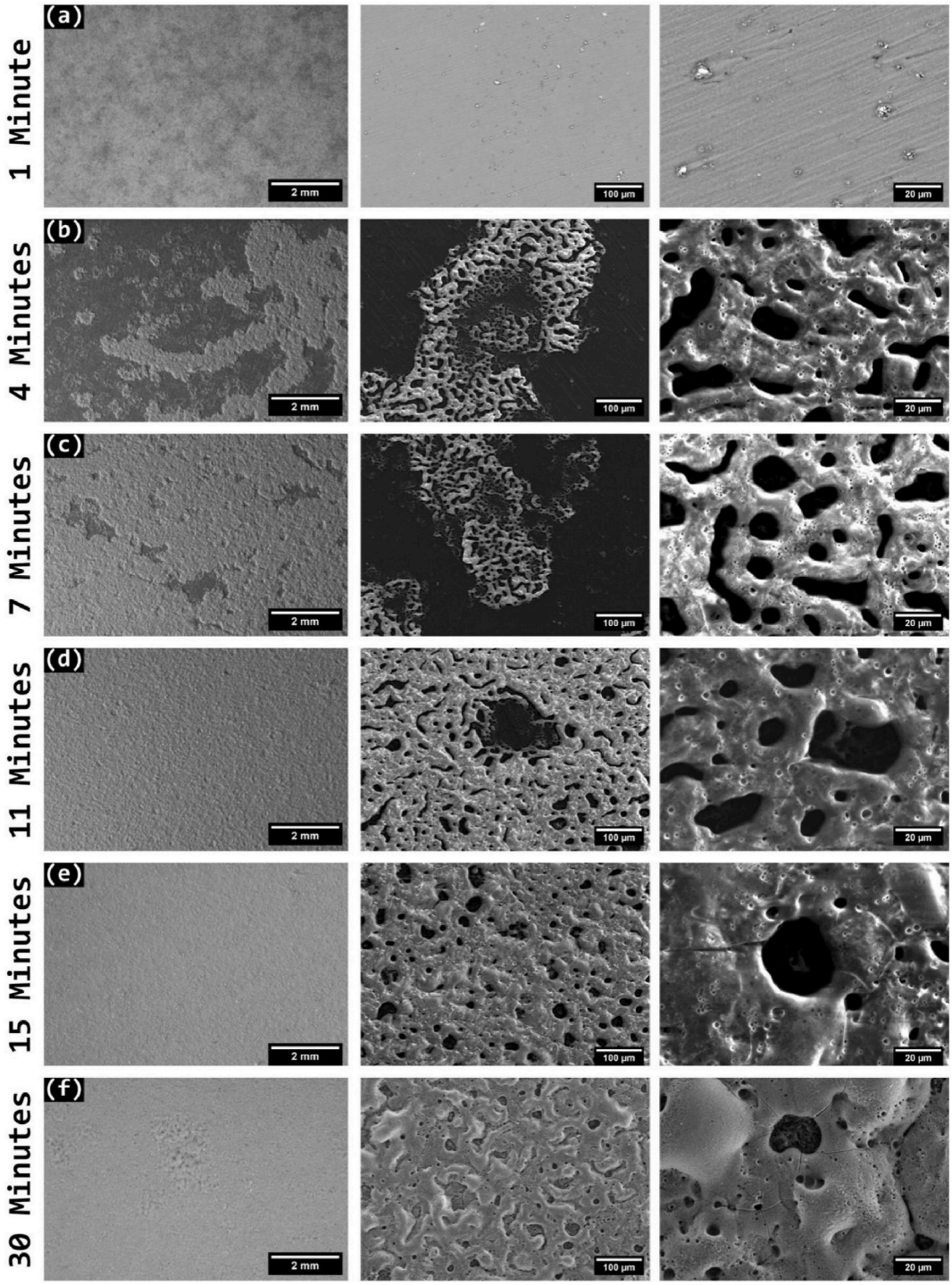

Fig. 2. Surface morphology of PEO coatings at different time periods [50].

stem cells, and Mg^{2+} have a significant promotion effect on their proliferation, adhesion, and osteogenic differentiation. Mg bone implants not only provide sufficient mechanical support in the early stages of implantation, but also degrade gradually as bone tissue recovers. Therefore, Mg alloys are regarded to be the most promising biodegradable implants in the field of medical materials and have received widespread attention as potential bone implant materials.

However, Mg alloys have poor corrosion resistance and tribological properties [5], while in clinical bone repair surgery, bone implant grafts are often subject to unavoidable scraping and damage. As bone implants, the excessively fast degradation rate of Mg alloys may lead to rapid degradation of the bone plate in the healing phase, which cannot provide sufficient stress to the fracture location and most likely lead to the fracture of the bone plate *in vivo*, and the improper degradation rate of Mg alloys may also lead to pitting and excessive H_2 bubble generation to appear as H_2 gas pockets, resulting in exacerbating inflammation and even necrosis in the tissue, thereby delaying the healing process [6]. Also, the poor tribological properties may lead to wear of the bone plate during grafting, which seriously limits the widespread use of Mg alloys as bone implants.

Usually, alloying [7] and surface modification can ameliorate the fast corrosion rate and poor wear resistance of Mg and its alloys. The major approach to ameliorate the characteristics of Mg alloys is still the surface modification using various techniques, including physical vapor deposition [8,9], electrochemical plating [10,11], conversion coating [12–14], anodic oxidation [15], plasma spray [16,17], which are generally environmentally unfriendly and insufficient in corrosion resistance and adhesion strength, offering very limited protection for Mg alloys [18]. Hence, these surface modification techniques are limited in the practical application of Mg alloys. While plasma electrolytic oxidation (PEO), which is also referred to as microarc oxidation (MAO), is based on the metal substrate as the anode and electrode as the cathode (usually graphite and stainless steel) under high voltage and forms oxides on the external surface of the Mg substrate. PEO equipment is simple, and the porous PEO ceramic coating has high adhesion to the substrate metal, which can effectively avoid scraping during implantation of Mg alloys; and the rough porous surface structure facilitates the adhesion of cells [19]. Meanwhile, the PEO process has been a proven surface modification technology for Mg alloys [20]. Despite the many compelling advantages of PEO, it still has some drawbacks. The conventional porous PEO-coated Mg alloys does not meet the corrosion resistance requirements for long-term *in vivo* implants [21], due to the continuous, intense sparking and gas evolution on the PEO-coated surface, which results in a large pore size and excessive microcracks on the surface, aggressive corrosive materials can penetrate into these pores and cracks and severely damage the substrate, thus reducing the corrosion resistance [22–25], and too fast corrosion rate may not only seriously affect the long-term cell adhesion, and will lead to early failure of Mg alloys, limiting its application.

The ideal biodegradable Mg alloys coating needs to have good corrosion resistance, biocompatibility, high adhesion with strong bonding to the substrate Mg alloys, and both biological functions: antibacterial and drug-carrying capacity [19]. In recent years, many studies have been reported on the amelioration of PEO coatings on biodegradable Mg alloys, such as Ca–P-PEO coating [26–28], LDH-PEO coating [29–31], ZrO_2 incorporated-PEO coating [32–35], antibacterial ingredients-PEO coating [36–39], drug-PEO coating [40–43], polymer-PEO composite coating, PEF coating [44–48] and self-healing coating, as well as graphene-PEO coating [49]. This paper will review the improved PEO coatings on biodegradable Mg alloys that have been studied in the last five years from the perspective of preparation methods, coating structures and properties, for expounding the development and prospect of PEO coating in biodegradable Mg and providing researchers with future research interests.

2. Formation mechanism

The PEO treatment process is a reaction in which Mg loses e^- as an anode, as shown in equation (1), and combines with anions in the electrolyte to form compounds, as shown in equation (2) and (3).

$$Mg \rightarrow Mg^{2+} + 2e^- \tag{1}$$

$$2H_2O \rightarrow O2 + 4H^+ + 4e^- \tag{2}$$

$$Mg^{2+} + O^{2-} \rightarrow MgO \tag{3}$$

Sobrinho et al. [50] recorded the instantaneous voltage-time curves of AZ31B treated with PEO under the fixed condition (as shown in Fig. 1(a)) and the surface morphology of the PEO coatings generated in different periods (as shown in Fig. 2). In the first stage of coating formation (Fig. 2(a)), anodic oxidation of the substrate occurs to form a dense oxide layer, which increases the resistance of Mg alloys, therefore the voltage rises. When the voltage gradually rises beyond the breakdown, the plasma discharge occurs, this is the second stage of the coating formation (Fig. 2 (b, c)), the breakdown-reformation cycle occurs, and the coating is regenerated after being broken down with a generation rate greater than the coating dissolution rate. At this period, the outermost layer is porous. In the third stage, as shown in Fig. 2(d and e), the voltage continues to rise and Sobrinho et al. found that there is no increase in coating thickness in this stage, probably because the temperature of the electrolyte increases and leads to faster dissolution of the coating, resulting in the same rate of generation and dissolution, but the porous coating expands and covers more area during this period. Unlike stage II and stage III (Fig. 1(b and c)), In stage IV (Fig. 2(f)), two different discharge mechanisms can be inferred from the voltage variation pattern in Fig. 1(d), one is the breakdown of the thinner layer separating the large pores from the substrate; the other is the breakdown of the horizontal pores at the junction of the substrate and the coating that are connected to the electrolyte through cracks. The surface of the coating at this stage has a typical PEO pancake structure.

The above four stages discuss the overall formation process of the coating, but for each point of constant breakdown, there may be a cycle of stages II-IV. In addition, the PEO-coated AZ91 and AZ31 Mg alloys prepared by Rakoch et al. [51] can be divided into three

layers according to the cross-sectional morphology (Fig. 3(a–f)), which are the porous outer layer, inner layer, as well as the dense anodic layer. For phase IV of PEO, they observed two types of discharges and also concluded that two different discharge mechanisms existed simultaneously, similar to the view of Sobrinho et al. Among them, the mechanism promoting the thickening of the inner layer is mainly the breakdown of horizontal pores, the oxide is formed only in the inner layer due to the blockage of high-temperature ionized gas [52], while the thickening of the outer layer mainly relies on the melt ejection brought by the breakdown of the vertical large pore to contact with the cold electrolyte for condensation. However, these two discharge mechanisms seem to be considered contradictory in previous studies [20].

3. Conventional effective parameters

The electrical parameters affect the coating formation. Lu et al. [53] applied PEO treatment on KBM10 Mg alloys at direct current (DC), respectively, and found that the coating surface was smoother at lower voltages. With the voltage increases, the size and quantity of pores increase. The surface is rougher, which may be attributed to the growth in discharge size. Yuan et al. [54] investigated the impact of current output pattern on coating formation as well as performance, the parameters are shown in Table 1. They found that at a certain current density, the coatings treated under the current reduction mode (G852) with the lowest energy consumption show the best corrosion resistance and have the thickest dense inner layer, while the outer layer of large pores is sealed, which may be attributed to the fact that the current density was reduced twice resulting in sealing the large pores formed by the initial high current density. Lou et al. [55] performed PEO treatment of AZ31 in bipolar current mode at 1000 Hz and found that the order of influence of various factors to the corrosion resistance is anode on-time, cathode on-time, anode current setting, and cathode current setting (from large to small). Furthermore, increasing the anode on-time and anode current can increase the thickness of PEO anodic layer.

The treatment time is also one of the parameters affecting the microstructure of PEO coatings. Yong et al. [56] found that the surface roughness of PEO coatings increased when treatment time enhances, while the porosity decreased. Due to the coating being too thick to penetrate, the number of sparks decreases as the size of spark discharges grows, which leads to larger pores. In most cases, the increase in treatment time will increase the coating thickness, Mohedano et al. [57] found the coating thickness rises significantly with increasing oxidation time and the addition of fluoride accelerates coating generation. However, a long treatment time will probably lead to the breakage of the coating [58].

It is well known that the higher the conductivity of the electrolyte, the lower the breakdown voltage of the coating [20]. And the breakdown voltage often determines the spark size during PEO discharge, affecting the porosity, the pore size and the surface roughness of the coating [59]. The factors affecting electrolyte conductivity include electrolyte concentration. Ono et al. [60] found that the thickness and corrosion resistance of PEO-AZ31 increase with decreasing electrolyte concentration under constant current conditions. Also, surface roughness decreases with decreasing electrolyte concentration. However, A. Fattah-alhosseini et al. [59] chose a KOH electrolyte to prepare PEO coatings with different concentrations (1–3 M) and found that the coating treated at a concentration of 2.5 M has the best corrosion resistance. At 1–2.5 M, the pore size and porosity reduce as electrolyte concentration is raised, hence the corrosion resistance is positively correlated with the electrolyte concentration, while at 2.5–3 M, the pore size, porosity, and roughness of coating surface increase as electrolyte concentration is raised, and the corrosion resistance decreased significantly, which was consistent with the research of Ono and A. Keyvani [61]. The reason may be that low electrolyte concentration

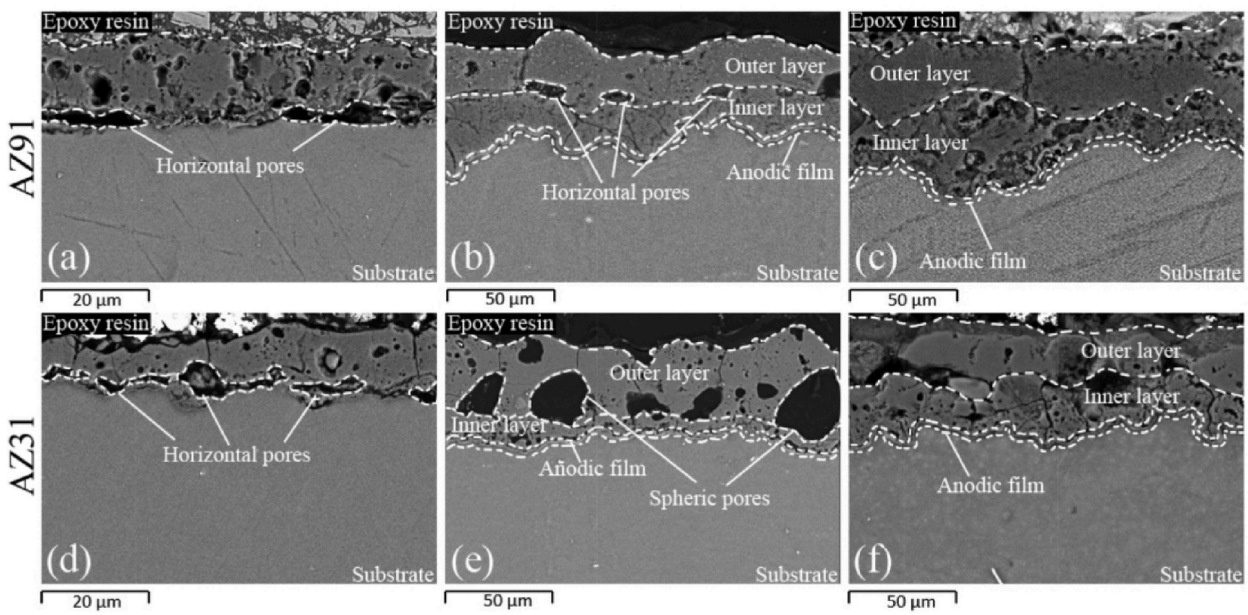

Fig. 3. Cross section morphology of PEO-coated AZ91 (a–c) AZ31, (d–f) [51].

Table 1
Current output modes of three groups [54].

		Current density (A dm^{-2})		
Tep	Time (min)	C5	G258	G852
I	0–10	5	2	8
II	10–20	5	5	5
III	20–30	5	8	2

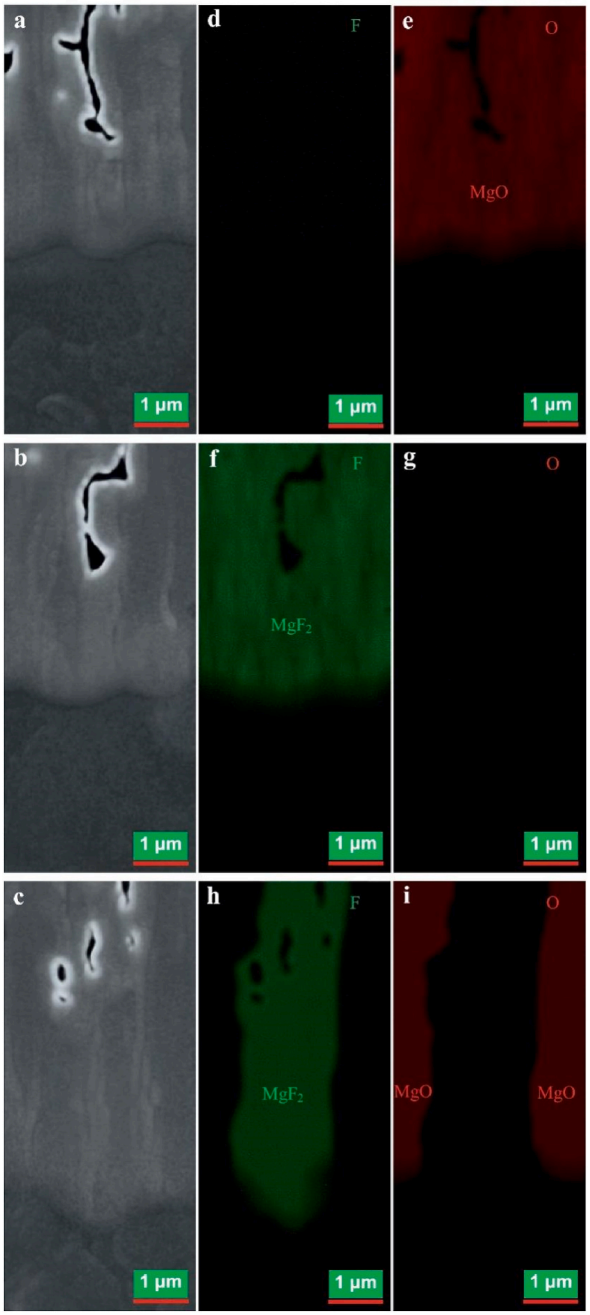

Fig. 4. Compositional analysis of the inner layer of typical coatings with α = 0.1, 10.7 and 1.3, respectively: (a–c) Cross-sectional morphology. (d, f, h) F maps of (a–c), respectively. (e, g, i) O maps of (a–c), respectively [62].

leads to low conductivity, which makes breakdown difficult, hence spark size becomes larger, and an appropriate increase in electrolyte concentration can reduce spark concentration, whereas a high electrolyte concentration will lead to a significant increase in solution conductivity, which makes the diffusion of spark discharge severe.

Apart from electrolyte concentration, the concentration ratio of electrolyte components can also affect the coating properties. Zhang et al. [62] treated AZ61 with an electrolyte (KOH concentration of 5 g/L and KF-2H_2O concentration of 140 g/L). They found the inner layer of this coating composed mainly of MgO or MgF_2 (Fig. 4(a–g)) could not prevent the intense melt eruption occurring during PEO treatment, i.e., traditional discharge (TD), which can lead to large aperture discharge channels on the surface, as shown in (Fig. 5 (b and c)). His improved method was to control α (the mass ratio of MgF_2 to MgO) by changing the concentration ratio of KOH to KF-2H_2O in the electrolyte, resulting coatings with different porosity (Fig. 5(a)). They discovered that at α = 1.3, the coating surface has small discharge pores, as shown in Fig. 5(d), showing the best corrosion resistance, which resulting from the sequential discharge (OD) caused by the different dielectric constants (Ds) of MgO and MgF_2 (the distribution of MgO and MgF_2 is shown in Fig. 4(c–i)), where MgF_2 with low Ds will undergo electric breakdown, but its surrounding MgO with higher Ds can inhibit the strong eruption of MgF_2 instead of occurring violent breakdown itself. More melt will be retained in the discharge channel, making the inner dense layer thicker, accompanied by a small aperture of the discharge channel during eruption. Thus, enhancing the corrosion resistance. Moreover, the addition of some particles in the electrolyte can also affect the corrosion resistance by affecting the conductivity of electrolyte, thus changing the morphology the coating [63], which is mostly shown in sealing pores. The interaction of particles with the electrolyte anion will also be affected by different anion types [64].

In general, the parameters mentioned above tend to affect the surface micromorphology of the coating by regulating the thickness and the size and distribution of the sparks in the process of discharging, thus influencing corrosion resistance as well as biocompatibility.

The substrate also affects the morphology of PEO coatings. For example, AZXX, which is often used as a substrate for medical Mg, Rakoch et al. [51] discovered that PEO coating on AZ91 was denser and its inner layer was thicker than that formed on AZ31. AZXX Mg alloys are also multiphase Mg alloys, and the increase of its β phase (Mg_xAl_y) will lead to coating perforation at the boundary of α and β phase [65]. In the extreme case without β-phase, the coating is not homogeneous and has poor corrosion resistance because there is no dense Al oxide in the coating and the severe local oxidation behavior around the AlMn precipitates [66]. In spite of the effect of β-phase content mentioned above, Chen et al. [66] also found that for AZ31 after solid solution treatment, the β-phase is finer and more uniformly distributed, and the coating morphology is more uniform with fewer defects after PEO treatment, thus the corrosion resistance is improved.

And it is worth noting the Taguchi method has been used in most of the studies. And in multi-parameter experiments, the use of the Taguchi method allows the use of the minimum possible combination matrix to determine the best PEO process conditions, avoiding the control of a single variable resulting in more experimental times [67].

4. Amelioration of the pretreatment

Before PEO treatment of Mg alloys, pretreatment by laser [68–70], hydrofluoric acid (HF) [71], ultrasonic [72,73], and solid solution treatment [74] can improve the Mg alloys matrix and form a denser PEO coating on its surface to ameliorate the mechanical integrity and corrosion resistance of matrix.

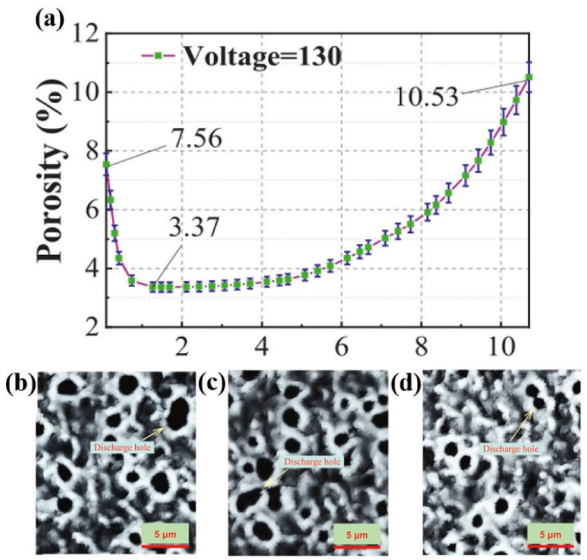

Fig. 5. (a) The variation curve of porosity with α at a voltage of 130 V. (b)–(d) Surface morphologies of typical coatings with α = 0.1, 10.7 and 1.3, respectively [62].

4.1. Laser shock peening

Laser shock peening (LSP), is a form of non-contact surface treatment that uses high power and short pulses of laser light to impact the surface of the sample, which causes plastic deformation to occur on the Mg alloys, forming a nanoparticle layer and inducing residual compressive stresses in the surface layer of the metal [68]. Pretreatment using LSP technique improves the mechanical integrity and corrosion resistance of Mg-based implants *in vivo* [69,70].

Xiong et al. [75] formed a fine particle layer about 30 μm thick on the surface of AZ80 Mg plate by Nd: YAG laser. Different from the single PEO coating shown in Fig. 6(c), the cross-section of LSP/PEO coating on Mg alloy is shown in Fig. 6(d), part of the fine particle layer was oxidized to the outer layer of PEO, and the unoxidized particle layer was the inner layer. The LSP-nanocrystal layer has self-healing properties, which can effectively reduce the adsorption of Cl^- and give the passivation film a high nucleation density. As illustrated in Fig. 7, once the external PEO coating is subjected to external corrosion, the LSP layer can quickly form a dense passivation film at the damage location to obstruct the corrosive medium's penetration [70]. On the one hand, the passivation film enables a large amount of corrosion products to accumulate in the corrosion channel, which ameliorates the corrosion resistance of the samples. On the other hand, the LSP-treated refined grain surface can provide more discharge channels for the spark discharge during PEO, which makes the formed PEO coating denser and enhances the corrosion resistance of PEO coating. As shown in Fig. 6 (a, b), compared with the PEO coating alone, the surface of the LSP pretreated coating shows lower porosity, which is about 78 times higher than that of the LSP/PEO coating. The electrochemical corrosion experiments manifested that the polarization resistance (Rp) of the LSP/PEO-treated samples ($1.19 \times 10^5\ \Omega\ cm^2$) was one order of magnitude greater than in of the PEO-treated samples ($2.63\times 10^4\ \Omega\ cm^2$). In a long-term immersion corrosion experiment conducted in simulated body fluid (SBF), Xiong et al. [70] found that the PEO coating was close to peeling off at the final stage of immersion (1800 h), while the LSP/PEO coating remained well bonded to the substrate.

In vivo, Mg alloy implants are subjected to mechanical loads as well as corrosive environments, which can cause stress corrosion cracking (SCC) and premature implant failure. While the corrosion resistance of Mg alloys is improving, its mechanical properties may not be improved simultaneously. Therefore, in addition to corrosion resistance, the maintenance of mechanical integrity of biodegradable implants after implantation in humans is another crucial factor. For samples loaded under tension, the compressive residual stresses on the surface of LSP-treated samples can retard the generation of cracks in corrosive environments, while the PEO-treated samples still have tensile residual stresses on their surfaces, which are not conducive to stress corrosion resistance. The slow strain rate tensile (SSRT) experiments by Xiong et al. [70] confirmed that although PEO coating can enhance the mechanical properties of the material, it did not significantly improve its stress corrosion susceptibility in a corrosive environment. In contrast, the LSP/PEO treated specimens showed significantly higher elongation (5.8 %) and ultimate tensile strength UTS (221 MPa), the longest SSRT test duration (32 h), and better mechanical properties than the PEO coating.

4.2. Ultrasonic cold forging technology

The ultrasonic cold forging technology (UCFT) technique uses ultrasonic vibrations to produce plastic deformation on the metal surface to form nanocrystalline structures, which can reduce the porosity of subsequent PEO coatings and significantly improve the

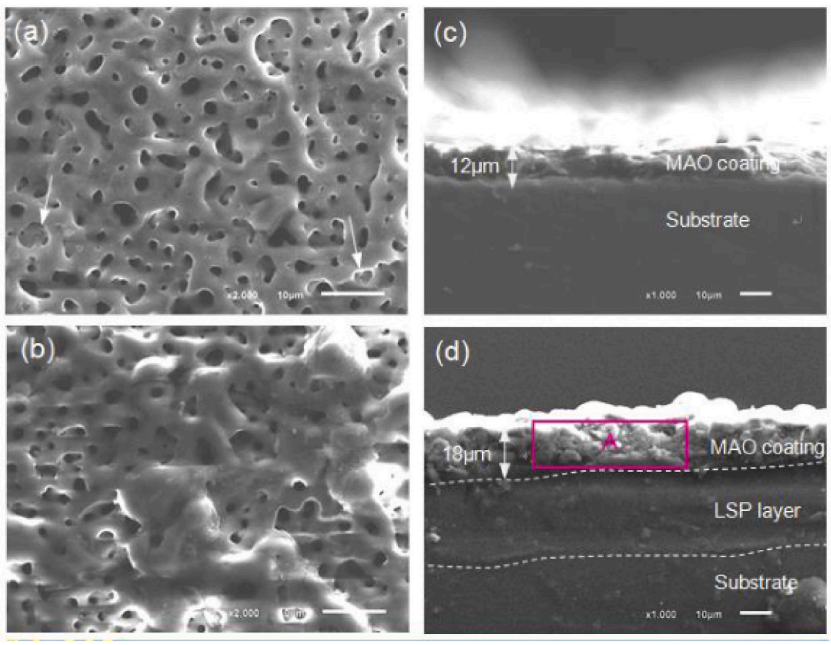

Fig. 6. SEM morphologies of surface and cross-section of PEO Mg alloy (a, c) and LSP/PEO Mg alloy (b, d) [75].

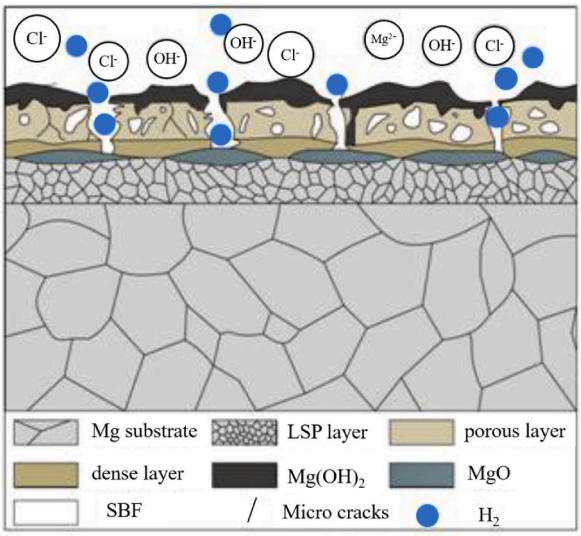

Fig. 7. Schematic diagram of the SCC behavior of LSP/PEO samples in simulated body fluid. The LSP layer is able to form a passivation film rapidly at the damage site, preventing further erosion of the substrate by corrosion ions [70].

metal surface hardness. UCFT is simple to operate, highly efficient to treat and environmentally friendly [72]. Yang et al. [73] used an ultrasonic device equipped with tungsten carbide balls to treat AZ31B Mg alloys with ultrasonic cold forging technique. On the surface of the Mg alloys, the finer grains provide more discharge channels for the PEO coating, so the PEO coating on the sample after UCFT treatment is denser and more uniform than that formed directly on the substrate, which improves the corrosion resistance of Mg. The corrosion current density of UCFT-treated PEO Mg alloy was proved to drop by one order of magnitude lower compared to the non-UCFT-treated PEO Mg alloy in electrochemical studies. Mg as an implant material is subjected to relative motion in the human body, which may lead to wear damage and accompany corrosive erosion of body fluids, and the effect of frictional corrosion generated should not be neglected. The antifriction corrosion experiments confirmed that the UCFT-PEO samples have a flat and dense surface with a friction coefficient of about 0.1, which is lower than that of PEO samples, indicating that they have better friction corrosion performance than PEO samples. the same is true for electrochemical impedance spectroscopy (EIS) and potentiodynamic polarization (PDP) measurements, where the lowest friction corrosion current density (2.4×10^{-4} A/cm^2) and maximum friction corrosion impedance (23.38 kΩ cm^2) were found in UCFT-PEO samples.

4.3. Ultrasonic fluorination treatment

The formation of a MgF_2 coating by hydrofluoric acid treatment tends to be integrated in the passive oxide coating, which can induce surface arcing during PEO, thus making it easier to reach the breakdown voltage. The results showed that the HF-treated samples were in the third stage of the PEO process for a longer time than the untreated samples, indicating that the PEO coatings formed by the pretreatment were more uniform and denser. The application of ultrasound (US) in pretreatment resulted in denser coatings and increased their fluorine content. Wei et al. [71] pretreated AZ91 Mg alloys by HF (9.8 wt%) at 40 kHz, 60 W ultrasound for 30 s with ultrasonic fluorination. Observation using scanning electron microscopy (SEM) revealed that, PEO coating was deficient in its inner layer on its own, while which treated by ultrasonic fluorination was intact and free of defects. According to the electrochemical test, the PEO coating deposited on the surface of AZ91 pretreated with HF and US had higher corrosion resistance than the PEO coating formed directly on AZ91.

4.4. Solid solution processing

Yan et al. [74] subjected Mg-0.06Cu alloy ingots to solid solution treatment, i.e., heating at 510 °C for 10 h and quenching with water. In antibacterial experiments with *Staphylococcus aureus* (S. aureus), the solid solution alloy exhibited similar antibacterial effects as the cast alloy. The corrosion rate of the Mg–Cu alloy was determined by micro-electro-couple corrosion, with α-Mg and Mg_2Cu second-phase particles acting as the cathode and anode, respectively. The majority of the second-phase particles were dissolved by heat treatment, resulting in a reduction of the galvanic coupling corrosion. The solid solution alloy has a more uniform composition distribution than the as-cast (AC) alloy, resulting in a tighter layer of corrosion products. In electrochemical tests, both the surface layer resistance (Rf) and polarization resistance (Rct) of AS-PEO were twice as large as those of AC-PEO. Immersion tests revealed that PEO-coated solid-solution alloys corroded at a lower rate than cast alloys.

5. Typical amelioration of PEO coating on Mg alloys

In order to meet the requirements for an ideal biodegradable Mg alloys implant coating, i.e., corrosion resistance, biocompatibility, wear resistance to avoid large wear debris during implantation, tight bonding to the substrate Mg alloys, antibacterial properties and drug loading ability as mentioned above, different PEO coating Amelioration methods have been proposed focusing on different behavior enhancements. Their main coating techniques as well as characteristics are shown in Table 2.

5.1. Calcium phosphate-PEO coating

Calcium (Ca), and phosphorus (P) are important for human life activities. Biologically relevant calcium phosphate (Ca–P) is found in human bones and is a major component of bones [76,77]. In addition, large amounts of Ca–P facilitate wound healing [78]. Ca–P coating is a commonly used implant coating that can increase significantly the corrosion resistance, biocompatibility, and bioactivity of the substrate [76,79,80]. Most remarkably, the bioactivity of Ca–P coating allows the adhesion, proliferation, and diffusion of osteoblasts, which facilitates bone regeneration, while improving osseointegration by promoting the binding of the implant to the surrounding bone tissue [81,82]. These make Ca–P-coated implants put to use in the field of bone repair, and bone replacement [83]. Ca–P exists in various forms, such as hydroxyapatite (HA), calcium deficient hydroxyapatite (CDHA), octacalcium phosphate (OCP), dicalcium phosphate anhydrous (DCPA), biphasic calcium phosphates (BCP), β-tricalcium phosphate (TCP), etc. [78,84]. Among them, the most commonly used Ca–P is HA ($Ca_{10}(PO_4)_6(OH)_2$) [26], which is easy to manufacture and the main inorganic component of bone

Table 2
Coating techniques and characteristics of typical Amelioration methods.

Amelioration of PEO coating	Coating techniques	Surface morphology Amelioration	Improved behaviors vs. conventional PEO coating	Disadvantages
Calcium phosphate (Ca–P)-PEO coating	Sol-gel method: prepare Ca–P sol-gel and coat on PEO-coated samples; - Hydrothermal method; - Flame spraying; - Electrochemical deposition (ECD); - Electrophoretic deposition (EPD)	- Smaller pore size - Shallow cracks	– High corrosion resistance - Good bioactivity and biocompatibility - Suitable mechanical property	–
Layered double hydroxide (LDH)-PEO coating	Hydro-thermal treatment; immersion process; two-step method (immersion and hydrothermal treatment)	- Smaller pores size - Fewer cracks	- High corrosion resistance - Better biocompatibilities - Drug loading capacity	Porous structure still exists.
ZrO_2 incorporated-PEO coating	ZrO_2 nanoparticles are incorporated into electrolytes or in electrolytes containing Zr element during the PEO process.	- Increased compactness - Smaller pore size - Smoother surface	- Better wear resistance - Better corrosion resistance - Better biocompatibilities	The coating formed in the electrolyte containing Zr element has more defects compared to the electrolyte containing ZrO_2 nanoparticles.
Antibacterial ingredients-PEO coating	PEO: add antimicrobial agents directly to the electrolyte.	- Smaller pore size - Shallow cracks	- High corrosion resistance - Outstanding antibacterial property	Metallic inorganic antimicrobial agents can be cytotoxic in excess.
Drug-PEO coating	Dip-coating: dip the PEO-coated samples into drug solution.	- Smaller pore size - Shallow cracks	- High corrosion resistance - Superior drug release capability For treatment: - Excellent antibacterial property - Inductive osteogenesis potential - Inhibiting osteosarcoma (OS)	–
Polymer-PEO composite coating	Dip coating method; rotary coating method; electropolymerization method; electrophoretic deposition method	- Smoother surface - No obvious pores and cracks	- High corrosion resistance - Better wear resistance - Some have better biocompatibility - Some have good drug-loading properties	- Some have low adhesive strength; - Some have poor wettability (depending on polymer selection), resulting in poor biocompatibility.
Plasma electrolytic fluorination (PEF) coating	PEF typically with highly saturated hydrofluoric acid (HF) as the electrolyte.	- Smaller pore size - Smoother surface - No cracks	- High corrosion resistance - Better biocompatibilities	–

with excellent biocompatibility, bioactivity, and osteoconductivity [27,85,86]. HA is not toxic in the human body, easily binds to surrounding bone tissue [28], forms chemical bonds at the implant-bone tissue interface, and releases Ca^{2+} which is harmless to the body and can induce and accelerate new bone growth [87].

PEO can be used directly to prepare Ca–P coating [26,73,77,80,82,88–93], which requires the addition of a salt solution containing Ca, P to the electrolyte, and the final form of Ca–P produced depends on the Ca/P ratio [83,84]. It is worth mentioning that Tang et al. [88] found that the control of the Ca/P ratio can be achieved by adjusting the applied voltage during PEO, where the Ca/P ratio of the coating at 500 V ratio (1.68) is extremely close to the Ca/P ratio of HA (1.67), as shown in Fig. 8.

To date, diversified surface modification techniques have also arisen for the preparation of Ca–P coating on PEO coating surfaces to obtain composite coating and further get superior coatings, such as hydrothermal method [94], Flame Spraying [95], electrochemical deposition (ECD) [27,96], electrophoretic deposition (EPD) [87], sol-gel method [28,97,98] and so on. Among them, the sol-gel method is the most popular. Hydrothermal treatment (HT) is simple and low cost [99], but the degradation of Mg alloys which formed Mg^{2+} will prevent the crystallization of HA, and it is difficult to form HA coating, some research shows that this problem can be improved by adding a chelating agent or doping F^{-} in HA [100]. The advantages of thermal spraying include easy control of working parameters and mass fabrication, but the thermal expansion coefficient difference between HA coating and metal substrate during the cooling process is large, and residual stresses will be generated, which can be improved by adding a PEO interlayer [95]. Compared with thermal spraying, ECD, and PEO such coating structure formed in the electrolyte is more similar to that of skeletal inorganic materials [78]. EPD and ECD have many similarities, both have the advantages of short working time, low working temperature, simple operation, green environment, and can form a uniform and stable coating on the porous or complex-shaped substrate, and the coating thickness can be controlled [27,101–103]. The main difference between them is whether the redox reaction occurs during the deposition process. However, the ECD and EPD-formed coatings have low bonding strength and are easy to peel off [78]. Many advantages like controllable structural composition, high adaptability to complex-shaped substrates, low cost, and environmental cleanliness are inherent to sol-gel coatings [104]. Additionally, the PEO coating with porous structure is added to the interior of the coating system, which can improve the disadvantage of low bonding strength of the sol-gel coatings [98]. However, it has been shown that it is difficult for the sol-gel to fill the porous PEO coating by reason of the presence of microbubbles at atmospheric pressure, and this problem can be solved by the method of excluding microbubbles at low pressure [28].

Ca–P coating can notably improve the ability of preventing the invasion of corrosive media of PEO-coated Mg alloys. When preparing HA coating using PEO, the mixture of appropriate HA particles can fill the micropores formed by the PEO coating, reduce the porosity and make it dense, which can enhance the barrier capacity against corrosive media. The variation of porosity and thickness of coatings is related to the concentration of added HA particles. Zheng et al. [89] found that compared with PEO coating without HA, the surface micropores of PEO coating prepared by electrolyte containing 1 g/L HA particles were filled with HA particles, the number of micropores was significantly reduced, and the coating thickness was thinner, indicating a denser coating construction, and the highest coating corrosion resistance at this time. However, when the concentration of HA additives arrived 2 g/L, micropores' sealing effect decreased and the coating was looser, and at 3 g/L clusters of particles appeared on the coating surface, with the increasing of micropores, and the barrier capacity of coatings decreased. It was also found that the opposite conclusion was obtained at high HA concentrations. Yang et al. [90] demonstrated that the increase in HA concentration helped to make the coating surface dense while filling the surface pores, thus enhancing the corrosion resistance of coating. The addition of 5 g/L HA particles resulted in a small improvement for a porous surface in comparison to the PEO coating alone, and while the concentration was raised to 10 g/L, the

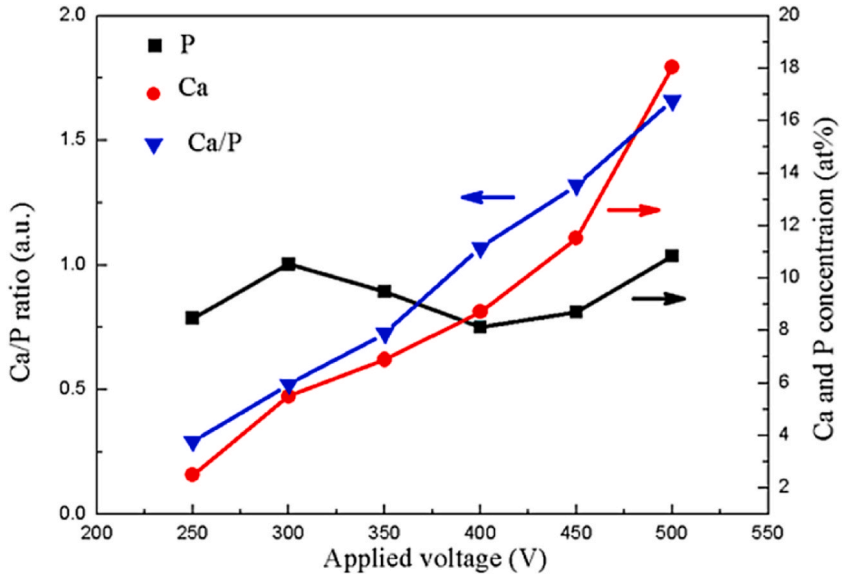

Fig. 8. Adjust the applied voltage to control the Ca and P content and Ca/P ratio of PEO coating [88].

porosity decreased sharply, and the number of micropores decreased further at 20 g/L, probably because the HA particles improved the spark discharge behavior during PEO. What is noteworthy is that the number of micropores is inversely proportional to its size, with smaller sizes having more pores. The effect of different concentrations (5, 10, and 15 g/L) of HA nanoparticles (HA NPs) on PEO coating properties was investigated by Chaharmahali et al. [26]. It was also found that the porosity decreased with the increasing concentration of HA NPs, while the thickness increased, as shown in Fig. 9(a–f). This may be since the capacitive voltage of the sample was also higher at higher concentrations, and the discharge generated more energy, which facilitated the continuation of the reaction and the formation of a thicker coating. Meanwhile, the electrochemical test results display the lowest corrosion current density and the highest corrosion resistance with the concentration of HA NPs set to 15 g/L.

Wang et al. [87] developed a HA/PEO coating by depositing HA on PEO coating through EPD. The samples immersed in SBF for different times were analyzed by EIS and their corrosion behavior was explained using a composite coating degradation model. As shown in Fig. 10(a–c), with the immersion time increased (5, 15, 20 days), in the first stage, the HA coating was exposed to SBF and decomposed, forming Ca–P compound deposits on the coating surface to prevent the invasion of corrosive media to Mg alloys. Then, as the immersion time increased, SBF penetrated deeply into the HA layer through microcracks, and the rate of HA layer degradation accelerated and microcracks expanded. In the third stage, the HA layer continuously degraded, the surface became too loose and porous to block the SBF, and the corrosion solution further extended to the internal PEO layer and even reached the substrate.

Ca–P coating can notably improve the bioactivity and biocompatibility of Mg alloys with PEO coating, while there are fewer relevant *in vivo* studies, so we mainly focus on what effects it can bring on osteogenic activity and cell behavior (cell adhesion, spreading, proliferation, and differentiation behavior).

Dou et al. [77] found that after 21 days of SBF immersion experiments, micropores on the surface were observed to be filled with spherical or striated apatite prepared through PEO, indicating that the Ca–P coating had excellent bioactivity. Attarzadeh et al. [93] performed elemental analysis of TCP/PEO coating surface precipitation by EDS after 7 days of SBF immersion experiment and found that higher concentrations detected higher Ca/P ratios on the exterior of the coating, implying that more apatite compounds formed, representing a possible superior osseointegration ability. Tang et al. [28] combined the sol-gel method with PEO to prepare a HA/PEO composite coating. 72 h SBF immersion experiments showed that more apatite precipitation could be observed on the outside of the composite coating in comparison to PEO coating with bare Mg alloys.

Combining PEO with the sol-gel method, Liu et al. [98] prepared calcium metaphosphate (CMP)/PEO composite coating on AZ31B. Through detecting the number of cells at different cell adhesion stages, it was found that the CMP/PEO composite coating accelerated the cell adhesion rate of human bone marrow-derived mesenchymal stem cells (hBMSCs) compared to bare Magnesium alloys. As shown in Fig. 11(a–d), analysis of the results of vinculin and F-actin staining revealed that more extensive stress fibers with a larger cell spreading area were observed on the CMP/PEO composite coating. Ki-67 (cell proliferation-associated protein) analysis was consistent with the results of the cell counting kit-8 assay, which revealed that the CMP/PEO composite coating effectively improved the cell proliferation capacity of Mg alloys. In addition, the expression levels of osteogenesis-related genes (alkaline phosphatase (ALP), type I

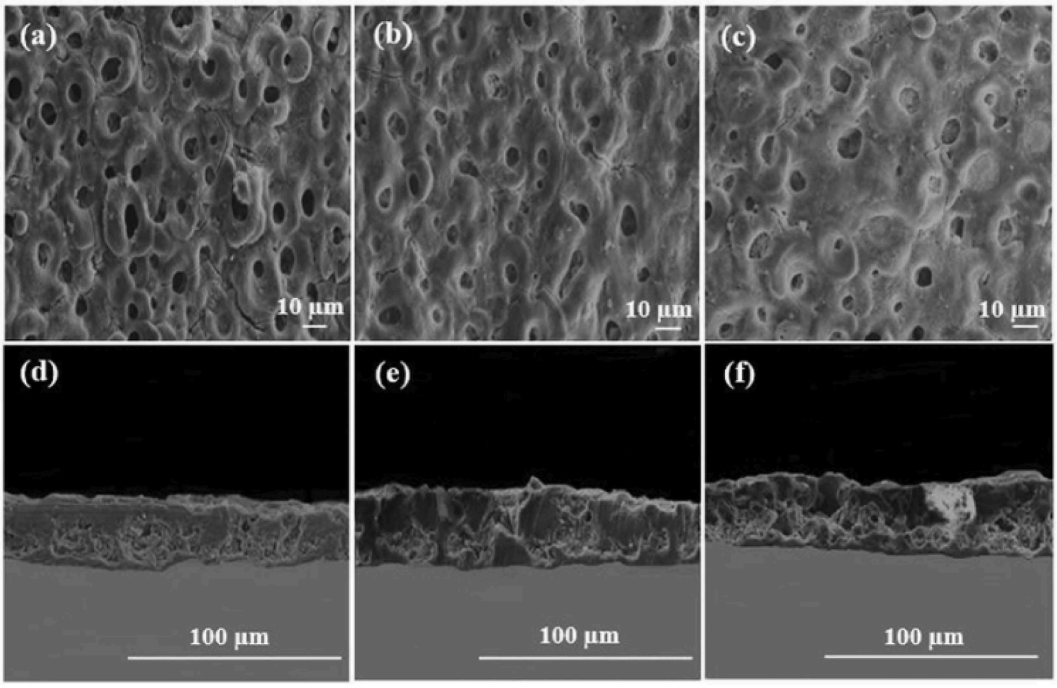

Fig. 9. SEM images of the surface (a–c) and cross-section (d–f) of samples with different concentrations of HA added. (a, d) 5 g/L HA, (b, e) 10 g/L HA, (c, f) 15 g/L HA [26].

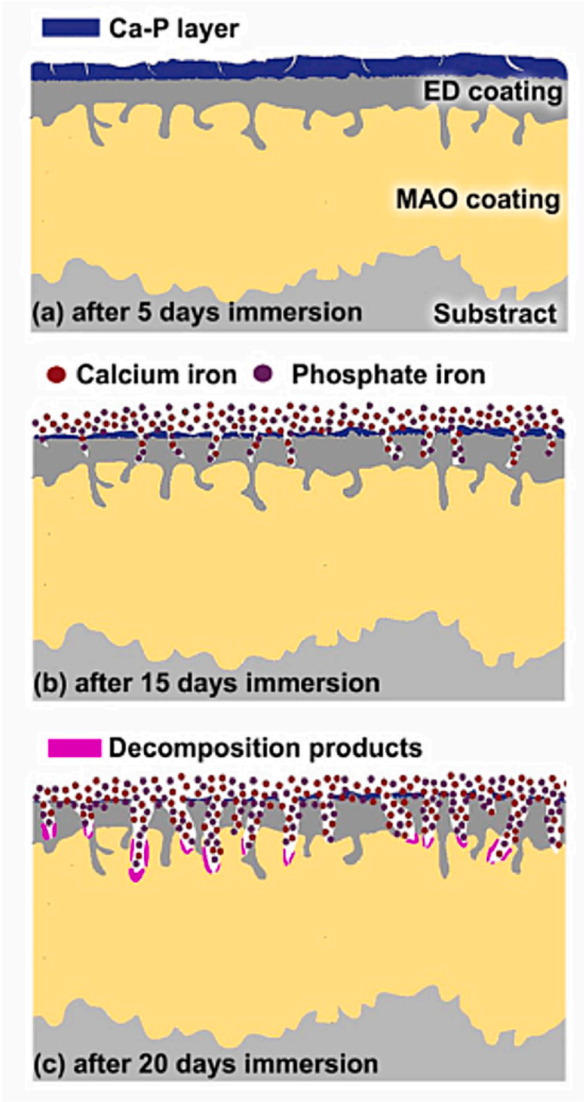

Fig. 10. Degradation model of PEO-EPD samples in SBF at various stages. (a) Ca–P compound deposition, (b) HA layer crack extension, (c) internal PEO layer corrosion [87].

collagen (COL1), and runt-related transcription factor 2 (RUNX2)) were significantly increased in the CMP/PEO composite-coated samples, demonstrating superior osteogenic ability. Yu et al. [94] developed fluoride-doped hydroxyapatite (FHAp)/PEO composite coating on AZ31B Mg alloys by combining PEO with the hydrothermal method. As shown in Fig. 12(a–d), more mouse caldaria bone cells (MC3T3-E1) pseudopod extensions could be observed on the FHAp/PEO coating compared with the undoped Ca–P/PEO coating and the uncoated sample, indicating that the fluoride ions promoted the adhesion and diffusion of osteoblasts. Meanwhile, the results of MTT experiments showed that the number of cells exposed to the FHAp/PEO coating was significantly higher than Ca–P/PEO coating, showing a stronger proliferation ability. In addition, higher activity of ALP was detected in FHAp/PEO-coated samples, suggesting that the coating also facilitates osteoblast differentiation. However, it has also been found that the morphology of Ca–P particles affects cellular behavior [96]. When platelet-like Ca–P particles accumulate, forming ridges, the cells are hindered from spreading on their surface. Therefore, more extensive cell adhesion was observed on the PEO-coated surface comparison to the Ca–P/PEO coating.

By adding in the electrolyte $Ca_3(PO_4)_2$ and $C_{10}H_{16}N_2O_8$ (ethylenediaminetetraacetic, EDTA), Jian et al. [105] prepared the PEO coatings containing Ca–P in the magnesium alloy surface, with no cytotoxicity in cytotoxicity test. 3 weeks after planting Ca–P/PEO-coated magnesium alloy screws into the femur of rabbits, bone healing around the screws occurred, the screws were firmly integrated with the bone, and no gas was observed, indicating that rapid degradation of the samples did not occur. 12 weeks after surgery, different from the bare magnesium alloy screws and the PEO-coated screws without Ca–P, some new bone appeared around Ca–P/PEO-coated screws, showing better bone tissue healing ability. Ca–P coating can also give suitable mechanical properties to

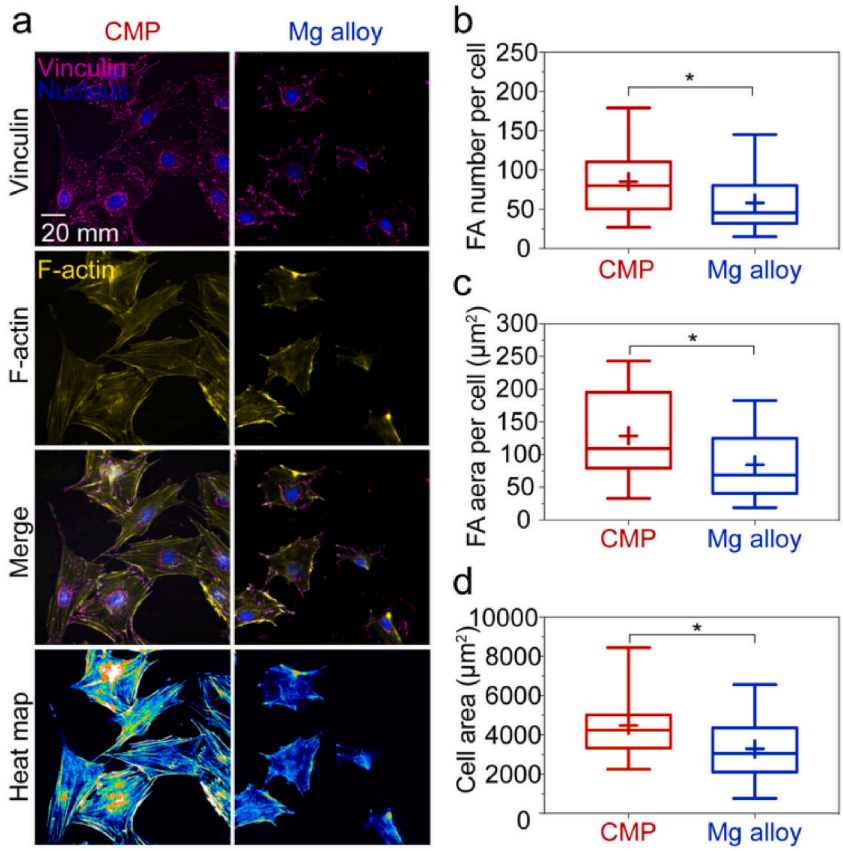

Fig. 11. Qualitative analysis: (a) Fluorescence images of vinculin (purple), nucleus (blue) and F-actin (yellow) of hBMSCs on CMP/PEO-coated Mg alloys and bare Mg alloy. Quantitative analysis: (b) focal adhesion (FA) number per cell, (c) FA area per cell, (d) cell area [98]. (For interpretation of the references to colour in this figure legend, the reader is referred to the Web version of this article.)

PEO-coated Mg alloys, which has an expansive range of applications in the biomedical field. Jin et al. [27] prepared Ca–P/PEO composite coating on AZ91D Mg alloys through ECD together with PEO. After soaked in SBF for 5 days and tested for mechanical properties, it was found that the fatigue life of Ca–P/PEO composite coated samples after soaking was much higher than that of single coating samples after soaking, and bare samples before soaking. Rúa et al. [91] found that Ca–P-coated AZ31 porous Mg alloys samples prepared by PEO, specimens before and after coating exhibited close compressive strength and Young's modulus, so they can meet bone tissue needs.

5.2. *Layered double hydroxide-PEO coating*

Layered double hydroxide (LDH) is a layered sandwich-like structural material, as shown in Fig. 13, consisting of positively charged double metal hydroxide main laminate and interlayer of anions and water molecules overlapped, with the chemical formula $[M^{2+}_{1-x}M^{3+}_{x}(OH)_2]^{x+}$ $[A^{y-}]_{x/y}\cdot nH_2O$, where M^{2+} represents divalent metal cation while M^{3+} is the trivalent metal cation, and A^{y-} represents the anion [29].

As shown in Fig. 14(c and d), the small size of LDH can be uniformly formed on the PEO porous layer, which can effectively cover the gaps and cracks of the original coating and increase its corrosion resistance compared to the single MAO coating as shown in Fig. 14 (a and b). At the same time, LDH has anion exchange property, and the loaded anions (mainly nitrate) can exchange with Cl^- in the corrosive environment to reduce the concentration of Cl^- in the solution and prevent the Cl^- from entering the alloy substrate and causing damage [30]. In addition, LDH as a nanostructured material allows cells to be immobilized on the LDH surface, significantly improving osseointegration and osteoblast adhesion, making it suitable for implant applications. The preparation methods and properties of commonly used LDH coatings are shown in Table 3.

Peng et al. [106] used HT to prepare Mg–Al-LDH coatings, i.e., a container containing 0.02 M aluminum nitrate for 12 h at 120 °C, whose pH is adjusted by NaOH to 12.8. On PEO-coated surfaces, a uniform dense nanoflake-like structure was created (Fig. 15(b)), which successfully closed the defects of the PEO coating (Fig. 15(a)). The coating is two-layered, with the outer layer being Mg–Al LDH (~2 μm) and the inner layer being PEO coating (~5 μm). Electrochemical and hydrogen evolution tests manifested that the PEO/LDH composite coating has better corrosion resistance than the PEO coating. The cell adhesion and cytotoxicity tests of rat bone marrow

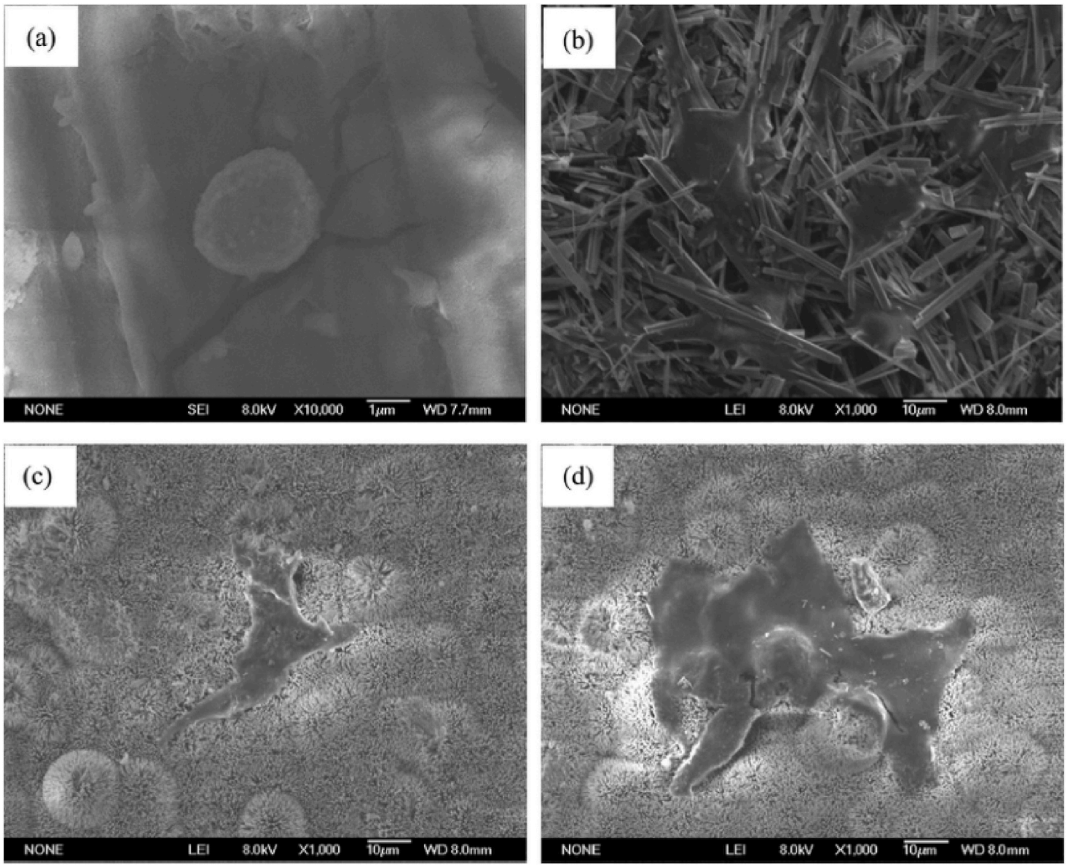

Fig. 12. SEM images of MC3T3-E1 on the surface of (a) uncoated, (b) Ca–P coated, and (c, d) FHAp/PEO-coated samples [94].

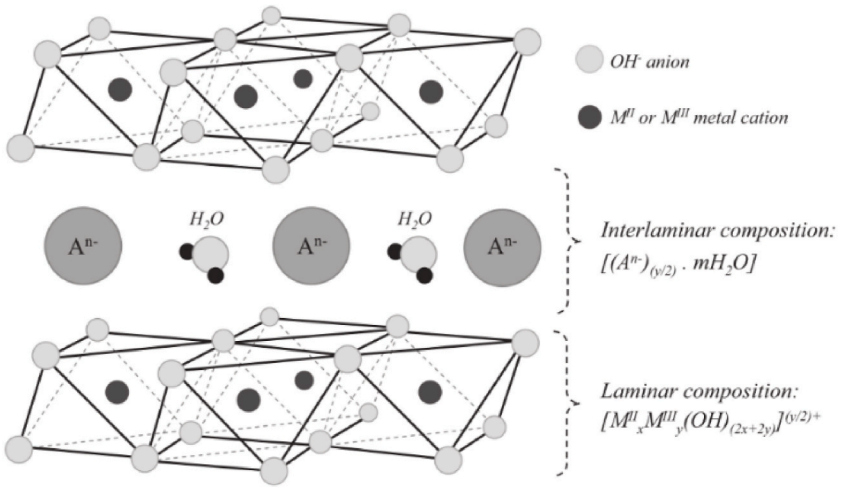

Fig. 13. Schematic diagram of LDH structure. The main hydroxide laminate consists of an oxygen octahedron composed of divalent and trivalent metal ions and OH^-, and between the laminates are anions and bound water [29].

stem cells (rBMSCs) showed that the PEO/LDH coating significantly improved the cytocompatibility of the substrate. When the incubation time was increased to four days, the cell viability of PEO/LDH extract increased to more than 80 %, indicating mild cytotoxicity. In contrast, cells in PEO extracts were completely dead. In addition, the unique anion exchange ability of LDH conferred good drug release from the PEO/LDH composite coating. The interlayer anions (mostly hydroxyl, nitrate, and carbonate) were replaced by 5-Fluorouracil (5-FU) via ion exchange when the Mg–Al-LDH coated samples were immersed in 5-F solution.

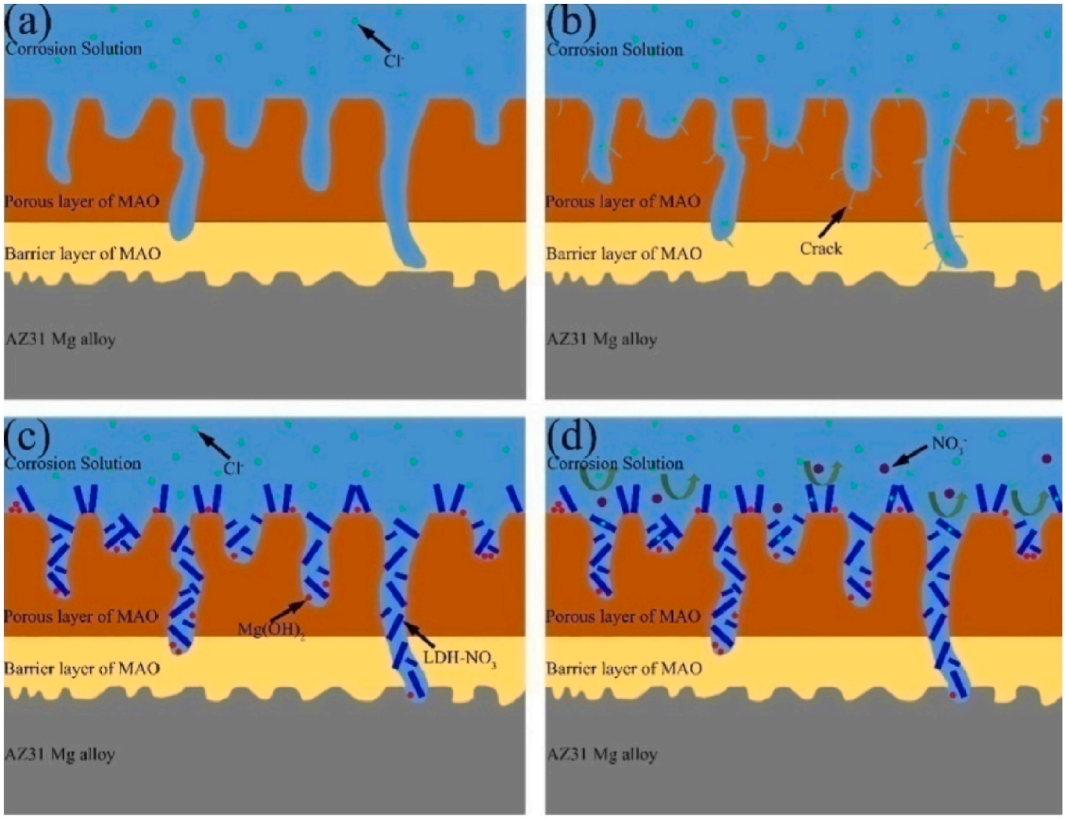

Fig. 14. Schematic diagram of the corrosion process of different coatings. (a, b) MAO coating, (c, d) MAO/LDH composite coating [30].

However, for the preparation of Mg–Al-LDH coatings, too high temperatures can lead to an inability to balance between the rate of dissolution of PEO coatings and the rate of growth of LDH coatings. Therefore, Li et al. [31] prepared coatings at low temperature (60 °C) to retard the dissolution rate of PEO coatings. For the PEO-LDH coating, the corrosion current density was lowered by two orders of magnitude when compared with the PEO coating alone, according to electrochemical studies. In addition, Wang et al. [107] confirmed that the thickness of the LDH coating linked positively with time. The inner layer (PEO layer) and outer layer (LDH layer) thicknesses of the coating treated with 2 h LDH were 4.45 ± 0.55 μm and 2.32 ± 0.08 μm, respectively, while the thicknesses of the outer and inner layers of the coating treated with 12 h LDH were 2.93 ± 0.13 μm and 3.47 ± 0.07 μm, respectively. Therefore, with the increase of HT time, the PEO layer was dissolved and gradually became thinner, while the LDH layer grew on the PEO layer and gradually became thicker. The PEO-coated Mg alloys after 12h HT demonstrated a milder inflammatory response and an increase in bone mineral density (BMD), trabecular thickness (Tb.Th) in the rat femur implantation experiment.

Peng et al. [108] prepared PEO/Mg–Al–Zn-LDH coatings by HT. Electrochemical and hydrogen evolution experiments confirmed that the inclusion of Zn^{2+} improved the corrosion resistance compared to the PEO/Mg–Al-LDH composite coating. Furthermore, due to the release of Zn^{2+}, the composite coating displays a powerful antibacterial capability against Gram-positive *S. aureus*. With the synergistic effect of Zn^{2+} and Mg^{2+}, cells displayed higher ALP activity and osteopenia (OPN) expression on the composite coating, and the coating had osteogenic differentiation ability, which facilitated its application in implants.

Al has been associated with neurotoxicity and Alzheimer's disease, so its use in biomedical applications may not be safe [109]. While Fe, as one of the essential trace elements, plays an important biological function *in vivo*, Zhang et al. [110] successfully prepared PEO/Mg–Fe-LDH coatings on Mg alloys using a two-step method of immersion and HT. In addition, the prepared coatings showed a significant reduction in the number of colonies after near-infrared light (NIR) (808 nm) irradiation, demonstrating the good photothermal antibacterial activity of the PEO/Mg–Fe-LDH coatings. Another study by Zhang et al. [111] similarly confirmed that PEO/Mg–Fe-LDH coatings are highly corrosion resistant and biocompatible. In addition, LDH coatings include PEO/Mg–Ni-LDH coatings, and Chen et al. [112] compared PEO/Mg–Zn-LDH, PEO/Mg–Al-LDH, and PEO/Mg–Ni-LDH coatings in their experiments. Since Al^{3+} are acidic under experimental conditions, they will react with MgO to destroy the original PEO coating. It is difficult for Zn and Mg to form trivalent cations, so only a small amount of Al elements contained in Mg alloys can form LDH with Zn through the discharge channel, resulting in Zn^{2+} can only locally produce LDH coating. Electrochemistry confirmed that, compared to PEO/Mg–Zn-LDH and PEO/Mg–Al-LDH coating, the corrosion current density of PEO/Mg–Ni-LDH coating was markedly decreased. Wang et al. [113] prepared PEO/Mg–Al–Co-LDH coating by in situ growth method. The electrochemical and immersion experimental results indicated that the coating outperforms pure PEO coating and untreated Mg alloys in corrosion resistance. Although excessive

Table 3
Preparation methods and performance of PEO-LDH coatings on Mg alloys substrates.

Mg substrate	Solution	Condition	Synthesis approach	LDH	Thickness (μm)		Electrochemical corrosion test						Cytocompatibility and Osteogenic activity			Ref
							E_{corr} (V)			I_{corr} (A/cm-2)			Cell types	Cell Viability		Relative ALP activity	
					PEO	PEO/LDH (PEO layer, LDH layer)	substrate	PEO	PEO/LDH	substrate	PEO	PEO/LDH		PEO	PEO/LDH		
AZ31	0.02 M aluminum nitrate (pH = 12.8)	120 °C, 12 h	hydro-thermal treatment	Mg–Al	6.5	7 (5, 2)	−1.45	−1.22	−1.2	1.66×10^{-5}	0.945×10^{-5}	3.92×10^{-6}	rat bone marrow stem cells (rBMSCs)	PEO/LDH > PEO		/	[106]
AZ31	Zn-1: 0.02 M $Al(NO_3)_3$, $Zn(NO_3)_2$ (10 μM Zn^{2+}) (pH = 12.8)	120 °C, 12 h	hydro-thermal treatment	Mg–Zn–Al	/	/	−1.61	/	−0.6	2.76×10^{-5}	/	1.56×10^{-5}	rBMSCs	Zn-2 > Zn-1, Mg–Al LDH > Zn-3 (3 days); Zn-2 showed a poor long-term cytocompatibility while Mg–Al LDH and Zn-1 showed high cell viability (14 days)		Zn-1 > Mg–Al LDH > Zn-2 (14 days)	[108]
	Zn-2: 0.02 M $Al(NO_3)_3$, $Zn(NO_3)_2$ (100 μM Zn^{2+}) (pH = 12.8)								−0.7			1.28×10^{-5}					
	Zn-3: 0.02 M $Al(NO_3)_3$, $Zn(NO_3)_2$ (1000 μM Zn^{2+}) (pH = 12.8)								−0.68			8.59×10^{-5}					
	0.02 M $Al(NO_3)_3$ (pH = 12.8)			Mg–Al					−1.33			2.37×10^{-5}					
Pure Mg (>99.95 wt%)	0.02 mol/L $Al(NO_3)_3$ (pH = 12.8)	120 °C, 2h	hydro-thermal treatment	Mg–Al	5.12 ± 0.37	4.45 ± 0.55, 2.32 ± 0.08	/						rBMSCs	completely died (<15 %) at all periods	> 60 %	PEO/LDH-12h > PEO/LDH-2h > PEO	[107]
		120 °C, 12h				2.93 ± 0.13, 3.47 ± 0.07									> 90 %		
AZ31	0.05 mol/L Al $(NO_3)_3 \cdot 9H_2O$ (pH = 10.5)	125 °C, 24 h	hydro-thermal treatment	Mg–Al	8.62		−1.58	−1.47	−1.34	1.20×10^{-5}	4.31×10^{-9}	1.78×10^{-10}	/				[116]
AZ31	40 g/L NaOH, 50 g/L EDTA-2Na and 5 g/L pure Al wire (PH = 13.76)	60 °C, 48 h	hydro-thermal treatment	Mg–Al	5.60 ± 0.43	7.83 ± 0.47 (4.00 ± 1.08, 3.83 ± 0.62)	−1.43	−1.47	−1.49	1.28×10^{-5}	3.94×10^{-7}	6.81×10^{-9}	Mouse calvaria bone cells (MC3T3-E1) pre-osteoblasts	PEO-LDH (> 90 %) > PEO		/	[31]
AZ31	$Al(NO_3)_3 \cdot 9H_2O$ (0.01 mol), NH_4NO_3 (0.06 mol)	95 °C, 1h	hydro-thermal treatment	Mg–Al	16.7		Zn-LDH coating > Ni-LDH coating > Al-LDH coating			Al-LDH coating > Ni-LDH coating > Zn-LDH coating			/				[112]
	$Ni(NO_3)_2 \cdot H2O$ (0.001 mol), NH_4NO_3 (0.006 mol)			Ni-LDH	16.8												

(*continued on next page*)

Table 3 (*continued*)

Mg substrate	Solution	Condition	Synthesis approach	LDH	Thickness (μm)		Electrochemical corrosion test						Cytocompatibility and Osteogenic activity				Ref
							E_{corr} (V)			I_{corr} (A/cm-2)			Cell types	Cell Viability		Relative ALP activity	
					PEO	PEO/LDH (PEO layer, LDH layer)	substrate	PEO	PEO/LDH	substrate	PEO	PEO/LDH		PEO	PEO/LDH		
	$Zn(NO_3)_2{\cdot}H_2O$ (0.01 mol), NH_4NO_3 (0.06 mol)			Zn-LDH	17.5												
AZ31	12 g/L of $MnCl_2{\cdot}4H_2O$ for 9 h and then in 2 g/L of $FeCl_2{\cdot}4H_2O$ for 4 h		immersion process	Mn–Fe	/	/	/	−1.57	~-1.4	PEO > PEO/Mn–Fe-LDH			C3H10T1/2	PEO/Mn–Fe-LDH > PEO		PEO/Mn–Fe-LDH > PEO	[235]
AZ31	4 g/L $FeCl_2{\cdot}4H_2O$ solution for 1.5 h at room temperature, then in pure water at 120 °C for 10 h		two-step method (immersion and hydrothermal treatment)	Mg–Fe	3.8 ± 0.1	5.8 ± 0.2	/			PEO > PEO/MgFe-LDH			MC3T3-E1	PEO > PEO/MgFe-LDH (4 days,7 days)		/	[111]
AZ31	2 g/L $FeCl_2{\cdot}4H_2O$ solution for 0.5 h (Fe-1)/1h (Fe-2) at room temperature, then in pure water at 120 °C for 6h	Fe-1	two-step method (immersion and hydrothermal treatment)	Mg–Fe	4	/	/	~-1.5	~-1.7	/	8.63×10^{-7}	2.13×10^{-8}	MC3T3-E1	Fe-2 > Fe-1 > PEO (7, 14 days)		Fe-2 > Fe-1 > PEO (7 days)	[110]
		Fe-2							~-1.79			2.17×10^{-8}					
AZ31	0.05 mol/L $Al(NO_3)_3$, 0.02 mol/L $Co(NO_3)_2$ (PH = 10.5)	398 K, 24 h	hydro-thermal treatment	Mg–Al–Co	~8	10	−1.58	−1.47	−1.39	1.2×10^{-5}	4.32×10^{-8}	4.23×10^{-10}	/				[113]

amounts of Ni and Co can be harmful to the human body, they can still be applied to the human body by controlling them to trace concentrations [114,115].

Although the PEO/LDH system shows excellent performance, it still has a porous structure and there is still a possibility of corrosion media penetrating between the substrate and the coating. Therefore, Wang et al. [116] successfully constructed a superhydrophobic surface with good sealing effect by surface modification of Mg–Al-LDH/PEO coatings with stearic acid (SA). Electrochemical and immersion experiments showed that corrosion resistance of different coatings was in the following order: SA-PEO/LDH-24h > PEO/LDH-24h/PEO > PEO coating.

5.3. ZrO_2 incorporated-PEO coating

ZrO_2 itself is chemically stable and has a high melting and boiling point. In addition, the excellent properties of ZrO_2 include good corrosion resistance, mechanical properties, (e.g., high resistance to cracking, high hardness), and biocompatibility, which are the main reasons for its widespread use in medical applications. The good biocompatibility of ZrO_2 is reflected in its antibacterial and antioxidant properties. Moreover, ZrO_2 is not carcinogenic *in vitro* and does not cause chromosomal aberrations in cells [117,118]. In the choice of medical ceramic materials, ZrO_2 is also considered to be a suitable biomaterial for bone tissue regeneration due to its inherently stable chemical properties and better biocompatibility. This has led to ZrO_2 being used in many medical applications, such as bone implants [119,120], dentistry [121,122], and others.

ZrO_2 incorporated-PEO coating can be obtained by PEO treatment in electrolytes containing ZrO_2 nanoparticles or in electrolytes containing zirconium elements (e.g. , K_2ZrF_6, $Zr(NO_3)_4$, $ZrOCl_2$ etc. [32,123–127], of which K_2ZrF_6 is more commonly used).

Electrolytes containing Zr element are involved in the electrochemical reaction during PEO treatment and then ZrO_2 is incorporated into the coating mainly in the form of tetragonal (t-ZrO_2) structure. Liu et al. [125] found that the sparking phenomenon promoted the deposition of ZrO_2 on the surface and then ZrO_2 starts to deposit on the substrate when voltage potential exceeded sparking voltage. Finally, the distribution of Zr elements in PEO coatings formed in the electrolyte containing fluoro zirconates was inhomogeneous [124].

ZrO_2 nanoparticles cannot be dissolved in the electrolyte and thus the incorporation of them into the coating does not relate to the

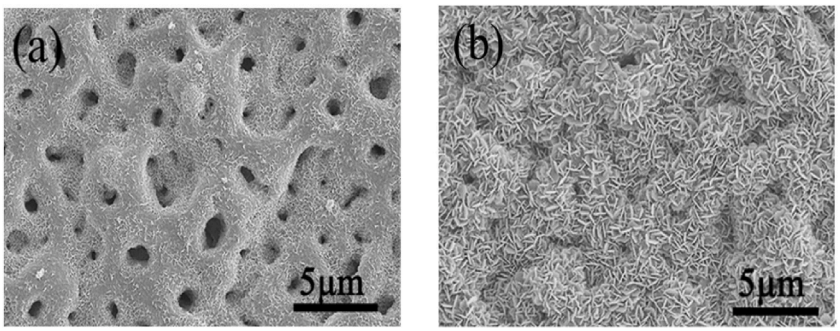

Fig. 15. Surface morphology of (a) PEO, (b) PEO/LDH [106].

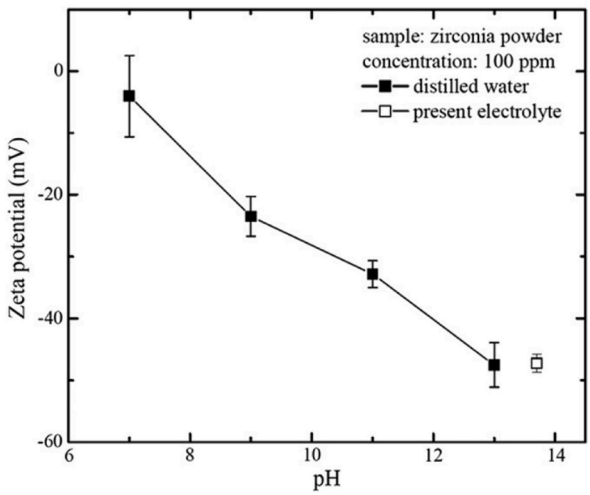

Fig. 16. The potential change of ZrO_2 nanoparticles at different pH (trace measurements during the PEO process) [133].

electrochemical reaction. However, the electrophoretic effect may be the reason for allowing ZrO_2 nanoparticles to move close to the substrate. Fig. 16 shows the variation of the zeta potential of ZrO_2 nanoparticles as pH rises. As the pH gradually increased with the PEO process, the zeta potential of ZrO_2 nanoparticles decreased sharply, and this kind of high negative potential promotes ZrO_2 nanoparticles to be adsorped by the substrate which served as anode. The mechanism of substrate adsorption of ZrO_2 nanoparticles is shown in Fig. 17. R. Arrabal et al. [128] used a tracer method in his study to explain that ZrO_2 nanoparticles were preferentially bound on the outside of the coating. Then they were subsequently delivered to the inner coating region through cracks and pores. Razieh et al. [33] proposed that after the oxidation process started, firstly, some ZrO_2 nanoparticles would be trapped in a protective film that rapidly formed on the substrate in an alkaline solution environment.

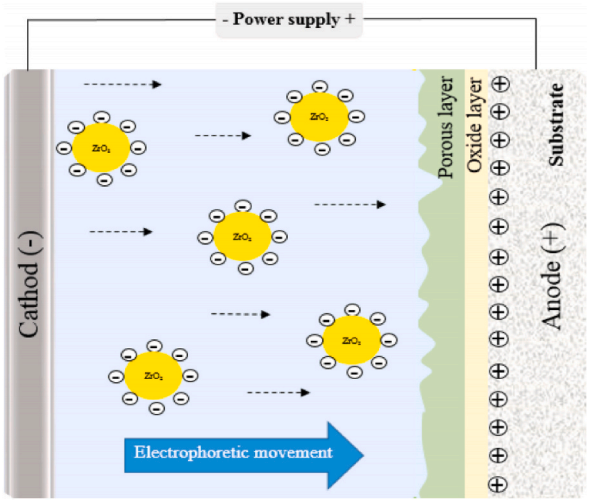

Fig. 17. ZrO_2 nanoparticles are continuously adsorbed during PEO [33].

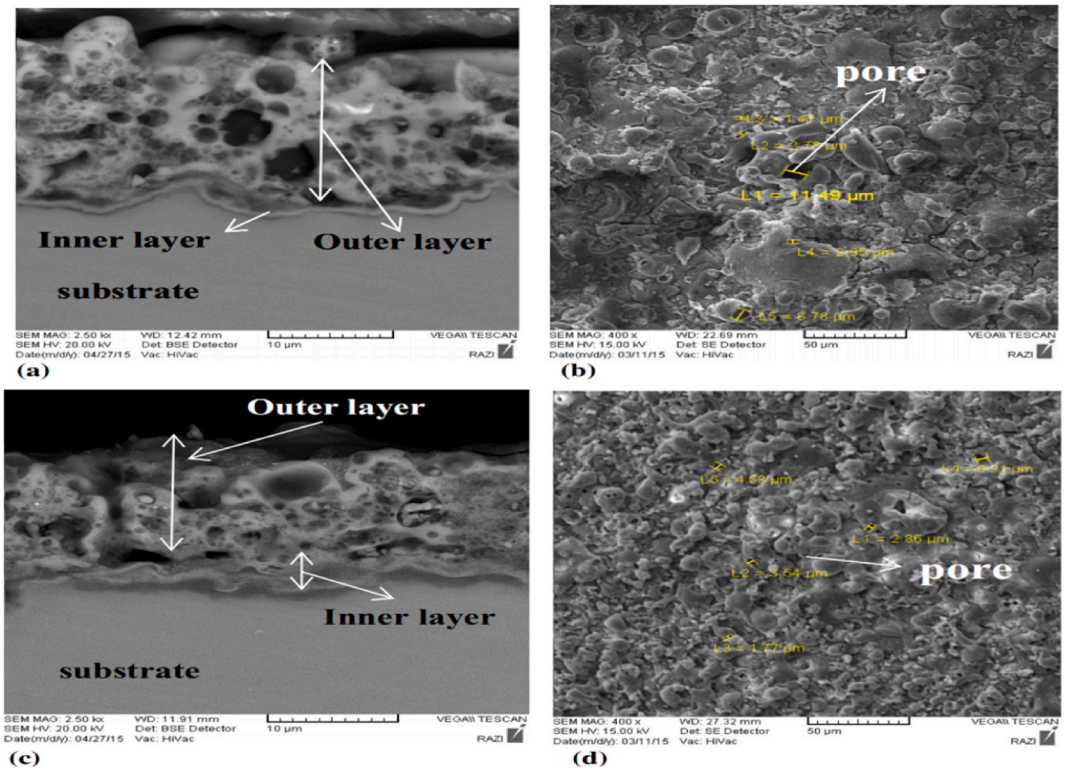

Fig. 18. Scanning electron micrographs of the surface and cross-section of the coating. (a, b) Treatment in a ZrO_2-free electrolyte. (c, d) Treatment in an electrolyte with 9 g/L ZrO_2 nanoparticles [130].

After breakdown occurs, because of contacting with the solution, the molten oxide solidifies rapidly, ZrO_2 NPs incorporating into the oxide film [129]. Subsequently, fluctuations in the molten oxide may also lead to admixture of nanoparticles in small quantity in the solution near the discharge site. ZrO_2 transport paths may be the defects inherent to the coating. Nasrollah et al. [130] and D.V. et al. found that [131] nanoparticles were in the outer layer instead of the inner layer, which was different from the presence of ZrO_2 nanoparticles in both the whole layers as stated in the above mechanism. This probably due to the different parameters when performing PEO, such as current density, etc. Song et al. [132] found that for PEO coatings containing ZrO_2 on AZ31, as the current density increased, the size of pores and coating thickness of the surface increased, while the number of pores decreased. There is uncertainty as to diffusion of coating composition, migration of coating composition along cracks and pores, and formation of new phases occurring at locally high temperatures.

ZrO_2 has three different crystalline forms. The stable low-temperature phase is monoclinic. The tetragonal phase gradually forms above 1000°. Above 2370°, it transforms into the cubic crystalline phase. Before and after the incorporation of ZrO_2 nanoparticles into the coating, sufficient heating at high local current density transforms the monoclinic ZrO_2 into tetragonal structure [133], which may serve as a marker of temperature change during PEO. However, ZrO_2 does not decompose or melt during PEO and undergoes only

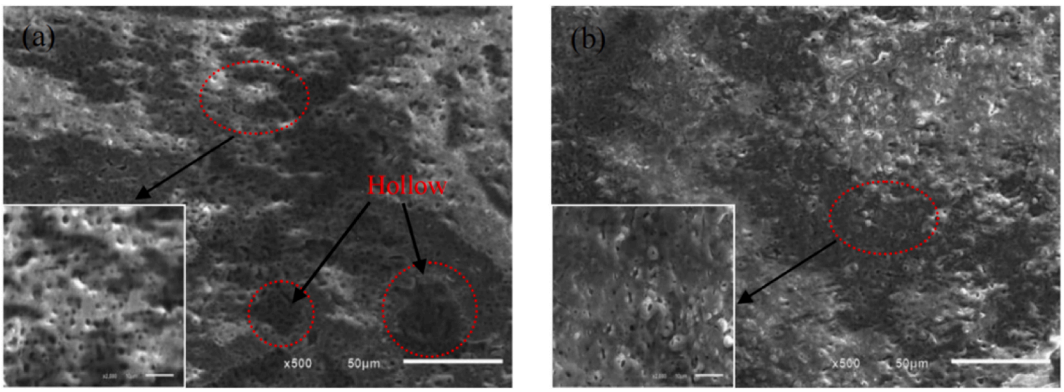

Fig. 19. Surface morphology of PEO coatings formed in electrolytes with (a) 0, (b) 2.5 g/L K_2ZrF_6 [123].

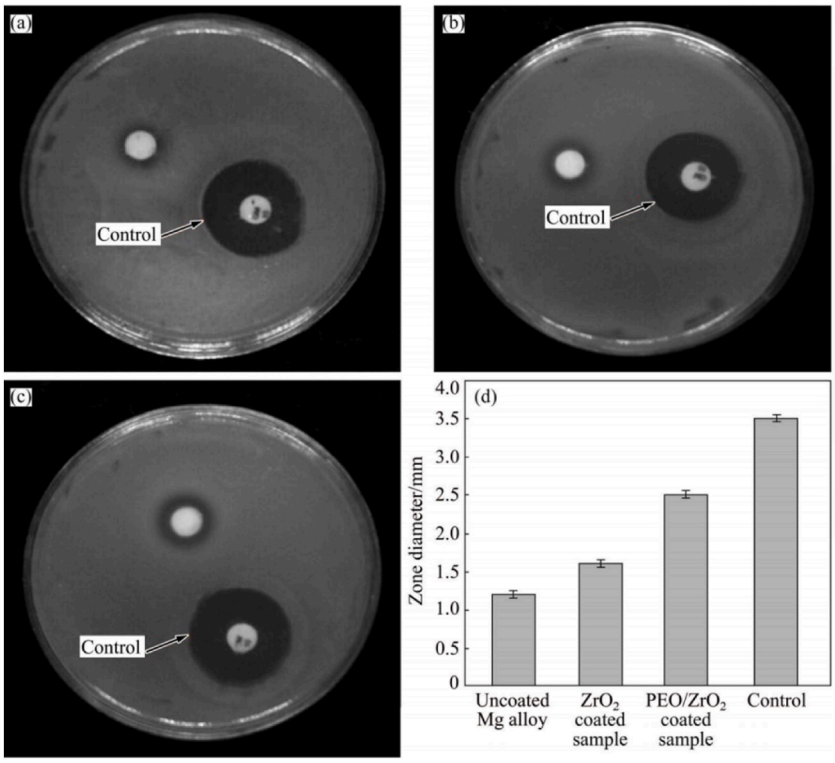

Fig. 20. Inhibition zones of (a) Mg alloy substrate, (b) ZrO_2 nanos free-PEO coating, (c) ZrO_2 nanos incorporated-PEO coating. (d) The diameter of growth inhibition zones against E. coli bacteria after 24 h of the three samples [35].

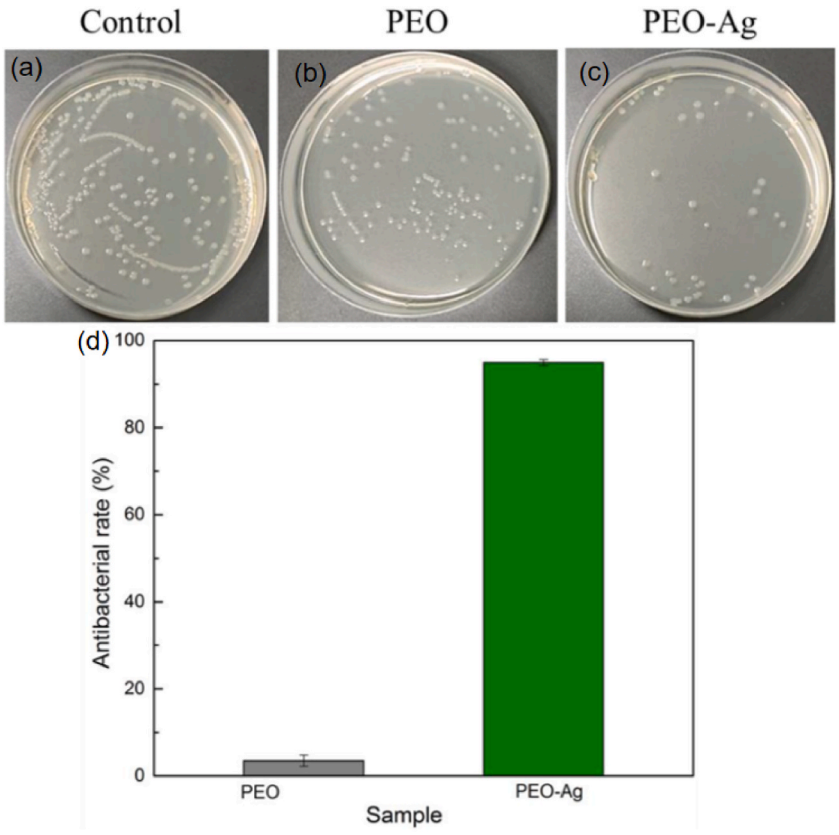

Fig. 21. Colony and antimicrobial rates of (a) control group, E. coli on (b) PEO-coated and (c) PEO-Ag-coated samples [158].

phase changes during PEO. Its chemical and physical properties are mostly unchanged, but the local high temperatures that result from different working parameters may cause some of the ZrO_2 nanoparticles to generate the $Mg_2Zr_5O_{12}$ phase, which may have an effect on the thermomechanical properties of the coating [134].

PEO coatings containing ZrO_2 nanoparticles improves the original morphological characteristics. Typically, the surface is more uniformly dense and the thickness of the inner layer increases evidently. Meanwhile, the coating compactness is improved compared to the PEO coating alone [34,124,135]. According to SEM of the surfaces of PEO coatings without ZrO_2 nanoparticles (Fig. 18(a and b)) and coatings with ZrO_2 nanoparticles (Fig. 18(c and d)), the size of the surface pores decreased. The reduction of cracks on the surface

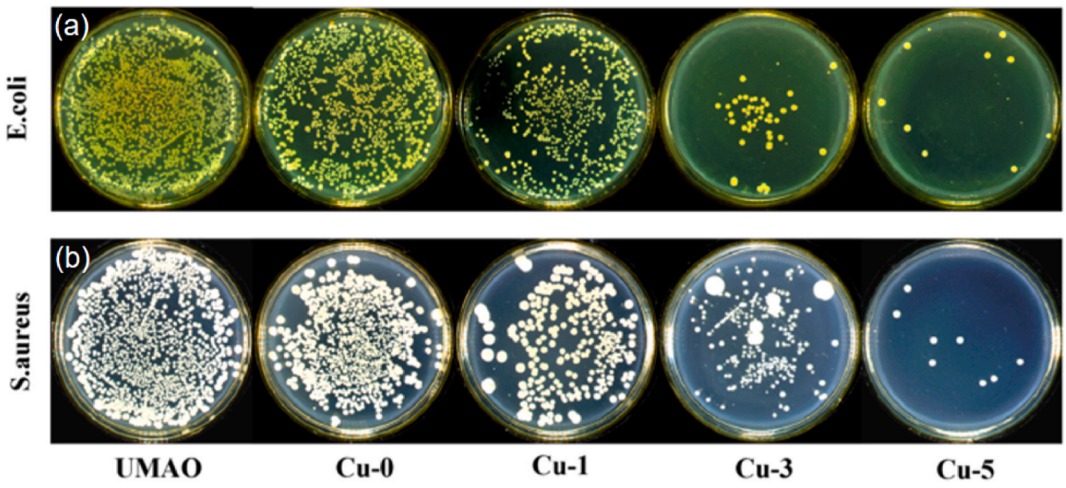

Fig. 22. Colony growth of (a) E. coli and (b) S. aureus in each group of media. (UMAO, Cu-0, Cu-1, Cu-3, and Cu-5, where 0, 1, 3, and 5 are Cu loading times (min)) [37].

was attributed to the great thermal stability of ZrO_2 itself, thus reducing the effect of thermal stress [136].

Compared to the method of incorporating ZrO_2 nanoparticles into the electrolyte, the surface of the coating forming in an electrolyte containing Zr element is not dense and present more defects, such as micropores and cracks. Zhuang et al. [123] treated AZ31 with PEO by adding K_2ZrF_6 to a phosphate-based electrolyte. Fig. 19 shows the surface morphology of the PEO coating formed without the addition of K_2ZrF_6 and formed under the addition of 2.5 g/L of K_2ZrF_6. It is clear that, in Fig. 19(a), the PEO coating is rough and has some cavities. After the addition of K_2ZrF_6, the roughness of the coating (Fig. 19(b)) is reduced and the coating is more compact. However, as the concentration of K_2ZrF_6 increases, the thickness of the coating firstly increases and then decreases.

Table 4
The antibacterial test and cytotoxicity assay of samples.

Coating Technology	Antibacterial agent		Antibacterial test		Cytotoxicity assay			Ref.
	Type	Concentration	Species	Antibacterial rate	Cell type	72h relative growth rate (RGR)	cell toxicity grade (CTG)	
PEO, self-assembly technique	Ag	0 g/L	*Staphylococcus aureus* (S. aureus)	67.24 % (24h)	/			[46]
		/		98.72 %				
PEO		0 % (wt.%)		/	/			[160]
		0.41 % (1 g/L, 400V)		74.13 % (24h)				
		1.07 % (1 g/L, 425V)		≈99.00 %				
		2.11 % (1 g/L, 450V)		≈99.00 %				
		0 g/L	Escherichia coli (E. coli)	3.52 % (6h)	Mouse caldaria bone cells (MC3T3-E1)	106.12 %	0 (no toxicity)	[158]
		1 g/L		94.90 %		90.04 %	1 (no toxicity)	
		0 g/L		11.74 % (24h)		30.80 %	3 (mild toxicity)	[159]
		1 g/L		3.98 %		95.50 %	1	
		2 g/L		90.89 %		98.20 %	1	
		3 g/L		91.11 %		93.80 %	1	
PEO	Cu	0.00 %	Porphyromonas gingivalis (P. gingivalis)	−52.00 % (72h)		85.61 %	1	[38]
		2.90 %		82.70 %		83.78 %	1	
		4.90 %		100.00 %		80.99 %	1	
UMAO, phytic acid conversion coating, electroless copper plating		0.00 %	E. coli	28.2 % (24h)		65.29 %	/	[37]
		0.18 % (1 min)		44.30 %		/		
		0.24 % (3 min)		94.60 %		44.96 %		
		0.69 % (5 min)		97.50 %		34.88 %		
		0.00 %	S. aureus	11.6 % (24h)		/		
		0.18 % (1 min)		56.00 %				
		0.24 % (3 min)		81.30 %				
		0.69 % (5 min)		97.50 %				
PEO		0.00 %		0.60 % (24h)		38.96 %	/	[36]
		0.15 % (0.1 g/L)		11.40 %		/		
		0.42 % (0.5 g/L)		48.50 %		61.99 %		
		0.58 % (1 g/L)		52.40 %		30.33 %		
		0.00 %		>99.00 % (24h)	Human osteosarcoma cells (MG63)	92.50 %	1	[39]
		0.44 % (1 g/L)		>99.00 %		98.75 %	1	
PEO	Zn	0.30 % (1 g/L)	S. aureus	28.5 % (6h)	/			[163]
		0.40 % (2 g/L)		29.30 %				
		0.70 % (3 g/L)		41.30 %				
		1.13 % (4 g/L)		45.50 %				
		0.30 % (1 g/L)	E. coli	21.10 %				
		0.40 % (2 g/L)		21.50 %				
		0.70 % (3 g/L)		22.40 %				
		1.13 % (4 g/L)		23.50 %				
PEO	TiO_2	0 g/L	S. aureus	61.48 %	/			[164]
		1 g/L		89.93 %				
		2 g/L		93.19 %				
		3 g/L		94.52 %				
		4 g/L		97.65 %				
PEO	TA	0 g/L	S. aureus	47.80 %	/			[165]
		2 g/L		92.29 %				
		0 g/L	E. coli	57.34 %				
		2 g/L		97.23 %				

Better wear resistance allows implants to produce less wear debris during and after implantation in the body, allowing them to last longer and reducing healthcare costs. Researchers' investigations into the wear behavior of coatings showed that coating's coefficient of friction could be reduced by adding nanoparticles [137]. S.V et al. [135] and DV et al. [131] studied the influence of ZrO_2 nanoparticles on the properties of coatings. The mechanical properties of the coatings were evaluated through microhardness measurement techniques. They found that coatings with nanoparticles were harder than those produced in the base solution and had a significantly higher increase in wear resistance by a factor of almost two. This was attributed to PEO coating adsorbing and trapping ZrO_2 nanoparticles in the pores, thus closing the exit of the pores and resulting in a lower porosity of the surface. The low porosity, high density, high surface hardness, high bond strength, low surface roughness, and lubricating effect of the nanoparticles resulted in a lower wear rate for this coating in comparison to the single PEO coating alone [138]. However, compared to the Nano-ZrO_2 incorporated-PEO coating, the PEO coating generated in the electrolyte containing Zr element has more surface defects and inconspicuous change in wear resistance.

For the corrosion resistance of ZrO_2/PEO-coated Mg alloys, PEO coatings with and without ZrO_2 NPs were developed and their corrosion resistance was evaluated. According to a study [130], the coatings containing ZrO_2 nanoparticles showed a greater reduction in corrosion current density and a greater polarization resistance of the coatings in comparison to the single PEO coating alone. J. Liang [126] et al. compared PEO coatings containing ZrO_2 nanoparticles with the single PEO coating and found that PEO coatings containing ZrO_2 nanoparticles provided effective corrosion protection. This is also consistent with the results of K.M. Lee's study [133]. The corrosion resistance of ZrO_2/PEO-coated Mg alloys formed in an electrolyte containing Zr element was similarly improved over the single PEO coating [123,127]. Zhuang et al. [123] showed that all coatings exhibit higher E_{corr} and lower I_{corr} than the AZ31 Mg alloys substrate. The PEO coatings formed in 2.5 g/L K_2ZrF_6-containing electrolyte show better resistance of corrosive media than the single PEO coatings and those generated in electrolytes with 5, 10 g/l K_2ZrF_6 added. ZrO_2 incorporated-PEO coatings show superior resistance of corrosion.

The coatings' improved resistance of corrosion jointly attribute to phase composition stability and microstructural integrity. This is because the presence of ZrO_2 on the coating results in a denser PEO layer and a series of enhanced surface characteristics: a reduction in the diameter of surface defects on the outer of the coating. In particular, the placement of nanoparticles within the pores of the coating forms a barrier against the passage of corrosion ions. This leads to a reduced distribution of corrosion ions into the substrate in the coating and this may explain for the enhanced barrier capacity against corrosive media of ZrO_2 incorporated-PEO coating compared to simple oxide coatings [130]. Therefore, the incorporation of ZrO_2 into PEO coatings is a suitable option to effectively prevent the invasion of corrosive media into the magnesium substrate in highly corrosive environments [127,133,139,140].

In terms of biocompatibility and bioactivity, ZrO_2 has comparable biocompatibility to titanium [141] and excellent osteogenic capacity. According to *in vivo* and *in vitro* experiments, the researchers found that ZrO_2 materials do not have cytotoxic effects on some cells, such as gingival fibroblasts [142], so ZrO_2-based materials can be used in dental implants [143]. In addition, using the disc diffusion technique, the researchers measured and compared the antibacterial properties of PEO-coated Mg alloys (with (Fig. 20(c)) and without (Fig. 20(b)) ZrO_2 nanoparticles) and bare Mg alloys against Gram-negative bacteria Escherichia coli (E. coli) (Fig. 20(a)). They found that ZrO_2 incorporated-PEO coating had a high antibacterial capacity against E. coli with an inhibition zone size of 2.5 mm. While the single PEO-coated Mg alloys and bare Mg alloys samples had inhibition zone sizes in the range of 1.6–1.2 mm, respectively (Fig. 20(d)). What's more, ZrO_2 is often used as a biomaterial that promotes bone tissue regeneration as a bioceramic material. Chen et al. [144] showed that ZrO_2 incorporated-PEO coating treated in electrolytes containing Zr element could induce the formation of hydroxyapatite after immersion in SBF, which further enhanced the osteogenic ability of the coatings. Besides, the mechanical properties of ZrO_2 may also be relevant for bone healing [145]. By culturing osteoblasts on ZrO_2 substrate, it was found that the newly formed osteoblasts had good adhesion and proliferation ability, and the cells also maintained the ability to differentiate into osteoblasts [146]. Scarano et al. [147] examined the bonding response of ZrO_2 implants implanted in rabbit tibiae after 1 month and the

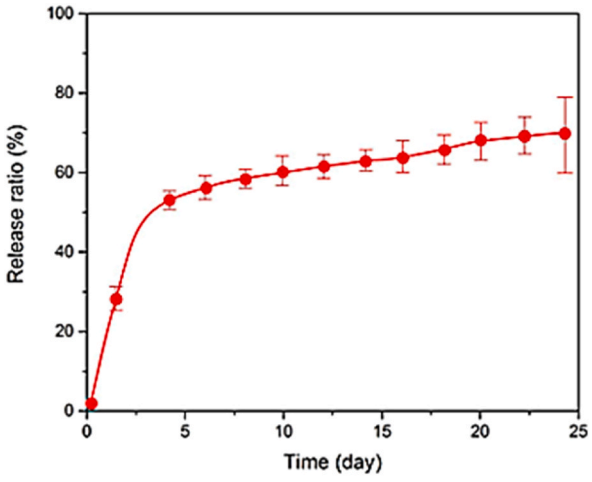

Fig. 23. The drug release rate of PEO/BSP composite coated samples for 24 days [42].

newly formed osteoblasts showed good activity. In addition to this, many other researchers have shown that ZrO_2 coatings, particularly monoclinic ZrO_2 coatings, support cell surface attachment and adhesion, thereby promoting cell proliferation enhancing the osseointegration of implants [141,148].

It is worth mentioning that the ZrO_2 nanoparticles that are used are not sintered. This is because during the sintering process, ZrO_2 nanoparticles undergo grain coarsening, and the enlarged grain size leads to a reduced driving force for the densification process and usually results in poor mechanical properties of the nanoparticles [149]. In addition to the enlarged grain size, the agglomeration of nanoparticles without the sintering process is reduced, which may affect the efficiency of nanoparticles in filling various defects in PEO coatings [150]. Also, ZrO_2 nanoparticles are inherently physicochemically stable and have lower radioactivity than human bone tissue, which leads to the fact that although ZrO_2 nanoparticles are not degradable *in vivo*, the un-sintered trace ZrO_2 nanoparticles of tiny size in ZrO_2 incorporated-PEO coating are non-toxic, non-hazardous and useable *in vivo*.

Although ZrO_2 alone shows excellent antimicrobial and osteogenic properties, there is a paucity of research specifically on the antimicrobial properties and osteogenic ability of ZrO_2 incorporated-PEO coated Mg alloys. Most studies focused on the formation mechanism, surface morphology and corrosion resistance. More studies on the antimicrobial properties and osteogenic ability of ZrO_2 incorporated-PEO coated Mg alloys should be carried out on specific bacteria that are commonly exposed. Meanwhile, more animal studies should be carried out to investigate the osteogenic ability to increase the potential of ZrO_2 incorporated-PEO coated Mg alloys for applications.

5.4. Antibacterial ingredients-PEO coating

Infection at the surgical site of magnesium implants is a common cause of treatment failure, often leading to tissue damage and stimulating the body to mount a defense response that triggers infectious inflammation [151]. Bacteria adhere to and accumulate on the implant surface, secreting extracellular polymeric substance (EPS) (mainly polysaccharide matrix and other macromolecular polymers) to surround themselves and form biofilms [152]. Biofilm formation can be divided into four stages: bacterial reversible adhesion, bacterial irreversible adhesion, biofilm maturation, and bacterial shedding and recolonization [153]. Biofilms are highly resistant to the external environment, protect bacteria and also store nutrients required for bacterial growth [152]. The biofilm acts as a barrier to antibiotics and host immune response, increasing the difficulty of treating the associated infection [154]. PEO coating alone is difficult to meet antibacterial standards, therefore, the development of new antibacterial coating is important for the prevention of postoperative infections in implants.

The preparation of antimicrobial coating based on PEO technology can be divided into two methods, one is to add antimicrobial agents directly to the electrolyte, and the second is to prepare a composite coating by introducing antimicrobial agents through other surface modification techniques. Inorganic antimicrobial agents, which can fight bacterial infections while avoiding the application of antibiotics and are non-cytotoxic within a certain concentration, have a broad market prospect in the field of antimicrobial materials [153]. The following mainly introduced Ag^+, Cu^{2+}, and Zn^{2+} all belong to inorganic antimicrobial agents.

Ag particles are oxidized and dissolved, and the released Ag^+ is adsorbed on the bacterial cell membrane, which affects the membrane permeability of bacteria [155]. After Ag^+ enters the cell, on the one hand, it affects DNA and RNA and their transcription reactions [156], interfering with cell replication and division activities [153], and on the other hand, it combines with the negatively charged thiol group of proteases to form covalent bonds, leading to inactivation of bacterial proteases and disruption of normal cellular respiration and metabolic functions [157]. In addition, Ag^+ can induce excessive production of reactive oxygen species (ROS) in bacteria, triggering oxidative stress reactions and damaging proteins, DNA, and other biological macromolecules [156]. Yu et al. [158] researched the influence of the addition of Ag particles (1 g/L) on the antibacterial ability of the coating. 6 h antibacterial tests showed that the antibacterial rate of E. coli of PEO-coated samples containing Ag^+ was higher than that of samples with PEO coating, up to 94.9 % (Fig. 21). Chen et al. [159] studied the influence of adding different concentrations of Ag^+ (0, 1, 2, and 3 g/L) to the electrolyte

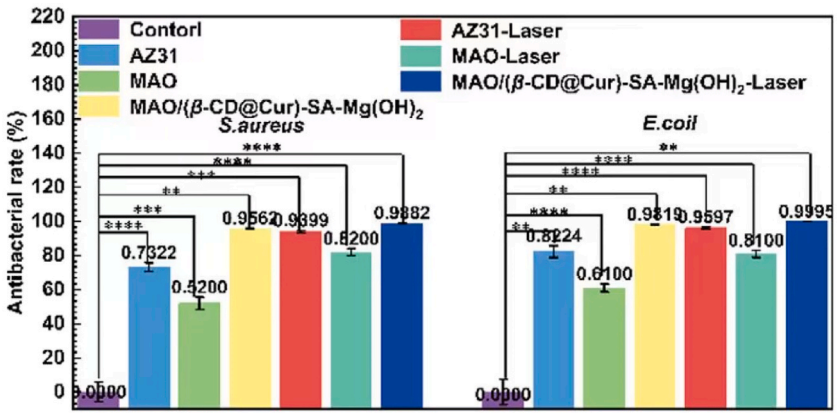

Fig. 24. The antibacterial rates of each group of samples against S. aureus and E. coli in the dark and after 30 min treatment with 808 nm NIR light [40].

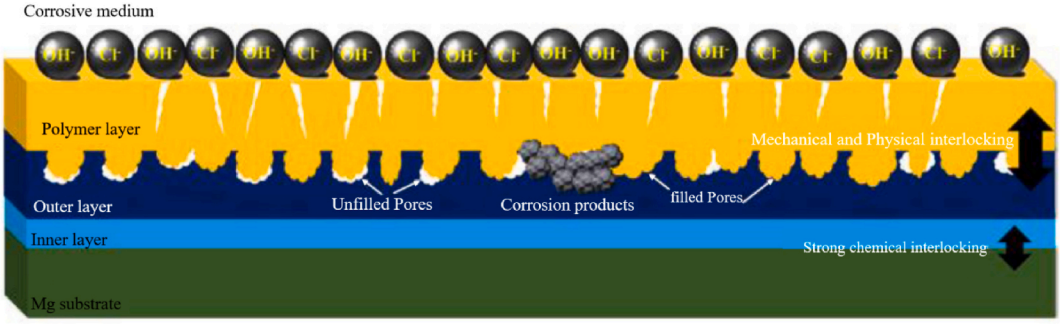

Fig. 25. Schematic diagram of the protection mechanism of PEO/polymer composite coating [176].

on the antibacterial ability of PEO coating. 24-h antibacterial test results revealed that the bactericidal rate of E. coli was higher when Ag^+ concentration added is 2 g/L and 3 g/L, and the highest rate was 90.89 % when 2 g/L Ag^+ was added, which proved that adding appropriate Ag^+ could improve the antibacterial ability of the coating. Han et al. [160] studied the effect of different voltages (400 V, 425 V, 450 V) on the antibacterial ability of silver-containing PEO coating against S. aureus. 24 h antibacterial test results showed that the higher voltage groups (425 V, 450 V) could maintain a consistently high antibacterial rate (~99 %) when sufficient Ag particles (>1 wt%) were added to the coatings. Wang et al. [46] combined PEO with a self-assembly technique to prepare silver nanoparticles (Ag NPs)/Polyethyleneimine (PEI)/PEO (APP) composite coating on AZ31 Mg alloys. The antibacterial test results revealed that the survival rate of S. aureus of APP-coated Mg alloys was much lower than that of PEO-coated Mg alloys and bare Mg alloys, which was only 1.28 %, indicating that APP coating has a good antibacterial property.

Cu-containing coating exerts its antibacterial functions by releasing Cu^{2+} and undergoing the following four toxic reactions [38,161,162]. (1) Cu^{2+} adsorbs onto bacterial cell membranes using electrostatic forces, disrupting the normal metabolic activities of bacteria. (2) Cu^{2+} damages the integrity of bacterial cell membranes, leading to cytoplasmic efflux. (3) Cu^{2+} induces excessive ROS production in bacteria, which affects the activity of respiratory enzymes and interferes with the gene replication process. (4) Cu^{2+} displaces iron atoms from the iron-sulfur atom cluster, causing damage to catabolic and biosynthetic pathways. Liang et al. [36] studied the influence of adding different concentrations of Cu^{2+} (0.1, 0.5,1 g/L) to the electrolyte on the antibacterial ability of PEO coating. 24 h antibacterial test results showed that the antibacterial ability was close at Cu^{2+} concentrations of 0.5 g/L and 1 g/L, and the inhibition rate of S. aureus was as high as 50 %. It is worth mentioning that excess Ag^+ and Cu^{2+} may be toxic to cells. The highest antibacterial rate of S. aureus was observed at a Cu^{2+} concentration of 1 g/L, but the cellular activity of MC3T3-E1 was low, indicating some cytotoxicity. Song et al. [37] combined UMAO, phytic acid (PA) conversion coating, and electroless copper plating on a pure magnesium substrate to prepare UMAO-PA-Cu composite coating, while Cu loading time (1, 3, and 5 min) was varied to regulate the Cu content in the coating. The most common pathogenic bacteria in bone implant surgery are E. coli and S. aureus, so these two bacteria were selected for antimicrobial test to evaluate the material's promise in the field of bone repair. The results of the antibacterial tests are shown in Fig. 22. The antibacterial effect increased significantly with increasing Cu content, where the coating reached the antibacterial criteria (antibacterial rate >90 %) when the Cu loading time was 3 and 5 min. Although the highest antimicrobial rate emerged when the Cu loading time was 5 min, subsequent cellular activity assays showed that the excess Cu was cytotoxic and affected the adhesion, proliferation, and differentiation of MC3T3-E1. Zhang et al. [38] prepared Cu-containing coatings with different mass fractions (0 %, 3 %, 5 %, and 7 %) by varying the treatment time of PEO. Pseudomonas gingivalis (one of the main causative agents of periodontitis) was selected for antibacterial tests to evaluate the potential of the samples in the field of jaw restoration. The antimicrobial tests explained that the antibacterial rate of the PEO coating group containing Cu was significantly

Table 5
Common types of polymer coatings and their coating methods and functions.

Substrate	Polymer layer	Coating method	Polymer coating function	References
AZ31B	Chitosan (CS)	Dip Coating	Reduce corrosion, improve biocompatibility, antimicrobial, poor adhesion strength	[189]
AZ31	Polylactic acid (PLA)	Spin Coating	High corrosion resistant, good biocompatibility, high adhesion strength	[192]
AZ31	Poly-L-lactic acid (PLLA)	Spin Coating	Corrosion resistance, good biocompatibility	[195]
Mg–4Zn-0.6Zr-0.4Sr	Polylactic acid-ethanolic acid (PLGA)	Dip Coating	Pores sealing, corrosion resistance	[191]
AZ31	Polyethyleneimine (PEI)	Dip Coating	High corrosion resistance, high adhesion strength to substrate	[46]
Mg–Zn–Ca	Polydopamine (PDA/PDAM)	Dip Coating	Corrosion resistance, hydrophilicity, high adhesion strength and good biocompability	[187]
AZ91		Electropolymerization		[180]
AZ31	Polycaprolactone (PCL)	Dip Coating	Good biocompatibility and corrosion resistance	[190]
WE42	Gelatin	Dip Coating	Good drug release and corrosion resistance	[177]
AZ31B	poly trimethylene carbonate (PTMC)	Dip Coating	Good biocompatibility, corrosion resistance, high mechanical strength and poor adhesion strength	[45]

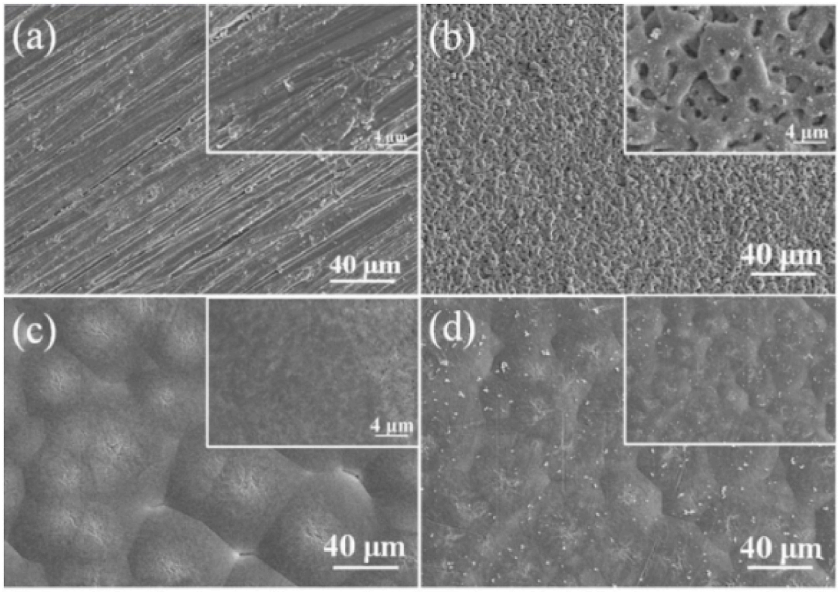

Fig. 26. Surface morphology of (a) AZ31 alloy, (b) PEO, (c) PEO/PCL and (d) PEO/PCL/PDAM under SEM [190].

higher than that of the PEO group and improved with increasing copper content. After 72 h, the antibacterial rate of the coatings containing 5 % and 7 % Cu^{2+} could even approach 100 %.

There are two main views on the antibacterial mechanism of Zn, one contacts bactericidal and the other is ROS bactericidal. Contact bactericidal means that the released Zn^{2+} binds to the bacterial cell membrane, which increases the membrane permeability and eventually leads to cell death [151]. ROS bactericidal means that the released Zn^{2+} induces bacteria to produce excess ROS, which destroys coenzyme A on the cell membrane, impairs cellular respiration and inhibits bacterial growth [163]. Seyfi et al. [163] studied the effect of different concentrations (1, 2, 3, and 4 g/L) of ZnO nanoparticles on the antibacterial ability of PEO coating. After 6 h, the colonies were counted and it was found that the antibacterial effect of the coating improved with the concentration of ZnO nanoparticles increasing, and the best antibacterial performance was achieved at a concentration of 4 g/L with 23.5 % inhibition of E. coli and 45.5 % inhibition of S. aureus.

The addition of TiO_2 nanoparticles (NPs) improves the antibacterial properties of PEO coatings. Its antimicrobial effect, on the one hand, reduces bacterial adhesion through forming reactive oxygen OH^- on the surface (most bacteria have a negatively charged surface). Meanwhile, the PEO coating increases the surface roughness and porosity, which allows bacteria to diffuse and makes the reaction between OH^- and bacteria more adequate [164]. Mozafarnia et al. [164] prepared an electrolyte by TiO_2-PEO coating was prepared by adding TiO_2 NPs to the electrolyte. After 6 h incubation (for S. aureus), the results of colony counting showed that the highest antibacterial rate of 97.65 % was achieved in the TiO_2-PEO coated sample group with high TiO_2 NPs concentration (4 g/L).

Tannic acid (TA) is used as an additive in antimicrobial applications because the phenolic hydroxyl group of TA damages bacterial

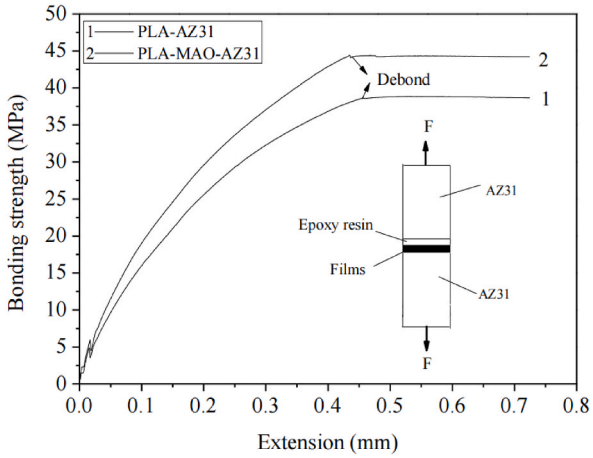

Fig. 27. Tensile tests on PLA-AZ31 samples and PLA-MAO-AZ31 samples [192].

cell walls and cell membranes, in addition, TA can chelate metal ions and decrease the activity of metalloenzymes [151]. Cui et al. [165] developed TA-PEO coating on AZ31 Mg alloys by adding PA and TA to the electrolyte. After incubation for 16 h (for S. aureus) or 12 h (for E. coli), the number of colonies was counted and the experimental results indicated that the antimicrobial ability of coating enhanced significantly because of TA.

In addition, chitosan (CS), a natural polymer, can act as an antimicrobial agent by contact killing, while facilitating cell growth [166].

As shown in Table 4, most of the above antibacterial experiments examined the antibacterial ability of the samples against E. coli and/or S. aureus, while some studies also selected Pseudomonas gingivalis for their experiments. However, many studies only performed antimicrobial experiments and lacked cellular activity experiments. Most of the antimicrobial agents currently introduced in PEO coating are metallic inorganic antimicrobial agents, which can be cytotoxic in excess. Therefore, it is crucial to conduct both antimicrobial experiments and cellular activity experiments to control the concentration of antimicrobial agents and finally screen out new antimicrobial coating with good antimicrobial properties and no cytotoxicity.

5.5. Drug-PEO coating

The exterior of the PEO coating is filled with pores, and the micro-pores facilitate drug adhesion to the coating surface either directly or after binding to the polymer to achieve storage of the drug. The drug release rate is related to the hydrophilicity, roughness, thickness, and pore size of the coating [43]. A variety of therapeutic drugs are covered in the included literature, including betamethasone sodium phosphate (BSP), berberine (BR), curcumin (Cur), geranium, and bisphosphonates (BP).

BSP ($C_{22}H_{28}FNa_2O_8P$) blocks the signaling pathways of transcription factors associated with inflammation, inhibits the production of pro-inflammatory mediators and cytokines [167], and has good anti-inflammatory effects [43]. Bordbar-Khiabani et al. [42] studied the drug release ability of PEO/BSP composite coating, and the experimental results demonstrated that PEO/BSP composite coating has good drug release ability. As shown in Fig. 23, the coating showed a burst release for the first 2 days and then could maintain a sustained drug release for about 24 days, probably because the hydrostatic force between BSP and PEO coating reduced the drug release rate. Berberine (BR) is the main component of the drug xanthan, which has anti-inflammatory, antibacterial, and anticancer pharmacological effects [168]. To control the appropriate drug release rate, Mu et al. [169] utilized degradable poly (lactic acid)-glycolic acid copolymer (PLGA) to carry drug. The researchers combined UMAO and self-assembly techniques to prepare UMAO/PLGA/BR composite coating on pure Mg alloys and demonstrated the good *in vitro* bioactivity and drug release capability of the

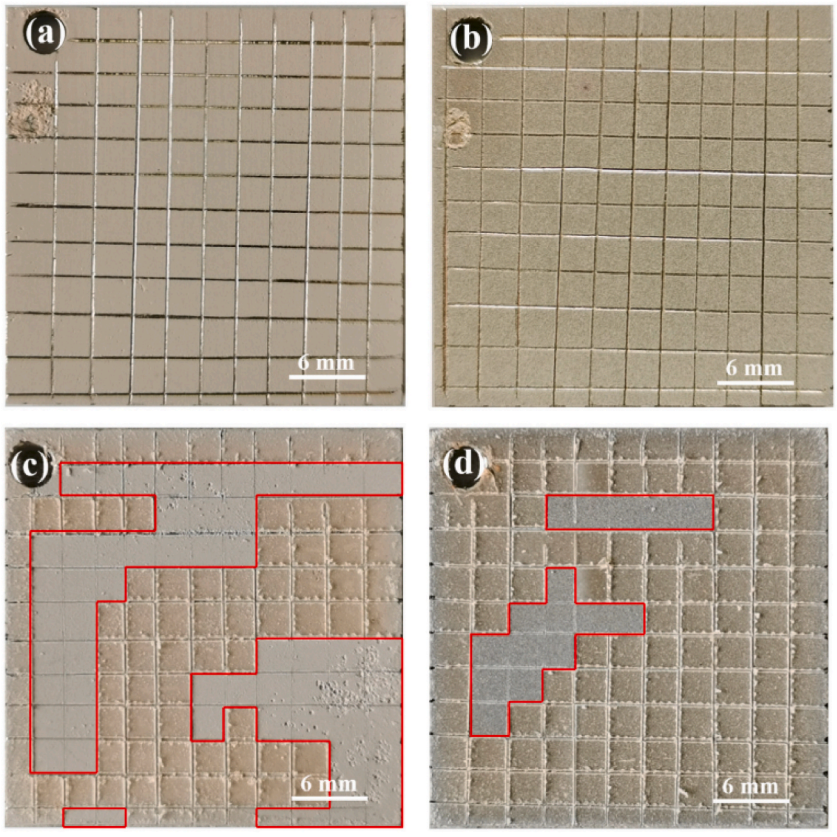

Fig. 28. Images of (a) PEO, (b) PEO/HT, (c) PEO/CS, and (d) PEO/HT/CS samples after adhesion tests according to ASTM D3359-09 [189].

composite coating.

Cur ($C_{21}H_{20}O_6$) is a highly lipophilic molecule that can freely pass through cell membranes, showing antibacterial, anti-inflammatory, anti-cancer, and antioxidant pharmacological effects [170]. Xue et al. [40] developed a composite coating of PEO containing Cur, having multiple antibacterial capabilities, and the antibacterial mechanism is divided into contact sterilization and

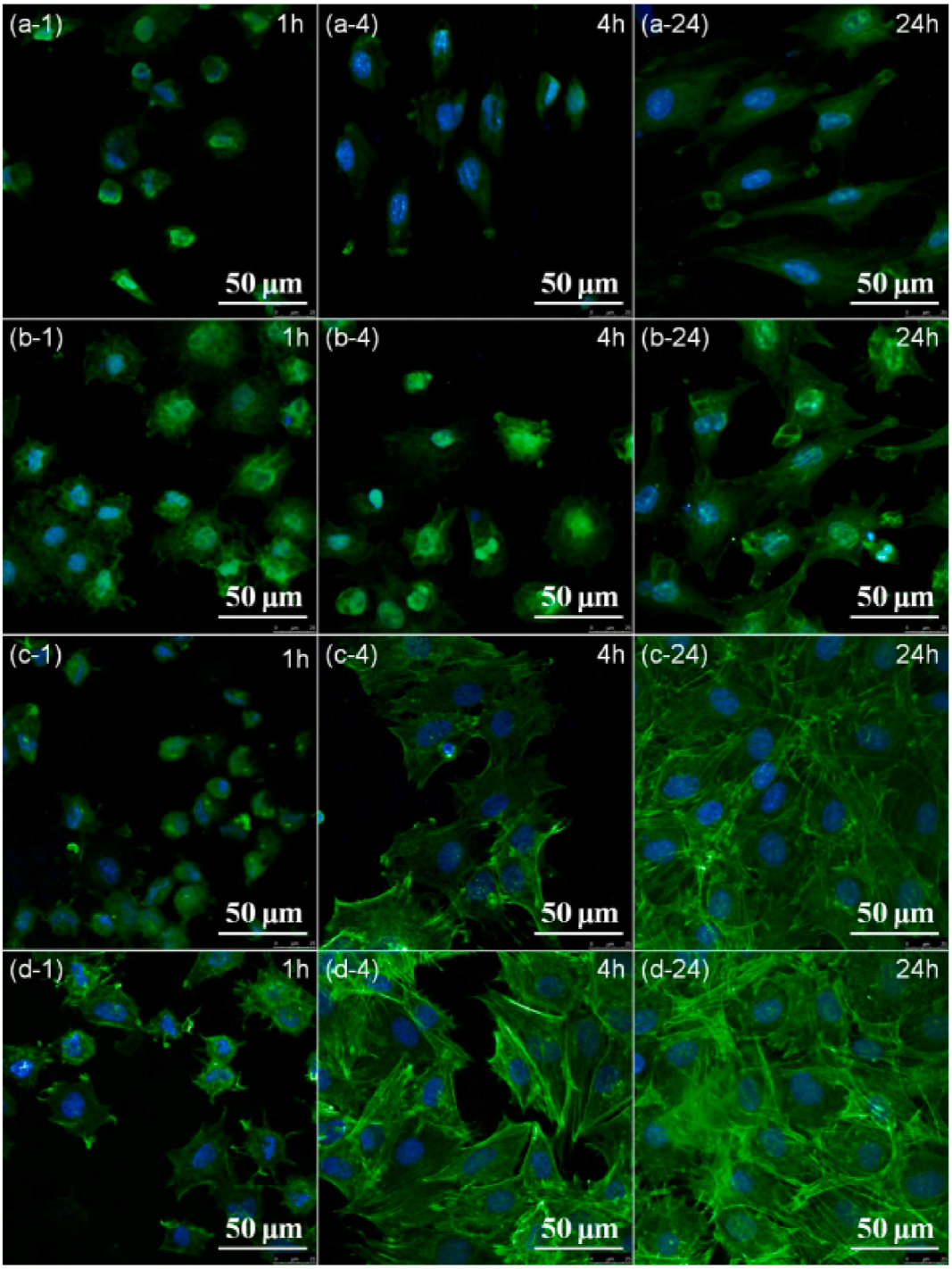

Fig. 29. Fluorescence microscopy images of MC3T3-E1 cells on different samples of (a) AZ31, (b) PEO, (c) PEO/PCL and (d) PEO/PCL/PDAM at 1 h (i-1), 4 h (i-4) and 24 h (i-24), respectively, with actin stained with fluorescein isothiocyanate (FITC) in the green part and the nucleus stained with PDAI in the blue part. PDAI-stained nuclei (blue) [190]. (For interpretation of the references to colour in this figure legend, the reader is referred to the Web version of this article.)

photothermal antibacterial. Among them, photothermal antimicrobial belongs to physical sterilization, in which the photothermal agent converts light energy into heat energy under near-infrared light, and the generated local high temperature eventually leads to bacterial death by destroying cell membranes, protein denaturation, etc. [171]. The results of the photothermal antibacterial test are shown in Fig. 24. After near-infrared light treatment, the antibacterial rate of the composite coating is up to 99.95 % for S. aureus and 98.82 % for E. coli, showing excellent antibacterial performance.

Puerarin can promote bone regeneration by promoting the proliferation and differentiation of osteoblasts and inhibiting bone resorption by osteoclasts [172]. Peng et al. [173] investigated the bioactivity of puerarin-loaded (PL) PEO coating. SBF immersion experiments clarified that the PL PEO coating showed better apatite formation and good osteogenic activity compared to the PEO coating. Some of the drug-loaded coatings related to osteogenesis have progressed to the *in vivo* phase. Osteosarcoma (OS) is the most common primary skeletal malignancy [174], and similar to geranium, BP can also induce osteoclast apoptosis, which in turn inhibits the activation of osteoclast-mediated osteolysis by OS cells, acting as an anti-OS agent [174]. Li et al. [41] developed a BP-loaded PEO composite coating and investigated the effect of the coating on OS inhibition at three levels: molecular, cellular, and *in vivo*. The results elucidated that the coating had the ability to inhibit the mevalonate pathway in OS cells, induce apoptosis and necrosis in OS cells, and then destroy tumor tissues and inhibit tumor regeneration, which has promising applications in the field of postoperative OS repair.

5.6. Polymer-PEO composite coating

Many researchers have thought of the possibility of forming a thin polymer layer on the PEO coating, and in this way, they expect the polymer-PEO composite coating to be effective in improving the drawbacks of PEO coating such as excessive micropores, insufficient hardness, limited corrosion resistance, and poor biocompatibility [175].

A range of corrosive media such as Cl^- can diffuse between the substrate and the PEO coating through pores and microcracks in the coating surface. However, the thin polymer layer can effectively refrain the corrosion rate and improve the tribological properties of the PEO coating by sealing these cracks or reducing the porosity (Fig. 25) [176]. After PEO treatment, the polymeric agent can penetrate through PEO layer and into these pores, and seal the inherent defects like cracks and pores on PEO surface, thus effectively preventing Cl^- from reaching Mg substrate, increasing the hydrophobicity and the corrosion resistance of the single PEO coating, and offering effective protection for Mg alloys. Polymer coatings have been used in medical applications such as wound dressings [177,178], stents [44,179], implants [180–182] and dentistry [183,184] due to their superior properties. Nevertheless, some polymer coatings may also suffer from defects such as poor adhesion strength and weak cytocompatibility, which can be addressed using HT or functionalized modifications etc.

Among the various polymer-PEO composite coatings of Mg alloys, the one that is currently more applied is the polydopamine (PDA) coating. PDA has good wettability, biocompatibility. In terms of adhesion, PDA improves the adhesion of improves mesenchymal stem cells, thus accelerating osteogenic differentiation. Moreover, PDA can spur the formation of bone-like apatite [185,186], and is widely used in antimicrobial coatings, and as a functional component in substrates for surface modification. Chitosan (CS), which is non-toxic and easily accessible has excellent biodegradability, biocompatibility, antimicrobial properties, and promotes wound healing. It has been widely used in antimicrobial materials, wound dressings, and can be embedded in dental adhesives. Gelatin coating, which is biocompatible, biodegradable, and has excellent drug-carrying properties, making it widely used in drug delivery systems. In addition, there are polylactic acid (PLA), poly (levulinic acid) (PLLA), poly (lactic acid-glycolic acid) (PLGA), PEI and poly trimethylene carbonate (PTMC) etc. These polymers can not only effectively seal pores, but also have good biocompatibility.

The preparation methods of these polymer-PEO composite coatings are also varied, and the effect of using different preparation methods for the same polymer varies greatly, among which the coating method is mostly by dip coating, i.e., the PEO- coated sample is directly immersed in polymer solution or dichloromethane solution of polymer. Feng et al. [187] prepared PDA/PEO-HA coatings by immersing Mg–Zn–Ca alloy samples containing HA in dopamine (DA) solution for 8 h. The more special one is the spin coating, which

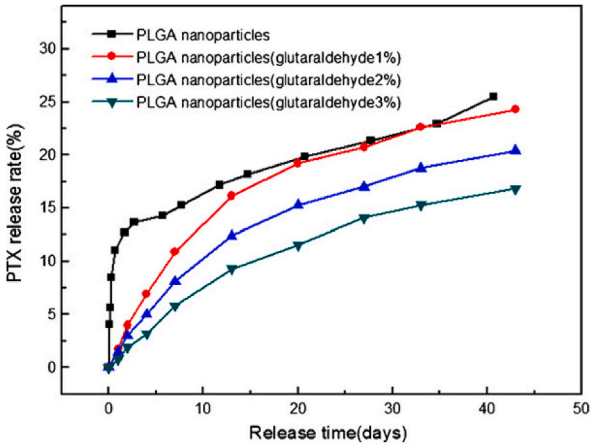

Fig. 30. *In vitro* release mode of paclitaxel in the cross-linked gelatin/PLGA nanoparticle composite coating at different levels [236].

can produce thinner and less microporous coatings compared to the dip coating [188]. For instance, Alabbasi et al. [188] dissolved PLLA and ester-terminated resin in 60 % dichloromethane and applied it to PEO coatings using a rotary coater. There are also a small amount of electropolymerization and electrophoretic deposition techniques have been used to prepare polymer-PEO composite coatings. Farshid et al. [180] added DA to two concentrations of 1 mg/mL and 1.5 mg/mL of sodium deoxysilicate solution for electropolymerization on AZ91 to prepare a PEO/PDA composite coating. The coating methods of common polymer coatings and their functions are shown in Table 5.

In order to prevent defects in the surface of the PEO coating from allowing corrosive substances to diffuse between the substrate and the PEO coating, researchers generally use polymer coatings to fill these defects. Xu et al. [189] prepared PEO/CS coating on AZ31. Randomly distributed volcano-like micropores of random size and microcracks penetrating the coating existed on the PEO-treated samples' surfaces, while the CS layer could completely seal the pores and microcracks of the PEO-treated sample. Meanwhile, the researchers found that the polymer coating not only can effectively seal the pores, but also its surface structure does not change significantly after other functionalization treatments. Tian et al. [190] prepared a PEO/polycaprolactone (PCL)/Polydopamine (PDAM) composite coating on AZ31 alloy using PCL and functionalized with PDA. The PEO coating demonstrates a porous surface character (Fig. 26(b)), compared to AZ31 alloy (Fig. 26(a)). After sealing by PCL layer, the PEO/PCL composite coating had a flatter surface morphology (Fig. 26(c)). And after further functionalization by PDA, the morphology of the PEO/PCL composite coating varied insignificantly, and merely few PDA particles appeared (Fig. 26(d)).

By applying the polymer layer on the PEO coating, the surface of the coating is smoother, where the effective sealing of inherent defects e.g., pores and cracks can further reinforce the corrosion resistance of the single PEO coating. Tian et al. [190] conducted a series of experiments such as electrochemical tests to verify the corrosion resistance of PCL/PEO polymer composite coatings. In the electrochemical test in SBF, compared to the corrosion current ($I_{corr} = 1.402 \times 10^{-5} A/cm^2$) and corrosion potential ($E_{corr} = -1.508V$) of AZ31 alloy, PEO has a slight decrease in E_{corr} value (−1.640 V) due to its porous structure. Nevertheless, the corrosion potential of the PEO/PCL samples was significantly higher (−1.342 V), and the corrosion current density was 5 orders of magnitude or so lower (3.260×10^{-10} A/cm^2) compared to AZ31 alloy. In subsequent local alkalinization experiments, hydrogen evolution experiments and immersion experiments, PCL/PEO polymer coatings showed superior corrosion resistance as well. Similarly, Chen et al. [191] performed immersion tests on PEO/PLGA composite coating samples to study hydrogen evolution and electrochemical behavior, and then obtained similar results. Within the first 30 h of the immersion experiment, the volume of hydrogen released from PEO/PLGA samples was much lower than the other two groups. And after 22 d, the hydrogen volume of PEO-coated samples increased rapidly, indicating that delamination of the coating occurred, while the PEO/PLGA group still maintained a lower hydrogen release volume. Compared with the other two groups, the corrosion potential of PEO/PLGA coating (E_{corr}) increased significantly, while the value of I_{corr} decreased significantly, demonstrating that the PEO/PLGA coating effectively ameliorated the corrosion resistance of the samples. The polymer can enormously reinforce the corrosion resistance of the implants and avoid premature degradation of the implants that can affect the function.

The polymer-PEO composite coating with smooth surface has better tribological properties than AZ31 alloy or PEO coating, which can effectively improve the wear rate and friction rate. Xu et al. [189] conducted tribocorrosion experiments on PEO/CS coating, PEO coating and untreated samples. The results demonstrated that the friction and wear rates of the CS layer samples were significantly lower than those of PEO and PEO/HT, and their average coefficients of friction (COFs) were also lower and more stable than those of the PEO coating. It indicates that by CS layer treatment, the samples are more wear-resisting and the possibility of coating peeling due to wear *in vivo* is reduced, thus ensuring the mechanical integrity of the magnesium substrate and avoiding the potential harm to the human body due to coating peeling. However, for the adhesion strength, only a few polymers such as PDA and PLA have high adhesion strength to the substrate since their functional groups enable to interact covalently and non-covalently with PEO coatings. Shi et al. [192] investigated the formation of PLA-AZ31 directly on AZ31 substrate. As Fig. 27 shown that, the adhesion strength of

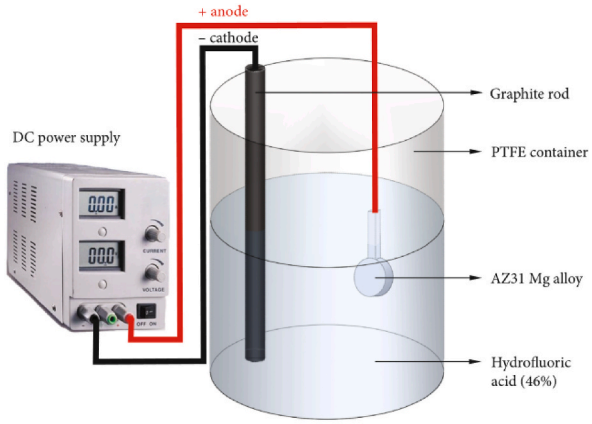

Fig. 31. Schematic of PEF treatment [198].

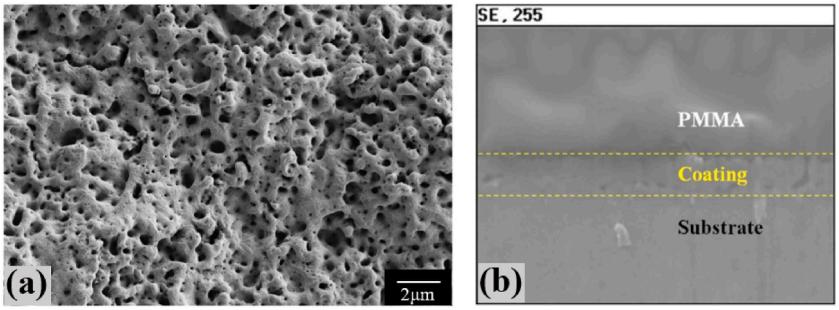

Fig. 32. (a) Surface and (b) cross-sectional morphology of PEF coating on AZ31 [6,198].

PLA-PEO-AZ31 was 45 MPa, and basing on ASTM F1147 [192]. The minimum adhesion strength required for medical implant coatings is currently 22 MPa, indicating that the PLA-PEO-AZ31 composite coating has a high adhesion strength, which can meet the requirements of medical implants. However, most polymer coatings have poor adhesion strength and require other surface treatment techniques such as HT or functionalized modifications to obtain greater adhesion strength. Xu et al. [189] found that there was no significant peeling of the PEO coating after the adhesion test under ASTM D3359-09 standard. In contrast, the peeling rate of the PEO/CS composite coating was approximately 41 % (Class 1B). The results indicated that the CS layer was prone to peeling, which affected the coating function. Addressing this problem, Xu et al. used HT to modified PEO/HT/CS coatings. As shown in Fig. 28(c) and (d), the peeling rate of PEO/HT/CS coating is lower compared to PEO/CS coating, which is only 12 % (Class 3B). After subsequent tribo-corrosion experiments, compared to the PEO sample (Fig. 28(a)), the HT-treated composite coatings (Fig. 28(b–d)) also had better corrosion resistance as well as wear resistance and abrasion rate, especially the PEO/HT/CS specimens had the lowest average covalent organic framework value (~0.11) and the lowest abrasion rate (~1.83×10^{-5} mm^3 N^{-1} m^{-1}) compared to the untreated substrate (~1.13×10^{-4} mm^3 N^{-1} m^{-1}), indicating that HT can effectively ameliorate the adhesion strength and wear resistance of polymer coatings. Besides, Ghanbari et al. [45] attempts to ameliorate the adhesion strength of PTMC/PEO coatings by functionalizing them with DA. The results show that compared with the class 1B of AZ31 and the class 2B of AZ/PEO/PTMC, the peel rate of AZ/PEO/DFP (the acronym for DA functionalized PTMC polymer) composite coating is less than 5 %, that is, class 4B, showing better adhesion strength improvement.

Wettability as a key surface property of the implant, affects the conformation of proteins [193], and has a significant effect on cell adhesion during the adhesion of various types of cells. The wettability of polymer-PEO composite coatings varies depending on the polymer type. Interestingly, most of them showed significant hydrophilicity, which is related the hydrophilicity of the polymer itself and the valid sealing of pores and cracks caused by PEO technology. Hydrophilic surfaces are more likely to bind water and proteins than hydrophobic surfaces and make a greater difference to the corrosion resistance and biocompatibility of the coating. Xu et al. [46] found by contact angle experiments that the contact angle (CA) of uncoated AZ31 was 32.85°, a hydrophilic surface, while the CA of the Ag NPs/PEI/PEO (APM) composite coating was 24.6°, showing that APM-AZ31 composite coating is more hydrophilic, which may be because of the sealing of defects by PEI that facilitates the hydrophilicity of the coating surface. PDA has better hydrophilicity, Feng et al. [187] conducted contact angle measurement experiments using static water and found that the CA of the PEO-HA coating was 100.5°, while the PDA/PEO-HA coating was 80.1°, indicating that the addition of the PDA coating made the PEO coating surface more hydrophilic. At the same time, researchers also found that a small amount of polymer coatings exhibited hydrophobicity. Lee et al. [194] measured the contact angles of AZ31 Mg alloys, PEO layer, and polymer layer with deionized water, and the contact angles were 63.7°, 60.7°, and 92.4°, respectively. The results showed that the coating changed from hydrophilic to hydrophobic after being coated by the polymer layer, and the polymer layer could effectively prevent the penetration of corrosive substances and improve the corrosion resistance. Therefore, it is reasonable to speculate that the fundamental reason for whether the polymer-PEO composite coating is hydrophobic may lie in the hydrophilicity of the polymer itself.

Polymer-PEO composite coatings are non-toxic and can effectively ameliorate the biocompatibility and bioactivity of PEO-coated Mg alloys, especially for osteoblasts. This review focuses on the effects of polymer coatings on cell activity, cell behavior, and cytotoxicity. Researchers found that some of the polymer-PEO composite coatings enables to effectively ameliorate osteoblasts in terms of the adhesion and proliferation. Feng et al. [189] observed the morphology of MC3T3-E1 cells on PDA/PEO-hydroxyapatite (PDA/-PEO-HA) and PEO-HA coatings. The cells developed well on the PDA/PEO-HA coating and adhered better to the coating surface, probably because the biomolecules, e.g., amino or hydroxyl groups contained in the polymer coating took a positive part in the adhesion and growth of the cells. In contrast, the cells did not grow well on the PEO-HA coating, which is perhaps because of the relatively inferior corrosion resistance, leading to a faster loss of a suitable living environment for the cells or the pore size of the PEO-HA coating and is not conducive to cell adhesion and proliferation [187]. Researchers have also identified some of the polymer-PEO composite coatings with poor adhesion at the initial stage of cell adhesion. While the biocompatibility of these polymers-PEO composite coatings can be effectively improved by functionalized modification. Tian et al. [190] improved the PEO/PCL coating by functionalizing PDA and use fluorescence microscopy to observe MC3T3-E1 cells in terms of the adhesion and proliferation. As shown in Fig. 5, at the 1st hour, cells adhered more poorly to PEO/PCL than other kinds of samples due to the hydrophobic nature of PCL (Fig. 29(a-1, b-1, c-1, d-1)). While the biocompatibility of these polymers-PEO composite coatings can be effectively improved by

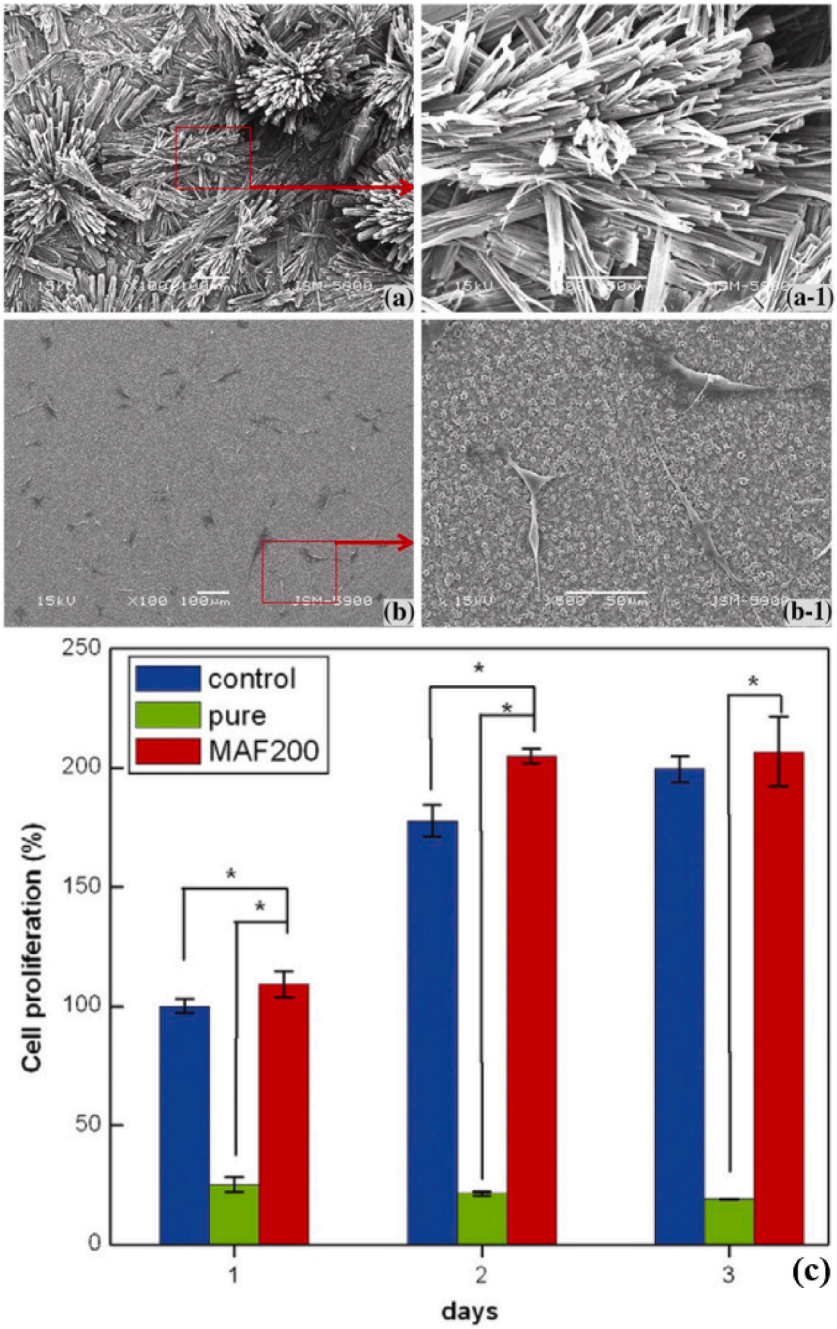

Fig. 33. Cell morphology of MC3T3-E1 cells after 3 days on (a) pure Mg, and (b) MAF-coated pure Mg; high magnification (a-1) pure Mg and (b-1) MAF-coated pure Mg, (c) Cell proliferation of MC3T3-E1 cells cultured for 1 day on pure Mg, MAF-coated pure Mg, and the control group. *$p < 0.05$ [199].

functionalized modification. After 4 h of incubation, cells on both PEO/PCL (Figs. 29(c-4)) and PEO/PCL/PDAM (Figs. 29(d-4)) spread excel at those on AZ31 alloy and PEO (Figs. 29(a-4, b-4). After 24h of incubation, cells on PEO/PCL (Figs. 29(c-24)) and PEO/PCL/PDAM (Figs. 29(d-24)) covered almost the entire surface of the samples compared to the bare and the PEO sample (Figs. 29 (a-24, b-24)), while the PDAM-modified coated samples had a larger cell spreading area, indicating that the functionalized modification of PDAM can effectively promote cell adhesion growth. In addition, researchers did not find significant cytotoxicity of the polymer coatings. Wei et al. [195] conducted cytotoxicity evaluation experiments on PEO/PLLA/PDA composite coating and PEO/PLLA coating samples with different concentrations of extracts. The results showed that all samples did not show significant cytotoxicity after 1 day of incubation. After 3 days of incubation, too high concentration of the extract slightly inhibited the

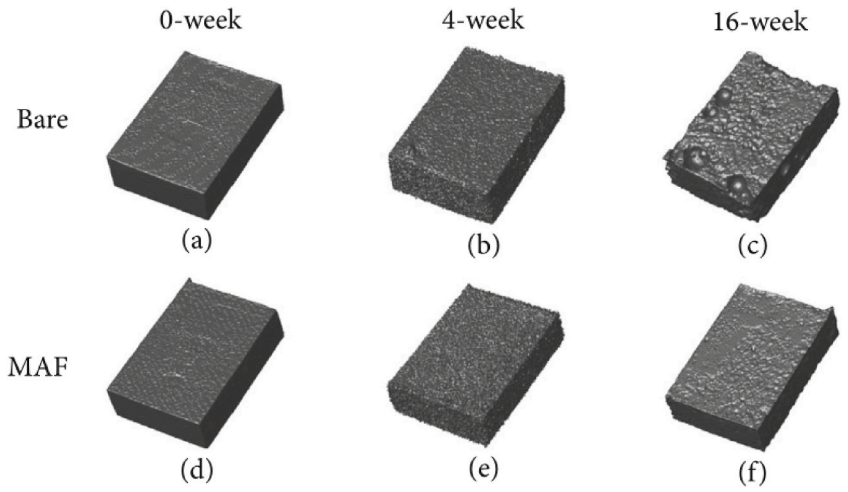

Fig. 34. Micro-CT scans of Bare and MAF-coated AZ31 from *in vivo* tests at three time points (0-week, 4-week, 16-week) [6].

multiplication of Human umbilical vein endothelial cells (HUVECs), while with dilution, the suppression of cell proliferation of HUVECs was gradually reduced in all samples until the restraint of cell proliferation by the samples completely disappeared at 40 % dilution, showing that the cytotoxicity was related to the concentration of corrosion products. Therefore, for medical implants, polymer-PEO coatings with better biocompatibility must be selected to obtain better osteogenic activity.

In addition, certain specific polymeric composite coatings have excellent drug-loading capacity, and the PEO coating has excellent slow-release capability. Xu et al. [177] cross-linked gelatin/PLGA nanoparticles/PEO coatings were prepared on WE42 by mixing equal volumes of glutaraldehyde solution (1 %, 2 %, 3 %) with gelatin solution (6 %). Fig. 30 shows the *in vitro* release mode of paclitaxel in the cross-linked gelatin/PLGA nanoparticle composite coating at different levels. The PLGA nanoparticles released rapidly in the first 5 days, and the release rate slowed down after 5 days. However, there was no significant burst release from the cross-linked gelatin/nanoparticle coating. Meanwhile, the release rate of paclitaxel in the early stage decreased when the glutaraldehyde concentration increased, indicating that the higher cross-linked gelatin could retard the release of paclitaxel.

In addition to the *in vitro* experiments mentioned above, the polymer-PEO composite coating also demonstrated an exceptional amelioration in the initial corrosion resistance of the magnesium implants in the *in vivo* experiments and an outstanding osteogenic ability. Kim et al. [196] coated pure Mg screws with the PCL 6 wt% + 4 cycles (i.e., PCL concentration of 6 wt%, dip coating cycles 4 times, abbreviated as PCL6/4) method that performed best in the previous *in vitro* experiments, and implanted them into rat tibiae. After 1 month, the PCL6/4-PEO composite coated Mg screws were largely intact, with only a small amount of wear on the threads. Meanwhile, osteocytes were formed on the surface of the screws, as well. The bone volume around the composite coated screw was larger compared to the single PEO coating. And after 2 months, compared to the faster corrosion of PEO-coated screws, the PCL6/4-PEO composite coated screws did not show significant air cavities and had significantly higher corrosion resistance. Further, many osteoblasts and new osteocytes were found on the screw surface, and many bone particles from the surrounding bone tissue appeared. Compared with PEO coating, the amount of bone tissue of PCL6/4-PEO composite coating was significantly increased, showing better osteogenic ability.

Although organic polymer coatings exhibit a better ability to seal the pore, some articles [197] also indicate that low thickness of the polymer layer will lead to coating detachment or cohesive failure, which provide insufficient protection for PEO coatings. In addition, the molecular weight of the polymer will affect the coating's hydrolysis rate, and the number of layers of the composite coating is going to impact on the thickness and density of the coating [166]. In summary, when developing polymer coatings, extra attention should be paid by researchers to the above parameters and appropriate surface modification techniques or functionalization modifications should be taken to address them.

5.7. Plasma electrolytic fluorination coating

Fluoride coatings are mainly prepared by plasma electrolytic fluorination (PEF), also known as micro-arc fluorination (MAF), which is similar to conventional PEO, utilizing electrochemical deposition techniques. Typically, as shown in Fig. 31 [198], under constant DC voltage, Mg is the anode, carbon is the cathode, and the electrolyte is acidic electrolyte such as high saturated HF acid or saturated fluoride salt solution or molten fluoride salt [6,198–200].

Gao et al. [6] prepared a fluoride coating of AZ31 with saturated NH_4HF_2 solution. The reactions are as followed:

$$Mg \rightarrow Mg^{2+} + 2e^{-}, \tag{4}$$

$$Mg^{2+} + 2F^{-} \rightarrow MgF_2 \tag{5}$$

Mg loses e^- and combines with F^- in the electrolyte to generate insoluble MgF_2 deposited on the Mg substrate, as shown in equations (4) and (5). Compared with the conventional PEO coating, the coating generated is without oxides, regardless of the use of high-concentration HF acid or saturated fluoride salt solution, or molten fluoride salt [198–200]. However, researchers discovered that the thickness of the coating varies by applying different electrolytes and substrates under the condition of similar voltage. And it is well known that the Pilling and Bedworth ratio (P–B ratio) of MgO is less than 1, which easily causes it to break. On the contrary, the P–B ratio of MgF_2 formed by the reaction of Mg and HF acid is between 1 and 2, the coating is passivating [199]. The fluoride coating prepared by MAF is uniform, compact without cracks, porous coral-like, and tightly bonded to the substrate, as shown in Fig. 32 (a, b) [6,198].

Similar to traditional PEO coating, the properties of PEF coating depend on electrical parameters, Jiang et al. [199] and Sun et al. [198] prepared fluoride coatings on pure Mg and AZ31 by PEF treatment with different voltages, respectively. PEF-treated pure Mg at 200 V has the best corrosion resistance when immersed in the SBF for 8 weeks, compared with those treated at 120 V and 160 V. Likewise, PEF-treated AZ31 at 200 V also has the lowest corrosion rate with higher surface roughness and smaller contact angle, which facilitated cell adhesion and proliferation, compared to 100 V, 150 V, 200 V, 250 V, and 300 V treatments. In another study by Jiang et al. [200], with the rise of applied voltage, the thickness of the coating increases, and the size of the micropores also increases simultaneously. And both the pore size and thickness are important factors affecting the corrosion resistance. Nevertheless, the effect is opposite, i.e., the larger the pore size, the lower the corrosion resistance; the thicker the coating, the higher the corrosion resistance. The coating with the best corrosion resistance is prepared under 130 V PEF treatment.

The rapid degradation rate is the primary reason for low biocompatibility, as it leads to rapid hydrogen release, elevated local pH and high local Mg^{2+}concentration [99]. Jiang et al. [199] evaluated the proliferation of MC3T3-E1 cells on MAF-coated pure Mg. As shown in Fig. 33(a–c), the cells of MAF-coated pure Mg extend multiple pseudopods to contact the coating surface and show the best adhesion and proliferation. The cell viability is also greater than that of the control and pure Mg groups, attributing to the high corrosion resistance and coral-like porous surface structure. Gao et al. [6] demonstrated the biocompatibility and corrosion resistance of MAF-coated pure Mg in rats, as shown in Fig. 34(a–f), the corrosion was uniform within 16 weeks, the volume loss was about 3.2 %, and the small amount of hydrogen gas released during the slow degradation of Mg was proved to be harmless. In contrast, the uncoated pure Mg showed severe pitting corrosion, the volume loss was about 14.9 %, and obvious large gas cavities can be found around the sample by Micro-CT scanning. In addition, numerous *in vivo* experiments have demonstrated the non-cytotoxicity of MgF_2 coating [47, 201], which slowly degrades and releases Mg^{2+} and F^- to the surrounding tissues. Mg^{2+}, as the main metal ions involved in bone formation and remodeling, have been widely demonstrated for their osteogenic effects [48], and low concentrations of F^- have also been shown to have antibacterial, tooth growth-promoting and osteogenic effects [47].

5.8. Self-healing coating

Self-healing materials enables to fix physical damage and autonomously restore their own function [202–205]. In the last five years, self-healing coatings have also been widely used in industrial, aerospace, and biomaterials applications. Currently, in terms of self-healing coatings applied on medical magnesium alloys loading PEO coating, the commonly used are the Ca–P-PEO coating and LDH-PEO coating mentioned above, which act as corrosion inhibitors or are loaded into the multilayer coatings [206–209] by incorporating corrosion inhibitors (e.g., 8-Hydroxyquinoline (8-HQ) [210,211], carboxylated carbon nanotube (CCNT-IL) [212], Ce ions [213]. The micropores in the PEO coatings or part of the combined coating strategy provide a "temporary storage compartment" for the corrosion inhibitors. When corrosive media such as Cl^- diffuse deeper, the release of these corrosion inhibitors will be triggered, and the majority of these corrosion inhibitors will react with OH^- or Mg^{2+} in the corrosion environment of magnesium or magnesium alloys to form a protective film to cover the damaged area, thus realizing self-healing [210,213]. Besides, using the synergistic healing effect between the corrosion inhibitors is a wise choice [214,215]. Some of them utilize their own physical properties, such as imidazolium-based ionic liquid (IN) [216] has hydrophobicity, which helps to repel corrosive substances. In addition, in industry, IN can also be adsorbed on the surface of PEO, filling the micropores on the outer surface of PEO, and the corrosion inhibitor (some possessing a hydrophobic structure) itself forms a protective film. Although this coating is a superhydrophobic coating that has been applied industrially, it can also provide inspiration to researchers in terms of innovations in bio-coatings for magnesium alloys. In addition, it is worth mentioning that the ultimate goal of preparing these self-healing coatings is to prevent the corrosive environment from continuing to invade the magnesium substrate. As mentioned above, the additional coating in the PEO self-healing multilayer coatings can provide sufficient space for the corrosion inhibitors, and also act as a barrier film to prevent corrosive substances from invading to a certain extent [210,214]. In addition, researchers have also directly utilized the self-healing ability of certain polymers to prepare a composite coating with both corrosion resistance and biological properties on the PEO coating. The specific mechanism has also been widely reported [217,218]. To summarize, polymers usually have elasticity and plasticity, and when the coating is broken, the polymer molecules can remove, arrange, and combine to fill the cracks and defects, thus restoring the integrity of the coating. S. Farshid et al. [180] used an electro-polymerization technique to deposit PDA on a PEO-coated magnesium alloy. The healing function of PDA can be explained by the pore-block mechanism and zipper-like mechanism [219].

Currently, the types of self-repairing coatings that can be applied on PEO-coated magnesium alloy biomaterials include primarily conversion coatings [31,180,213–215,220] and encapsulation coatings [210,221,222]. Conversion coatings include chemical conversion coatings, PEO-based coatings, and LDH-based coatings. Among chemical conversion coatings, only phytate conversion coatings (PACC) [213], chromate conversion coatings (CCC) [223], and phosphate conversion coatings (PCC) [224,225] can be applied on magnesium substrates. While CCC is strictly limited in clinical use due to the high toxicity and carcinogenicity of the hexavalent chromium in it. PA, an organophosphate compound extracted from the seeds of leguminous plants, germ of cereals, and bran, possesses

a strong chelating ability to produce insoluble compounds with metal ions, such as Mg^{2+}, which makes it an ideal choice for self-repairing coatings [226]. However, in practical applications, PA is more often combined with corrosion inhibitors (e.g., cerium), and this will be elaborated in the subsequent section of PEO-based coatings. By contrast, PEO-based coatings take into account the defects of PEO coatings. By adding corrosion inhibitors (e.g., cerium (Ce), CeO_2, Ce^{3+},8-HQ [227,228]), which combine with Mg^{2+} or OH^- around the defects to form a precipitate that settles in the damaged area. Alternatively, the inhibitor can be adsorbed to the damaged region to form a protective film, leading to self-healing. Among them, Yang et al. [223] found that cerium salt transformed film has similar self-healing properties with CCC, with much lower toxicity than CCC, and can effectively inhibit substrate corrosion. However, the Ce salt transformed film has low adhesion strength and can't be tightly bonded with the substrate so the effect is significantly reduced. While PA has a robust chelating ability, it can be used as a chelating agent to make Ce and PEO coating closely linked. Yang et al. took this opportunity to use hydrothermal treatment in the PEO-coated magnesium alloy and prepared about 5 μm thick phytate/cerium composite self-healing coating (PA/Ce). The composite coatings' adhesion strength and self-healing behavior can allow the substrate to provide long-term corrosion protection. In addition, biomaterial polyacrylamide (PAM) hydrogels can stimulate the release of triggered inhibitors when sensing elevated pH due to pH-responsive function [229,230]. Guo et al. [220] prepared PAM gels encapsulating the Ce^{4+} inhibitor on the surface of PEO-treated AZ31 Mg alloy. With the localized pH elevation caused by magnesium corrosion, the PAM releases Ce^{4+}, which is the most effective way to protect the substrate against the corrosion of magnesium. By growing in combination with other corrosion products to form a dense protective film, the corrosion resistance of the coating was improved greatly.

Exceptionally, PDA, mentioned in section 5.6. Polymer-PEO composite coating, is a catecholamine-based polymer, which also has some self-healing properties. Distinguishing from other inhibitors, PDA is non-toxic and PDA promotes bone-like hydroxyapatite production with some osteogenic activity. Farshid et al. [180] used electrodeposition to construct a PEO/PDA biphasic coating. Electrochemical experiments surface that Mg^{2+} are bond with the catechol groups of PDA when released from the breakage, thereby filling the defects (pore-block mechanism). At the same time, PDA can react with water ions to form new cross-links and thus achieve self-healing properties (zipper-like mechanism) [219]. In addition, the excellent biocompatibility of this coating is also mentioned in section 5.6. Polymer-PEO composite coating, which is an ideal material for orthopedic implants.

Encapsulation coatings have self-healing effects by encapsulating particles or containers with inhibitors in PEO coatings. LDH mentioned in section 5.2 can be used as layered ionic micro-nano containers to close the pores of PEO to achieve self-healing, in addition to properties such as ion exchange capacity. The self-healing mechanism of LDHs coatings is mainly divided into two aspects. On the one hand, when the LDHs coating is damaged, rare-earth elements are released and a new protective film is formed at the defects to enhance the protection of the magnesium substrate. In addition, LDHs coating relies on the ion exchange capacity, which can release interlayer inhibitors while trapping aggressive anions [231]. Xu et al. [215] prepared novel MgAlY-LDHs coatings loaded with salicylic acid on flash-PEO-coated AZ31 alloy using an intercalation method and a one-step hydrothermal method. The Y-salicylic acid complexes showed good corrosion protection against magnesium substrates by grafting onto LDHs and defects to realize dual self-healing of both sites. Some researchers have also found that graphene oxide (GO) accelerates the *in-situ* nucleation of LDHs [232]. It makes the LDHs appear as curled edges and corrugated sheets, which improves the tortuosity of the diffusion path of LDHs to corrosive media. In addition, GO also acts as a carrier so that the corrosion inhibitor can be stabilized and immobilized in the coating. Chen et al. [210] in this way reacted 8-HQ@GO composites by ring-opening reaction, doped the composites into LDHs flakes, and loaded them onto PEO coatings by hydrothermal reaction. This work is a new idea to introduce corrosion inhibitors and prevent corrosion inhibitor leakage to improve the corrosion resistance of LDHs coatings. In addition to micro-nano containers, particles such as zeolites and CS are also an option for loading Ce-based inhibitors. Zeolite is a compound composed of three kinds of silicon, aluminum, and oxygen, in which the silica-oxygen tetrahedra and aluminum-oxygen tetrahedra form an infinitely expandable three-dimensional space shelf structure between them, which is resistant to acid, alkali, and high temperature, and has strong adsorption capacity and ion exchange capacity. It is often used as catalysts and molecular sieves because its interior is full of fine pores as dense as a beehive. Zadeh et al. [233] have also found that the inhibitors in zeolites can be selectively released to damaged sites, which provides direction for zeolites as carriers of inhibitors. Chen et al. [222] therefore placed zeolite particles containing Ce^{3+} into the PEO coating. Ce^{3+} ions were released from the coating through ion exchange along with the dissolution of zeolite during the degradation of the coating, and the cerium hydroxide/oxide formed at the defects could form a passivation film to improve the barrier ability of the coating, which improved the corrosion resistance of the coating.

In addition, some researchers combine micro-nano containers with other coatings for the realization of multifunctional coatings. Layer-by-layer assembly (LBL) coatings typically use polymeric materials (e.g., polymers) that are adsorbed onto a substrate by electrostatic action. External stimulus-responsive coatings, on the other hand, induce the release of inhibitors from the coating by applying external stimuli (humidity, sunlight, pH), etc. Jia [221] utilized the "proton sponge" property of Ce that is sensitive to pH, and $(Ce(NO)_3)_3$–$6H_2O$ was doped into the CS. The pH was adjusted to 5.5, CS particles were used as micro-nano particle containers. They were deposited on the PEO coating by the LBL technique to form a robust composite coating structure. It was demonstrated that with the increase of pH during corrosion, Ce^{3+} dissociates, diffuses to the corrosion site and combines with the substrate surface to produce Ce_2O_3, depositing in the corrosion region. Meanwhile, Ce–NH_2 chelates formed by Ce and CS will also help in the immobilization and delivery of inhibitors to improve corrosion resistance. Meanwhile, cytocompatibility evaluation experiments also showed that the composite coating exhibited higher cell viability and low toxicity to MC3T3-E1 cells.

Self-repairing coatings, significantly extend the service life of coatings and prevent them from physical damage. Its sufficient potential and unique mechanism may lead to a significant step forward in the protection of magnesium alloys. However, there is a lack of research concerning self-healing coatings on whether the corrosion inhibitor affects the coating function and the synergistic effect between the substances, as well as a lack of research on the coating's biological properties, tensile strength, adhesion strength, and

other important mechanical properties, which is not conducive to its real application in medicine. Moreover, the current research on self-repairing coatings is still in the growth period, and the types and functions of coatings are too singular, which restricts the application of self-repairing coatings. In addition, although the use of inhibitors has been successful in achieving the function of self-repair coating, Feyerabend et al. [234] have experimentally shown that rare earth elements (REEs) such as Ce and La contained in the diluent show moderate toxicity to vascular and bone-related cells, and hinder their use in bone implant materials. Although the external stimulus-response coating is low in toxicity, the choice of coating materials and requirements for usage conditions is strict. More work should still be done to expand its application.

6. Summary, challenges and perspectives

For the major problem of traditional PEO coating: premature failure of biodegradable Mg alloys due to high corrosion rate, different amelioration methods can be categorized as generation of PEO composite coating to seal the pores of traditional PEO coating or alteration of electrolyte composition (without changing the main components: the addition of nanoparticles, soluble salts, antibacterial components; changing the main components to HF solution) so as to change the PEO coating composition and characterization. Especially the changes in pore size, porosity and thickness, improve the different behaviors of conventional PEO coatings. The focus is on the amelioration of corrosion resistance and biocompatibility, and the endowment of antibacterial properties, osteogenesis and drug-loading abilities of PEO coatings.

Currently, however, the following challenges remain for PEO coatings suitable for biomedical Mg alloys.

(1) Most researchers have focused on improving various properties of PEO coatings and endowing them with more biological functions, while the widely accepted formation mechanism of PEO coatings has still not been proposed. In addition, the study of the interaction between different treatment parameters is blank.
(2) Many of the current methods for improving the corrosion resistance of PEO coatings are aimed at magnesium alloys for industrial use. Some of the corrosion inhibitors and polymer-PEO coatings are toxic to the human body, therefore, conventional PEO coating of industrial magnesium alloy cannot meet the needs of biomedical magnesium alloys implanted in the human body.
(3) Among the PEO coatings generated by different amelioration methods, except for the biofunction-oriented Antibacterial ingredients-PEO coating and drug-PEO coating, there are still few studies on the biocompatibility of the other coatings, especially *in vivo* tests, and only some researchers have investigated the biocompatibility of new improved PEO coatings using *in vitro* tests. Among them, the good biocompatibility of ZrO_2 has been confirmed in other medical fields (e.g., bone tissue repair field, oral prosthesis field), but there are very few studies on the biocompatibility of ZrO_2 incorporated-PEO coating. In the case of biofunction-oriented coatings, most researchers focus on testing the achievement of bio-functionality and often ignore the cytotoxicity, especially for antibacterial ingredients-PEO coatings, i.e., the addition of excessive antibacterial ingredients may be harmful to human cells while efficiently inhibiting bacteria. Hence, it is necessary to determine the appropriate concentration of these antibacterial ingredients to achieve the best antibacterial effect while avoiding cytotoxicity.
(4) Although different amelioration methods have improved some of the behaviors of conventional PEO coatings, none of them have been able to develop a novel PEO coating that would meet the criteria for ideal biomedical magnesium implants.

Therefore, in future research, on the premise of investigating the formation mechanism of PEO and the influence mechanism of each parameter, as it is the basis for the development of other amelioration methods, it is required to take more attempts for the combination of different amelioration methods to develop novel PEO coatings that can satisfy the criteria and to conduct *in vitro* and *in vivo* experiments to examine its corrosion resistance, wear resistance, mechanical properties, biocompatibility, and antibacterial properties for the long-term implantation of biomedical Mg *in vivo*.

Data availability statement

No data was used for the research described in the article.

CRediT authorship contribution statement

Biying Shi: Writing – review & editing, Writing – original draft, Software, Conceptualization. **Yu Ru Li:** Writing – review & editing, Writing – original draft, Validation, Resources. **Jiaqi Xu:** Writing – review & editing, Writing – original draft, Resources, Investigation. **Jiawei Zou:** Writing – original draft, Resources. **Zili Zhou:** Writing – original draft, Resources. **Qi Jia:** Writing – original draft, Software. **Heng Bo Jiang:** Writing – review & editing, Validation, Supervision, Conceptualization. **Kai Liu:** Writing – review & editing, Project administration, Funding acquisition, Conceptualization.

Declaration of competing interest

The authors declare that they have no known competing financial interests or personal relationships that could have appeared to influence the work reported in this paper.

References

chaod [1] Global, regional, and national burden of bone fractures in 204 countries and territories, 1990-2019: a systematic analysis from the Global Burden of Disease Study 2019, Lancet Healthy Longev 2 (9) (2021) e580–e592.
[2] American Academy of Orthopaedic Surgeons website, Available from: www.aaos.org.
[3] S. Pina, J.M.F. Ferreira, Bioresorbable plates and screws for clinical applications: a review, Journal of Healthcare Engineering 3 (2) (2012) 243–260.
[4] M.P. Staiger, et al., Magnesium and its alloys as orthopedic biomaterials: a review, Biomaterials 27 (9) (2006) 1728–1734.
[5] J. Song, et al., Latest research advances on magnesium and magnesium alloys worldwide, J. Magnesium Alloys 8 (1) (2020).
[6] X. Gao, et al., In vivo corrosion behavior of biodegradable magnesium alloy by MAF treatment, Scanning 2021 (2021) 5530788.
[7] J.T. Zhang, et al., Optimal design of a rod shape ultrasonic motor using sequential quadratic programming and finite element method, Finite Elem. Anal. Des. 59 (2012) 11–17.
[8] M. Sivapragash, et al., Optimization of PVD process parameter for coating AZ91D magnesium alloy by Taguchi grey approach, J. Magnesium Alloys 6 (2) (2018) 171–179.
[9] D.F. Zhang, et al., Low temperature thermal oxidation towards hafnium-coated magnesium alloy for biomedical application, Mater. Lett. 190 (2017) 181–184.
[10] X.B. Chen, et al., Corrosion-resistant electrochemical plating of magnesium (Mg) alloys, in: Corrosion Prevention of Magnesium Alloys, 2013, pp. 315–346.
[11] L.P. Wu, et al., Progress of electroplating and electroless plating on magnesium alloy, Trans. Nonferrous Metals Soc. China 20 (2010) S630–S637.
[12] K. Brunelli, et al., Effect of HCl pre-treatment on corrosion resistance of cerium-based conversion coatings on magnesium and magnesium alloys, Corrosion Sci. 47 (4) (2005) 989–1000.
[13] X. Chen, N. Birbilis, T.B. Abbott, Review of corrosion-resistant conversion coatings for magnesium and its alloys, Corrosion 67 (2011) 1–16.
[14] V.S. Saji, Organic conversion coatings for magnesium and its alloys, J. Ind. Eng. Chem. 75 (2019) 20–37.
[15] Y.F. Zhang, et al., Formation mechanism and corrosion resistance of the hydrophobic coating on anodized magnesium, Corrosion Sci. 111 (2016) 334–343.
[16] T. Gurgenc, Microstructure, mechanical properties and ELM based wear loss prediction of plasma sprayed ZrO2-MgO coatings on a magnesium alloy, Mater. Test. 61 (8) (2019) 787–796.
[17] D. Thirumalaikumarasamy, V. Balasubramanian, S.S. Sabari, Prediction and optimization of process variables to maximize the Young's modulus of plasma sprayed alumina coatings on AZ31B magnesium alloy, J. Magnesium Alloys 5 (1) (2017) 133–145.
[18] F. Czerwinski, Magnesium Alloys: Design, Processing and Properties, IntechOpen, 2011.
[19] Z.-Z. Yin, et al., Advances in coatings on biodegradable magnesium alloys, J. Magnesium Alloys 8 (1) (2020) 42–65.
[20] W.H. Yao, et al., Micro-arc oxidation of magnesium alloys: a review, J. Mater. Sci. Technol. 118 (2022) 158–180.
[21] P.T. Guo, M.Y. Tang, C.Y. Zhang, Tribological and corrosion resistance properties of graphite composite coating on AZ31 Mg alloy surface produced by plasma electrolytic oxidation, Surf. Coating. Technol. 359 (2019) 197–205.
[22] T.W. Clyne, S.C. Troughton, A review of recent work on discharge characteristics during plasma electrolytic oxidation of various metals, Int. Mater. Rev. 64 (3) (2019) 127–162.
[23] G.B. Darband, et al., Plasma electrolytic oxidation of magnesium and its alloys: mechanism, properties and applications, J. Magnesium Alloys 5 (1) (2017) 74–132.
[24] T. Monetta, P. Parnian, A. Acquesta, Recent advances in the control of the degradation rate of PEO treated magnesium and its alloys for biomedical applications, Metals 10 (7) (2020).
[25] C. Blawert, et al., 8 - plasma electrolytic oxidation/micro-arc oxidation of magnesium and its alloys, in: T.S.N.S. Narayanan, I.-S. Park, M.-H. Lee (Eds.), Surface Modification of Magnesium and its Alloys for Biomedical Applications, Woodhead Publishing, 2015, pp. 193–234.
[26] R. Chaharmahali, A. Fattah-Alhosseini, H. Esfahani, Increasing the in-vitro corrosion resistance of AZ31B-Mg alloy via coating with hydroxyapatite using plasma electrolytic oxidation, Journal of Asian Ceramic Societies 8 (1) (2020) 39–49.
[27] J. Jin, W. Zhang, H. Li, A composite coating formed on AZ91D magnesium alloy by micro-arc oxidation and electrochemical deposition, Mater. Technol. 32 (12) (2017) 707–715.
[28] H. Tang, et al., Fabrication of hydroxyapatite coatings on AZ31 Mg alloy by micro-arc oxidation coupled with sol-gel treatment, Rsc Advances 8 (22) (2018) 12368–12375.
[29] R. Salomão, et al., Hydrotalcite synthesis via co-precipitation reactions using MgO and Al(OH)3 precursors, Ceram. Int. 37 (8) (2011) 3063–3070.
[30] J. Chen, et al., Design and in situ prepare a novel composite coating on Mg alloy for active anti-corrosion protection, J. Alloys Compd. (2020) 831.
[31] C.Y. Li, et al., In vitro degradation and cytocompatibility of a low temperature in-situ grown self-healing Mg-Al LDH coating on MAO-coated magnesium alloy AZ31, Bioact. Mater. 5 (2) (2020) 364–376.
[32] L. Wang, et al., Discharge characteristics, plasma electrolytic oxidation mechanism and properties of ZrO2 membranes in K2ZrF6 electrolyte, Membranes 12 (5) (2022).
[33] R. Chaharmahali, et al., Improving surface characteristics of PEO coatings of Mg and its alloys with zirconia nanoparticles: a review, Applied Surface Science Advances 6 (2021).
[34] S. Wang, et al., Comparison of corrosion resistance and cytocompatibility of MgO and ZrO2 coatings on AZ31 magnesium alloy formed via plasma electrolytic oxidation, Coatings 8 (12) (2018) 441.
[35] M. Daroonparvar, et al., Antibacterial Activities and Corrosion Behavior of Novel PEO/nanostructured ZrO2 Coating on Mg Alloy, Transactions of Nonferrous Metals Society of China, 2018.
[36] D.Y. Liang, et al., Copper coating formed by micro-arc oxidation on pure Mg improved antibacterial activity, osteogenesis, and angiogenesis in vivo and in vitro, Biomed. Microdevices 23 (3) (2021).
[37] J. Song, et al., Antibacterial properties and biocompatibility in vivo and vitro of composite coating of pure magnesium ultrasonic micro-arc oxidation phytic acid copper loaded, J. Mater. Sci. Mater. Med. 30 (5) (2019) 49.
[38] D. Zhang, et al., Antibacterial activities against Porphyromonas gingivalis and biological characteristics of copper-bearing PEO coatings on magnesium, J. Mater. Sci. Technol. 61 (2021) 33–45.
[39] J.X. Chen, et al., In vitro degradation and antibacterial property of a copper-containing micro-arc oxidation coating on Mg-2Zn-1Gd-0.5Zr alloy, Colloids and Surfaces B-Biointerfaces 179 (2019) 77–86.
[40] K. Xue, et al., In vitro degradation and multi-antibacterial mechanisms of beta-cyclodextrin@curcumin embodied Mg(OH)(2)/MAO coating on AZ31 magnesium alloy, J. Mater. Sci. Technol. 132 (2023) 179–192.
[41] M. Li, et al., Nitrogen-containing bisphosphonate-loaded micro-arc oxidation coating for biodegradable magnesium alloy pellets inhibits osteosarcoma through targeting of the mevalonate pathway, Acta Biomater. 121 (2021) 682–694.
[42] A. Bordbar-Khiabani, et al., Improved corrosion performance of biodegradable magnesium in simulated inflammatory condition via drug-loaded plasma electrolytic oxidation coatings, Mater. Chem. Phys. (2020) 239.
[43] A. Bordbar-Khiabani, B. Yarmand, M. Mozafari, Functional PEO layers on magnesium alloys: innovative polymer-free drug-eluting stents, Surf. Innovations 6 (4–5) (2018) 237–243.
[44] M. Sekkarapatti Ramasamy, et al., Combination of polydopamine and carbon nanomaterials coating enhances the piezoelectric responses and cytocompatibility of biodegradable PLLA nanofiber scaffolds for tissue engineering applications, Mater. Today Commun. 33 (2022).
[45] A. Ghanbari, et al., PEO/Polymer Hybrid Coatings on Magnesium Alloy to Improve Biodegradation and Biocompatibility Properties, Surfaces and Interfaces, 2022.
[46] X. Wang, et al., Enhanced anticorrosive and antibacterial performances of silver nanoparticles/polyethyleneimine/MAO composite coating on magnesium alloys, Journal of Materials Research and Technology-Jmr&T 11 (2021) 2354–2364.
[47] C. Zhai, et al., Fluoride coatings on magnesium alloy implants, Bioinorgan. Chem. Appl. (2022) 1–21, 2022.

[48] A. Fattah-alhosseini, et al., A review of effective strides in amelioration of the biocompatibility of PEO coatings on Mg alloys, J. Magnesium Alloys 10 (9) (2022) 2354–2383.
[49] A. Fattah-alhosseini, R. Chaharmahali, Enhancing corrosion and wear performance of PEO coatings on Mg alloys using graphene and graphene oxide additions: a review, FlatChem 27 (2021) 100241.
[50] P.H. Sobrinho, et al., Statistical analysis of the voltage-time response produced during PEO coating of AZ31B magnesium alloy, Surf. Coating. Technol. 315 (2017) 530–545.
[51] A.G. Rakoch, et al., Plasma electrolytic oxidation of AZ31 and AZ91 magnesium alloys: comparison of coatings formation mechanism, J. Magnesium Alloys 8 (3) (2020) 587–600.
[52] W.B. Tu, et al., Plasma electrolytic oxidation of AZ31 magnesium alloy in aluminate-tungstate electrolytes and the coating formation mechanism, J. Alloys Compd. 725 (2017) 199–216.
[53] J.P. Lu, et al., Effects of voltage on microstructure and corrosion resistance of micro-arc oxidation ceramic coatings formed on KBM10 magnesium alloy, J. Mater. Eng. Perform. 27 (1) (2018) 147–154.
[54] J.W. Yuan, et al., Effects of current output modes on the growth kinetics and corrosion resistance of micro-arc oxidation coatings on magnesium alloy, Mater. Res. Express 8 (6) (2021).
[55] B.S. Lou, et al., Effects of processing parameters on the adhesion and corrosion resistance of oxide coatings grown by plasma electrolytic oxidation on AZ31 magnesium alloys, Journal of Materials Research and Technology-Jmr&T 10 (2021) 1355–1371.
[56] J. Yong, et al., Effect of (NH4)2ZrF6, voltage and treating time on corrosion resistance of micro-arc oxidation coatings applied on ZK61M magnesium alloys, Materials 14 (23) (2021).
[57] M. Mohedano, et al., Bioactive plasma electrolytic oxidation coatings on Mg-Ca alloy to control degradation behaviour, Surf. Coating. Technol. 315 (2017) 454–467.
[58] Z.U. Rehman, D.J. Choi, Investigation of ZrO2 nanoparticles concentration and processing time effect on the localized PEO coatings formed on AZ91 alloy, J. Magnesium Alloys 7 (4) (2019) 555–565.
[59] A. Fattah-alhosseini, M.S. Joni, Effect of KOH concentration on the microstructure and electrochemical properties of MAO-coated Mg alloy AZ31B, J. Mater. Eng. Perform. 24 (9) (2015) 3444–3452.
[60] S. Ono, et al., Effect of electrolyte concentration on the structure and corrosion resistance of anodic films formed on magnesium through plasma electrolytic oxidation, Electrochim. Acta 240 (2017) 415–423.
[61] A. Keyvani, et al., Role of incorporation of ZnO nanoparticles on corrosion behavior of ceramic coatings developed on AZ31 magnesium alloy by plasma electrolytic oxidation technique, Surface. Interfac. 22 (2021) 100728.
[62] W. Zhang, Y. Du, P. Zhang, Excellent plasma electrolytic oxidation coating on AZ61 magnesium alloy under ordinal discharge mode, J. Magnesium Alloys 10 (9) (2022) 2460–2474.
[63] A. Fattah-alhosseini, R. Chaharmahali, K. Babaei, Effect of particles addition to solution of plasma electrolytic oxidation (PEO) on the properties of PEO coatings formed on magnesium and its alloys: a review, J. Magnesium Alloys 8 (3) (2020) 799–818.
[64] T. Zehra, et al., Anionic assisted incorporation of WO3 nanoparticles for enhanced electrochemical properties of AZ31 Mg alloy coated via plasma electrolytic oxidation, J. Alloys Compd. 916 (2022) 165445.
[65] Z. Shi, G. Song, A. Atrens, Influence of the β phase on the corrosion performance of anodised coatings on magnesium–aluminium alloys, Corrosion Sci. 47 (11) (2005) 2760–2777.
[66] Y. Chen, et al., Influence of second phase on corrosion performance and formation mechanism of PEO coating on AZ91 Mg alloy, J. Alloys Compd. 718 (2017) 92–103.
[67] Z. Shahri, et al., Optimization of plasma electrolyte oxidation process parameters for corrosion resistance of Mg alloy, J. Magnesium Alloys 8 (2) (2020) 431–440.
[68] Y. Guo, M.P. Sealy, C. Guo, Significant improvement of corrosion resistance of biodegradable metallic implants processed by laser shock peening, CIRP Annals 61 (1) (2012) 583–586.
[69] L. Liu, Y. Li, F. Wang, Influence of grain size on the corrosion behavior of a Ni-based superalloy nanocrystalline coating in NaCl acidic solution, Electrochim. Acta 53 (5) (2008) 2453–2462.
[70] Y. Xiong, et al., Stress corrosion cracking behavior of LSP/MAO treated magnesium alloy during SSRT in a simulated body fluid, J. Alloys Compd. (2020) 822.
[71] F.F. Wei, et al., Microstructure and corrosion resistance studies of PEO coated Mg alloys with a HF and US pretreatment, Int. J. Electrochem. Sci. 12 (1) (2017) 155–165.
[72] B. Zhu, et al., Improving corrosion resistance and biocompatibility of AZ31 magnesium alloy by ultrasonic cold forging and micro-arc oxidation, J. Biomater. Appl. 36 (9) (2022) 1664–1675.
[73] J.H. Yang, et al., Tribocorrosion behavior and mechanism of micro-arc oxidation Ca/P coating on nanocrystallized magnesium alloys, Materials and Corrosion-Werkstoffe Und Korrosion 69 (6) (2018) 749–759.
[74] X.D. Yan, et al., Improvement of biodegradable and antibacterial properties by solution treatment and micro-arc oxidation (MAO) of a magnesium alloy with a trace of copper, Corrosion Sci. 156 (2019) 125–138.
[75] Y. Xiong, et al., LSP/MAO composite bio-coating on AZ80 magnesium alloy for biomedical application, Mater. Sci. Eng., C 75 (2017) 1299–1304.
[76] S. Shadanbaz, G.J. Dias, Calcium phosphate coatings on magnesium alloys for biomedical applications: a review, Acta Biomater. 8 (1) (2012) 20–30.
[77] J.H. Dou, G.C. Gu, C.Z. Chen, Effects of calcium salts on microstructure and corrosion behavior of micro-arc oxidation coatings on Mg-2Zn-1Ca-0.8 Mn alloy, Mater. Lett. 196 (2017) 42–45.
[78] R. Chaharmahali, A. Fattah-alhosseini, K. Babaei, Surface characterization and corrosion behavior of calcium phosphate (Ca-P) base composite layer on Mg and its alloys using plasma electrolytic oxidation (PEO): a review, J. Magnesium Alloys 9 (1) (2021) 21–40.
[79] G. Liu, et al., Self-adjustment of calcium phosphate coating on micro-arc oxidized magnesium and its influence on the corrosion behaviour in simulated body fluids, Corrosion Sci. 79 (2014) 206–214.
[80] J.H. Dou, et al., Preparation and characterization of a calcium-phosphate-silicon coating on a Mg-Zn-Ca alloy via two-step micro-arc oxidation, Phys. Chem. Chem. Phys. 19 (23) (2017) 15110–15119.
[81] S.V. Dorozhkin, Calcium orthophosphate coatings on magnesium and its biodegradable alloys, Acta Biomater. 10 (7) (2014) 2919–2934.
[82] J.H. Dou, et al., Formation of silicon-calcium-phosphate-containing coating on Mg-Zn-Ca alloy by a two-step micro-arc oxidation technique, Mater. Lett. 212 (2018) 37–40.
[83] H. Hornberger, S. Virtanen, A.R. Boccaccini, Biomedical coatings on magnesium alloys - a review, Acta Biomater. 8 (7) (2012) 2442–2455.
[84] M.M. Saleh, et al., Biodegradable/biocompatible coated metal implants for orthopedic applications, Bio Med. Mater. Eng. 27 (1) (2016) 87–99.
[85] N. Ramesh, S.C. Moratti, G.J. Dias, Hydroxyapatite-polymer biocomposites for bone regeneration: a review of current trends, J. Biomed. Mater. Res. B Appl. Biomater. 106 (5) (2018) 2046–2057.
[86] D. Arcos, M. Vallet-Regi, Substituted hydroxyapatite coatings of bone implants, J. Mater. Chem. B 8 (9) (2020) 1781–1800.
[87] Z.X. Wang, et al., Preparation and degradation behavior of composite bio-coating on ZK60 magnesium alloy using combined micro-arc oxidation and Electrophoresis deposition, Frontiers in Materials 7 (2020).
[88] H. Tang, et al., Synthesis and properties of hydroxyapatite-containing coating on AZ31 magnesium alloy by micro-arc oxidation, Appl. Surf. Sci. 400 (2017) 391–404.
[89] Z.R. Zheng, et al., Biodegradation behaviour of hydroxyapatite-containing self-sealing micro-arc-oxidation coating on pure Mg, Surf. Eng. 37 (7) (2021) 942–952.
[90] J.J. Yang, et al., Microstructure and corrosion behavior of Ca/P coatings prepared on magnesium by plasma electrolytic oxidation, Surf. Coating. Technol. 319 (2017) 359–369.

[91] J.M. Rua, et al., Micro-arc oxidation coating on porous magnesium foam and its potential biomedical applications, Surf. Coating. Technol. 360 (2019) 213–221.
[92] L. Pezzato, et al., Microstructural and corrosion properties of hydroxyapatite containing PEO coating produced on AZ31 Mg alloy, Materials 14 (6) (2021).
[93] N. Attarzadeh, et al., Multipurpose surface modification of PEO coatings using tricalcium phosphate addition to improve the bedding for apatite compounds, J. Alloys Compd. 877 (2021) 160275.
[94] W.T. Yu, et al., Novel fluoridated hydroxyapatite/MAO composite coating on AZ31B magnesium alloy for biomedical application, Appl. Surf. Sci. 464 (2019) 708–715.
[95] M. Mardali, et al., Microstructure and corrosion characterization of a MgO/hydroxyapatite bilayer coating by plasma electrolytic oxidation coupled with flame spraying on a Mg alloy, ACS Omega 5 (38) (2020) 24186–24194.
[96] M.B. Kannan, et al., Electrochemical surface engineering of magnesium metal by plasma electrolytic oxidation and calcium phosphate deposition: biocompatibility and in vitro degradation studies, RSC Adv. 8 (51) (2018) 29189–29200.
[97] J.H. Dou, H.J. Yu, C.Z. Chen, Preparation and characterization of composite coating on Mg-1.74Zn-0.55Ca alloy by micro-arc oxidation combined with sol-gel method, Mater. Lett. (2019) 255.
[98] Y.P. Liu, et al., Micro-arc oxidation-assisted sol-gel preparation of calcium metaphosphate coatings on magnesium alloys for bone repair, Mater. Sci. Eng., C (2021) 131.
[99] Z.Z. Yin, et al., Advances in coatings on biodegradable magnesium alloys, J. Magnesium Alloys 8 (1) (2020) 42–65.
[100] R.X. Sun, et al., Hydrothermal synthesis of microstructured fluoridated hydroxyapatite coating on magnesium alloy, Surf. Eng. 32 (11) (2016) 879–884.
[101] J.M. Zhang, et al., Mechanistic studies of electrodeposition for bioceramic coatings of calcium phosphates by an in situ pH-microsensor technique, J. Electroanal. Chem. 452 (2) (1998) 235–240.
[102] M.Y. Zakaria, et al., Incorporation of wollastonite bioactive ceramic with titanium for medical applications: an overview, Mater. Sci. Eng., C 97 (2019) 884–895.
[103] A.R. Boccaccini, et al., Electrophoretic deposition of biomaterials, J R Soc Interface 7 (Suppl 5) (2010) S581–S613.
[104] W. Shang, et al., Electrochemical corrosion behavior of composite MAO/sol-gel coatings on magnesium alloy AZ91D using combined micro-arc oxidation and sol-gel technique, J. Alloys Compd. 474 (1–2) (2009) 541–545.
[105] S.Y. Jian, et al., The potential of calcium/phosphate containing MAO implanted in bone tissue regeneration and biological characteristics, Int. J. Mol. Sci. 22 (9) (2021).
[106] F. Peng, et al., Sealing the pores of PEO coating with Mg-Al layered double hydroxide: enhanced corrosion resistance, cytocompatibility and drug delivery ability, Sci. Rep. 7 (2017).
[107] J. Wang, et al., Biocompatibility and bone regeneration of PEO/Mg-Al LDH-coated pure Mg: an in vitro and in vivo study, Sci. China Mater. 64 (2) (2021) 460–473.
[108] F. Peng, et al., PEO/Mg-Zn-Al LDH composite coating on Mg alloy as a Zn/Mg ion-release platform with multifunctions: enhanced corrosion resistance, osteogenic, and antibacterial activities, ACS Biomater. Sci. Eng. 4 (12) (2018) 4112–4121.
[109] S. El-Rahman, Neuropathology of aluminum toxicity in rats (glutamate and GABA impairment), Pharmacol. Res. 47 (3) (2003) 189–194.
[110] D.D. Zhang, et al., Mg-Fe LDH sealed PEO coating on magnesium for biodegradation control, antibacteria and osteogenesis, J. Mater. Sci. Technol. 105 (2022) 57–67.
[111] D.D. Zhang, et al., Comparison study of Mg(OH)(2), Mg-Fe LDH, and FeOOH coatings on PEO-treated Mg alloy in anticorrosion and biocompatibility, Appl. Clay Sci. (2022) 225.
[112] J.F. Chen, et al., Effect of alloy cations on corrosion resistance of LDH/MAO coating on magnesium alloy, Appl. Surf. Sci. 463 (2019) 535–544.
[113] Z.H. Wang, et al., Corrosion resistance enhancement of micro-arc oxidation ceramic layer by Mg-Al-Co layered double hydroxide coating, Trans. Indian Ceram. Soc. 79 (2) (2020) 59–66.
[114] D. Li, et al., Cancer therapy and fluorescence imaging using the active release of doxorubicin from MSPs/Ni-LDH folate targeting nanoparticles, Biomaterials 34 (32) (2013) 7913–7922.
[115] J. Lee, et al., Biofunctional layered double hydroxide nanohybrids for cancer therapy, Materials 15 (22) (2022).
[116] Z.H. Wang, et al., Enhanced corrosion resistance of micro-arc oxidation coated magnesium alloy by superhydrophobic Mg-Al layered double hydroxide coating, Trans. Nonferrous Metals Soc. China 29 (10) (2019) 2066–2077.
[117] D. Bakker, et al., Tissue/biomaterial interface characteristics of four elastomers. A transmission electron microscopical study, J. Biomed. Mater. Res. 24 (3) (1990) 277–293.
[118] V. Covacci, et al., In vitro evaluation of the mutagenic and carcinogenic power of high purity zirconia ceramic, Biomaterials 20 (4) (1999) 371–376.
[119] M. Catauro, et al., Biological response of human mesenchymal stromal cells to titanium grade 4 implants coated with PCL/ZrO(2) hybrid materials synthesized by sol-gel route: in vitro evaluation, Mater. Sci. Eng., C 45 (2014) 395–401.
[120] S.M. Shin, A.Y. Sung, Preparation and analysis of functional silicone hydrogel lenses containing ZrO_2 and antimony tin oxide nanoparticles, J. Nanosci. Nanotechnol. 21 (9) (2021) 4649–4653.
[121] I. Ahmad, Yttrium-partially stabilized zirconium dioxide posts: an approach to restoring coronally compromised nonvital teeth, Int J Periodontics Restorative Dent 18 (5) (1998) 454–465.
[122] A. Nevarez-Rascon, et al., Al(2)O(3(w))-Al(2)O(3(n))-ZrO(2) (TZ-3Y)(n) multi-scale nanocomposite: an alternative for different dental applications? Acta Biomater. 6 (2) (2010) 563–570.
[123] J.J. Zhuang, et al., A study on microstructure and corrosion resistance of ZrO2-containing PEO coatings formed on AZ31 Mg alloy in phosphate-based electrolyte, Appl. Surf. Sci. 357 (2015) 1463–1471.
[124] F. Liu, et al., Corrosion behavior of the composite ceramic coating containing zirconium oxides on AM30 magnesium alloy by plasma electrolytic oxidation, Corrosion Sci. 53 (11) (2011) 3845–3852.
[125] F. Liu, et al., Formation process of composite plasma electrolytic oxidation coating containing zirconium oxides on AM50 magnesium alloy, Trans. Nonferrous Metals Soc. China 21 (4) (2011) 943–948.
[126] J. Liang, et al., Comparison of electrochemical corrosion behaviour of MgO and ZrO2 coatings on AM50 magnesium alloy formed by plasma electrolytic oxidation, Corrosion Sci. 51 (10) (2009) 2483–2492.
[127] H.H. Luo, et al., Study on the microstructure and corrosion resistance of ZrO2-containing ceramic coatings formed on magnesium alloy by plasma electrolytic oxidation, J. Alloys Compd. 474 (1–2) (2009) 551–556.
[128] R. Arrabal, et al., Incorporation of zirconia particles into coatings formed on magnesium by plasma electrolytic oxidation, J. Mater. Sci. 43 (5) (2008) 1532–1538.
[129] A. Bordbar-Khiabani, B. Yarmand, M. Mozafari, Enhanced corrosion resistance and in-vitro biodegradation of plasma electrolytic oxidation coatings prepared on AZ91 Mg alloy using ZnO nanoparticles-incorporated electrolyte, Surf. Coating. Technol. 360 (2019) 153–171.
[130] N. Eslamzadeh, et al., An investigation into the corrosion behavior of MgO/ZrO2 nanocomposite coatings prepared by plasma electrolytic oxidation on the AZ91 magnesium alloy, J. Mater. Eng. Perform. 26 (9) (2017) 4255–4264.
[131] S. Bratan, et al., Formation and Properties of Composite Nanostructured PEO-Coatings on Metals and Alloys, MATEC Web of Conferences, 2017, p. 129.
[132] J.J. Zhuang, et al., Effect of current density on microstructure and properties of PEO ceramic coatings on magnesium alloy, Surf. Eng. 33 (10) (2017) 744–752.
[133] K.M. Lee, et al., Electrochemical response of ZrO2-incorporated oxide layer on AZ91 Mg alloy processed by plasma electrolytic oxidation, Surf. Coating. Technol. 205 (13) (2011) 3779–3784.
[134] Z. Liu, A.E. Spargo, Identification of various phases in HRTEM images of MgO-PSZ, Journal of electron microscopy 50 (6) (2001) 443–446.
[135] S. Gnedenkov, et al., Fabrication of coatings on the surface of magnesium alloy by plasma electrolytic oxidation using ZrO 2 and SiO 2 nanoparticles, J. Nanomater. 2015 (2015) 1–12.

[136] W. Shang, et al., Electrochemical corrosion behavior of composite MAO/sol–gel coatings on magnesium alloy AZ91D using combined micro-arc oxidation and sol–gel technique, J. Alloys Compd. 474 (1) (2009) 541–545.
[137] G. Rapheal, et al., Effect of current density on the microstructure and corrosion properties of plasma electrolytic oxidation (PEO) coatings on AM50 Mg alloy produced in an electrolyte containing clay additives, Surf. Coating. Technol. 289 (2016) 150–164.
[138] M. Molaei, K. Babaei, A. Fattah-alhosseini, Improving the wear resistance of plasma electrolytic oxidation (PEO) coatings applied on Mg and its alloys under the addition of nano- and micro-sized additives into the electrolytes: a review, J. Magnesium Alloys 9 (4) (2021) 1164–1186.
[139] M. Daroonparvar, et al., Corrosion resistance investigation of nanostructured Si- and Si/TiO2-coated Mg alloy in 3.5% NaCl solution, Vacuum 108 (2014) 61–65.
[140] J. Liang, L.-t. Hu, J. Hao, Preparation and characterization of oxide films containing crystalline TiO2 on magnesium alloy by plasma electrolytic oxidation, Electrochim. Acta 52 (2007) 4836–4840.
[141] S. Schultze-Mosgau, et al., Osseointegration of endodontic endosseous cones: zirconium oxide vs titanium, Oral Surg. Oral Med. Oral Pathol. Oral Radiol. Endod. 89 (1) (2000) 91–98.
[142] M. Uo, et al., Cytotoxicity and bonding property of dental ceramics, Dent. Mater. 19 (6) (2003) 487–492.
[143] J.H. Dubruille, et al., Evaluation of combinations of titanium, zirconia, and alumina implants with 2 bone fillers in the dog, Int. J. Oral Maxillofac. Implants 14 (2) (1999) 271–277.
[144] H. Chen, J. Hao, Study on preparing of ZrO2 ceramic coating and bone biological activity of magnesium alloys for medicine, Xiyou Jinshu Cailiao Yu Gongcheng/Rare Metal Materials and Engineering 43 (2014) 150–153.
[145] Y. Ichikawa, et al., Tissue compatibility and stability of a new zirconia ceramic in vivo, J. Prosthet. Dent 68 (2) (1992) 322–326.
[146] Y. Josset, et al., In vitro reactions of human osteoblasts in culture with zirconia and alumina ceramics, J. Biomed. Mater. Res. 47 (4) (1999) 481–493.
[147] A. Scarano, et al., Bone response to zirconia ceramic implants: an experimental study in rabbits, J. Oral Implantol. 29 (1) (2003) 8–12.
[148] G. Wang, et al., Microstructure, bioactivity and osteoblast behavior of monoclinic zirconia coating with nanostructured surface, Acta Biomater. 6 (3) (2010) 990–1000.
[149] X.L. Phuah, et al., Ultra-high heating rate effects on the sintering of ceramic nanoparticles: an in situ TEM study, Materials Research Letters 9 (9) (2021) 373–381.
[150] M.L. Eggersdorfer, et al., Mass-mobility characterization of flame-made ZrO2 aerosols: primary particle diameter and extent of aggregation, J. Colloid Interface Sci. 387 (1) (2012) 12–23.
[151] A. Fattah-alhosseini, et al., Antibacterial activity of bioceramic coatings on Mg and its alloys created by plasma electrolytic oxidation (PEO): a review, J. Magnesium Alloys 10 (1) (2022) 81–96.
[152] D. Lindsay, A. von Holy, Bacterial biofilms within the clinical setting: what healthcare professionals should know, J. Hosp. Infect. 64 (4) (2006) 313–325.
[153] S. Ferraris, S. Spriano, Antibacterial titanium surfaces for medical implants, Mater. Sci. Eng., C 61 (2016) 965–978.
[154] Z.Y. Chen, et al., Antibacterial biomaterials in bone tissue engineering, J. Mater. Chem. B 9 (11) (2021) 2594–2612.
[155] J.R. Koduru, et al., Phytochemical-assisted synthetic approaches for silver nanoparticles antimicrobial applications: a review, Adv. Colloid Interface Sci. 256 (2018) 326–339.
[156] X. Fan, L. Yahia, E. Sacher, Antimicrobial properties of the Ag, Cu nanoparticle system, Biology 10 (2) (2021).
[157] X. He, et al., Antibacterial ability and osteogenic activity of porous Sr/Ag-containing TiO2 coatings, Biomed Mater 11 (4) (2016) 045008.
[158] K. Yu, et al., Investigation of biodegradability, cytocompatibility and antibacterial property of plasma electrolytic oxidation coating on Mg, Surface. Interfac. 30 (2022).
[159] Y. Chen, et al., Ag-containing antibacterial self-healing micro-arc oxidation coatings on Mg-Zn-Sr alloys, Surf. Eng. 37 (7) (2021) 926–941.
[160] Q. Han, et al., Fabrication of Ag containing antibacterial PEO coatings on pure Mg, Mater. Lett. (2021) 293.
[161] L. Zhang, et al., The dual function of Cu-doped TiO2 coatings on titanium for application in percutaneous implants, J. Mater. Chem. B 4 (21) (2016) 3788–3800.
[162] M. Hans, et al., Physicochemical properties of copper important for its antibacterial activity and development of a unified model, Biointerphases 11 (1) (2015) 018902.
[163] M. Seyfi, et al., Effect of ZnO nanoparticles addition to PEO coatings on AZ31B Mg alloy: antibacterial effect and corrosion behavior of coatings in Ringer's physiological solution, Journal of Asian Ceramic Societies 9 (3) (2021) 1114–1127.
[164] H. Mozafarnia, et al., Corrosion, wear, and antibacterial behaviors of hydroxyapatite/MgO composite PEO coatings on AZ31 Mg alloy by incorporation of TiO2 nanoparticles, Coatings 12 (12) (2022) 1967.
[165] L.Y. Cui, et al., In vitro corrosion and antibacterial performance of micro-arc oxidation coating on AZ31 magnesium alloy: effects of tannic acid, J. Electrochem. Soc. 165 (11) (2018) C821–C829.
[166] A. Fattah-Alhosseini, et al., Performance of PEO/polymer coatings on the biodegradability, antibacterial effect and biocompatibility of Mg-based materials, J. Funct. Biomater. 13 (4) (2022).
[167] D. Wang, et al., Betamethasone suppresses the inflammatory response in LPS-stimulated dental pulp cells through inhibition of NF-κB, Arch. Oral Biol. 98 (2019) 156–163.
[168] K. Wang, et al., The metabolism of berberine and its contribution to the pharmacological effects, Drug Metab. Rev. 49 (2) (2017) 139–157.
[169] L.T. Mu, et al., Corrosion behavior and biological activity of micro arc oxidation coatings with berberine on a pure magnesium surface, Coatings 10 (9) (2020).
[170] H.S. Batra, Pawar, D. Bahl, Curcumin in combination with anti-cancer drugs: A nanomedicine review. Pharmacol Res 139 (2019) 91–105.
[171] Y. Zou, et al., Photothermal bactericidal surfaces: killing bacteria using light instead of biocides, Biomater. Sci. 9 (1) (2021) 10–22.
[172] Y. Wang, et al., Puerarin stimulates proliferation and differentiation and protects against cell death in human osteoblastic MG-63 cells via ER-dependent MEK/ERK and PI3K/Akt activation, Phytomedicine 20 (10) (2013) 787–796.
[173] S.H. Peng, et al., Corrosion behavior and biological activity of micro-arc oxidation coating with puerarin on pure magnesium surface, Results Phys. 12 (2019) 1481–1489.
[174] T. Ohba, et al., Bisphosphonates inhibit osteosarcoma-mediated osteolysis via attenuation of tumor expression of MCP-1 and RANKL, J. Bone Miner. Res. 29 (6) (2014) 1431–1445.
[175] T. Zehra, A. Fattah-alhosseini, M. Kaseem, Surface properties of plasma electrolytic oxidation coating modified by polymeric materials: a review, Prog. Org. Coating 171 (2022) 107053.
[176] A. Fattah-alhosseini, R. Chaharmahali, K. Babaei, Impressive strides in amelioration of corrosion and wear behaviors of Mg alloys using applied polymer coatings on PEO porous coatings: a review, J. Magnesium Alloys 10 (5) (2022) 1171–1190.
[177] X. Ma, et al., Chitosan/polydopamine layer by layer self-assembled silk fibroin nanofibers for biomedical applications, Carbohydr. Polym. 251 (2021) 117058.
[178] Y. Liu, et al., Preparation and in vitro evaluation of ε-poly(L-lysine) immobilized poly(ε-caprolactone) nanofiber membrane by polydopamine-assisted decoration as a potential wound dressing material, Colloids Surf. B Biointerfaces (2022) 220.
[179] K. Kopec, et al., Polydopamine and gelatin coating for rapid endothelialization of vascular scaffolds, Biomater. Adv. 134 (2022) 112544.
[180] S. Farshid, M. Kharaziha, M. Atapour, A self-healing and bioactive coating based on duplex plasma electrolytic oxidation/polydopamine on AZ91 alloy for bone implants, J. Magnesium 11 (2) (2022) 592–606.
[181] Y. Sun, et al., A polydopamine-assisted strontium-substituted apatite coating for titanium promotes osteogenesis and angiogenesis via FAK/MAPK and PI3K/AKT signaling pathways, Mater. Sci. Eng., C 131 (2021) 112482.
[182] P. Xian, et al., Polydopamine (PDA) mediated nanogranular-structured titanium dioxide (TiO2) coating on polyetheretherketone (PEEK) for oral and maxillofacial implants application, Surf. Coating. Technol. (2020) 401.
[183] J. Zhang, et al., A novel dental adhesive containing Ag/polydopamine-modified HA fillers with both antibacterial and mineralization properties, J. Dent. 111 (2021) 103710.

[184] A. Alcudia, et al., Development of porous silver nanoparticle/polycaprolactone/polyvinyl alcohol coatings for prophylaxis in titanium interconnected samples for dental implants, Colloid and Interface Science Communications 48 (2022).
[185] P. Salazar, M. Martín, J.L. González-Mora, Polydopamine-modified Surfaces in Biosensor Applications, 2016.
[186] Z.S. Wang, et al., Efficacy and safety of traditional Chinese medicine on thromboembolic events in patients with atrial fibrillation: a systematic review and meta-analysis, Compl. Ther. Med. 32 (2017) 1–10.
[187] Y.S. Feng, et al., Characterization and cytocompatibility of polydopamine on MAO-HA coating supported on Mg-Zn-Ca alloy, Surf. Interface Anal. 49 (11) (2017) 1115–1123.
[188] A. Alabbasi, et al., Biodegradable polymer for sealing porous PEO layer on pure magnesium: an in vitro degradation study, Appl. Surf. Sci. 301 (2014) 463–467.
[189] L.Y. Xu, et al., Corrosion and tribocorrosion protection of AZ31B Mg alloy by a hydrothermally treated PEO/chitosan composite coating, Prog. Org. Coating (2022) 170.
[190] P. Tian, D. Xu, X. Liu, Mussel-inspired functionalization of PEO/PCL composite coating on a biodegradable AZ31 magnesium alloy, Colloids Surf. B Biointerfaces 141 (2016) 327–337.
[191] L.X. Chen, et al., Influence of a MAO plus PLGA coating on biocorrosion and stress corrosion cracking behavior of a magnesium alloy in a physiological environment, Corrosion Sci. 148 (2019) 134–143.
[192] P. Shi, et al., Preparation and characterization of PLA coating and PLA/MAO composite coatings on AZ31 magnesium alloy for improvement of corrosion resistance, Surf. Coating. Technol. 262 (2015) 26–32.
[193] M. Jurak, et al., What affects the biocompatibility of polymers? Adv. Colloid Interface Sci. 294 (2021) 102451.
[194] H.B. Lee, et al., Study on the characteristics of MAO/polymer/Ni three-layer composite film formed on AZ31 magnesium alloy, Int. J. Electrochem. Sci. 16 (12) (2021).
[195] Z. Wei, et al., Hemocompatibility and selective cell fate of polydopamine-assisted heparinized PEO/PLLA composite coating on biodegradable AZ31 alloy, Colloids Surf. B Biointerfaces 121 (2014) 451–460.
[196] Y.K. Kim, et al., Improvement of osteogenesis by a uniform PCL coating on a magnesium screw for biodegradable applications, Sci. Rep. 8 (1) (2018) 13264.
[197] M. Kaseem, et al., Electrochemical response of MgO/Co3O4 oxide layers produced by plasma electrolytic oxidation and post treatment using cobalt nitrate, J. Magnesium Alloys 11 (3) (2023) 1057–1073.
[198] L. Sun, et al., Surface Characterization and Corrosion Resistance of Biomedical AZ31 Mg Alloy Treated by Microarc Fluorination, Scanning, 2020, p. 2020.
[199] H.B. Jiang, et al., Surface modification of anodized Mg in ammonium hydrogen fluoride by various voltages, Surf. Coating. Technol. 259 (2014) 310–317.
[200] H.B. Jiang, et al., Achieving controllable degradation of a biomedical magnesium alloy by anodizing in molten ammonium bifluoride, Surf. Coating. Technol. 313 (2017) 282–287.
[201] Z.Y. Yan, et al., Feasibility and efficacy of a degradable magnesium-alloy GBR membrane for bone augmentation in a distal bone-defect model in beagle dogs, Bioinorgan. Chem. Appl. 2022 (2022) 4941635.
[202] Y. Yang, X. Ding, M.W. Urban, Chemical and physical aspects of self-healing materials, Prog. Polym. Sci. 49–50 (2015) 34–59.
[203] S. Wang, M.W. Urban, Self-healing polymers, Nat. Rev. Mater. 5 (8) (2020) 562–583.
[204] S. Utrera-Barrios, et al., Evolution of self-healing elastomers, from extrinsic to combined intrinsic mechanisms: a review, Mater. Horiz. 7 (11) (2020) 2882–2902.
[205] X.K.D. Hillewaere, F.E. Du Prez, Fifteen chemistries for autonomous external self-healing polymers and composites, Prog. Polym. Sci. 49–50 (2015) 121–153.
[206] D. Zhang, F. Peng, X. Liu, Protection of magnesium alloys: from physical barrier coating to smart self-healing coating, J. Alloys Compd. (2021) 853.
[207] T. Zehra, A. Fattah-alhosseini, M. Kaseem, Surface properties of plasma electrolytic oxidation coating modified by polymeric materials: a review, Prog. Org. Coating (2022) 171.
[208] A.S. Gnedenkov, et al., Hybrid coatings for active protection against corrosion of Mg and its alloys, Polymers 15 (14) (2023).
[209] A.S. Gnedenkov, et al., New polycaprolactone-containing self-healing coating design for enhance corrosion resistance of the magnesium and its alloys, Polymers 15 (1) (2023).
[210] Y. Chen, et al., A self-healing corrosion protection coating with graphene oxide carrying 8-hydroxyquinoline doped in layered double hydroxide on a micro-arc oxidation coating, Corrosion Sci. (2022) 194.
[211] A.S. Gnedenkov, et al., Smart composite antibacterial coatings with active corrosion protection of magnesium alloys, J. Magnesium Alloys 10 (12) (2022) 3589–3611.
[212] H. Huangfu, et al., A smart composite coating with self-reporting and self-healing functions to enhance corrosion protection for magnesium alloys, Prog. Org. Coating (2023) 181.
[213] S. Yang, R. Sun, K. Chen, Self-healing performance and corrosion resistance of phytic acid/cerium composite coating on microarc-oxidized magnesium alloy, Chem. Eng. J. (2022) 428.
[214] Y. Chen, et al., Synergistic effect of graphene oxide/ternary Mg-Al-La layered double hydroxide for dual self-healing corrosion protection of micro-arc oxide coating of magnesium alloy, Colloids Surf. A Physicochem. Eng. Asp. (2022) 655.
[215] X. Dai, et al., Dual self-healing effects of salicylate intercalated MgAlY-LDHs film in-situ grown on the micro-arc oxidation coating on AZ31 alloys, Corrosion Sci. (2023) 220.
[216] N. Li, et al., Self-healing and superhydrophobic dual-function composite coating for active protection of magnesium alloys, Surf. Coating. Technol. (2023) 454.
[217] B. Li, et al., Intrinsically self-healing polymers: from mechanistic insight to current challenges, Chem Rev 123 (2) (2023) 701–735.
[218] Z.P. Zhang, M.Z. Rong, M.Q. Zhang, Self-healable functional polymers and polymer-based composites, Prog. Polym. Sci. (2023) 144.
[219] A. Stankiewicz, I. Szczygieł, B. Szczygieł, Self-healing coatings in anti-corrosion applications, J. Mater. Sci. 48 (23) (2013) 8041–8051.
[220] J. Guo, et al., An anti-stripping and self-healing micro-arc oxidation/acrylamide gel composite coating on magnesium alloy AZ31, Mater. Lett. (2020) 260.
[221] Z. Jia, et al., Inhibitor encapsulated, self-healable and cytocompatible chitosan multilayer coating on biodegradable Mg alloy: a pH-responsive design, J. Mater. Chem. B 4 (14) (2016) 2498–2511.
[222] Q. Chen, et al., Formation of self-healing PEO coatings on AM50 Mg by in-situ incorporation of zeolite micro-container, Corrosion Sci. (2022) 209.
[223] S. Pommiers-Belin, et al., Determination of the chemical mechanism of chromate conversion coating on magnesium alloys EV31A, Appl. Surf. Sci. 298 (2014) 199–207.
[224] H. Chai, et al., The effects of chemical conversion parameters on morphology and corrosion performance of calcium phosphate coating on AZ31 alloy, Mater. Chem. Phys. 296 (2023) 127338.
[225] L.T. Trang, et al., Formation and corrosion behavior of calcium phosphate coating layers on ZK60 alloy coated at various pH conditions by chemical conversion method, Surf. Coating. Technol. 444 (2022) 128639.
[226] X. Xue, et al., The research progress of self-healing coatings for magnesium/magnesium alloy, J. Alloys Compd. (2023) 960.
[227] Y. Chen, et al., A self-healing corrosion protection coating with graphene oxide carrying 8-hydroxyquinoline doped in layered double hydroxide on a micro-arc oxidation coating, Corrosion Sci. 194 (2022) 109941.
[228] C. Ding, et al., Design and fabrication of a novel stimulus-feedback anticorrosion coating featured by rapid self-healing functionality for the protection of magnesium alloy, ACS Appl. Mater. Interfaces 9 (24) (2017) 21034–21047.
[229] Q. Tang, et al., A simple route to interpenetrating network hydrogel with high mechanical strength, J. Colloid Interface Sci. 339 (1) (2009) 45–52.
[230] S. Nazari Pour, et al., Controlled in situ formation of polyacrylamide hydrogel on PET surface via SI-ARGET-ATRP for wound dressings, Appl. Surf. Sci. 349 (2015) 695–704.
[231] M.L. Zheludkevich, J. Tedim, M.G.S. Ferreira, Smart" coatings for active corrosion protection based on multi-functional micro and nanocontainers, Electrochim. Acta 82 (2012) 314–323.
[232] Y. Cao, G. Li, X. Li, Graphene/layered double hydroxide nanocomposite: properties, synthesis, and applications, Chem. Eng. J. 292 (2016) 207–223.

[233] M. Abdolah Zadeh, et al., Synergetic active corrosion protection of AA2024-T3 by 2D- anionic and 3D-cationic nanocontainers loaded with Ce and mercaptobenzothiazole, Corrosion Sci. 135 (2018) 35–45.
[234] F. Feyerabend, et al., Evaluation of short-term effects of rare earth and other elements used in magnesium alloys on primary cells and cell lines, Acta Biomater. 6 (5) (2010) 1834–1842.
[235] J. Xie, et al., Oxyhydroxide-coated PEO-treated Mg alloy for enhanced corrosion resistance and bone regeneration, J. Funct. Biomater. 13 (2) (2022).
[236] X. Xu, et al., Cross-linked gelatin/nanoparticles composite coating on micro-arc oxidation film for corrosion and drug release, Appl. Surf. Sci. 256 (8) (2010) 2367–2371.